Additive manufacturing of ceramics: Advances, challenges, and outlook

Journal of the European Ceramic Society 43 (2023) 6635–6664

Contents lists available at ScienceDirect

Journal of the European Ceramic Society

journal homepage: www.elsevier.com/locate/jeurceramsoc

Additive manufacturing of ceramics: Advances, challenges, and outlook

Mehran Dadkhah [a], Jean-Marc Tulliani [a], Abdollah Saboori [b,*], Luca Iuliano [b]

[a] Lince laboratory, INSTM R.U, Department of Applied Science and Technology, Politecnico di Torino, Corso Duca Degli Abruzzi 24, 10129 Torino, Italy
[b] Integrated Additive Manufacturing Center, Department of Management and Production Engineering, Politecnico di Torino, Corso Duca Degli Abruzzi 24, 10129 Torino, Italy

ARTICLE INFO

Keywords:
Additive manufacturing
3D printing
Ceramics
Density
Mechanical properties

ABSTRACT

Additive manufacturing (AM) of ceramics is relatively more challenging with respect to polymers and metals, owing to their high melting temperatures and inherent brittleness. Thus, this review aims to provide a comprehensive survey of recent AM technologies successfully employed to produce net shape ceramic components. In recent years, several techniques have been developed and the latest progress in this field are highlighted, as well as the current challenges in the complex shaped ceramic parts production via AM technologies. The state of the art concerning the various 3D printing processes applied to the fabrication of ceramic components is discussed with, for each method, the presentation of its advantages, disadvantages, and possible applications. The potential of AM for producing complex shape ceramic components and the challenges to overcome are discussed as well.

1. Introduction

Additive manufacturing (AM) technology was introduced to the engineering field to fabricate solid models with complex geometric through the deposition of powder, liquid, and solid sheets, in a layer by layer manner [1,2]. This process is called digital fabrication, layer manufacturing, rapid Prototyping, solid freedom fabrication, generative manufacturing, and 3D printing [3–5]. AM technology was first introduced in the 1980 s and was limited to producing small parts or prototypes [6]. From the industrial point of view, AM process has initially been used in medicine and dentistry [7,8]. Thereafter, this technology has extensively been utilized to create various open-source designs associated with the automotive, aerospace, aviation industries, and healthcare [9,10]. For instance, so far, AM has been employed to produce rocket engine components, artificial heart pumps, implants, cornea, bridges, dental implants and microwave guides, customized jewelry, food items, cementitious materials, automobile parts, armament parts (ceramic armour), heat exchangers and houses, energy, electronics and ceramic tooling for investment casting [11–14]. One of the main challenges AM faces is the number of available processable materials for this technology. Nevertheless, it is well documented that various materials, including metals, ceramics, polymers, biomaterials and smart materials can be generally processed through AM technologies [15,16]. Table 1 displays a range of available materials processed via the current AM systems [15,17].

Table 1 clearly shows that till now, despite all the efforts undertaken on polymeric and metallic materials, more attention should be paid to ceramics. One of the bottlenecks in ceramic part production through AM technologies is the lack of a reliable and comprehensive review of the latest achievements and challenges in AM of ceramics. Hence, the main target of this comprehensive review is to overview the latest progress in this field and highlight the current challenges in the complex shape ceramic part production via AM technologies.

This review describes the state of art concerning the various 3D printing processes applied to the fabrication of ceramic components. For this reason, each method with its advantages, disadvantages, and applications will be described in detail hereafter. The potential of AM for producing complex shape ceramic components and the challenges will be discussed.

2. Additive manufacturing technologies

AM was firstly commercialized by Charles Hull in the early 1980 s using the stereolithography manufacturing process [18,19]. Since 2009, AM technology has been intensively developed and utilized in engineering applications and diverse industrial sectors. Fig. 1 displays the timeline of the landmark achievements in AM from the 1980 s to 2018 [6].

* Corresponding author.
E-mail address: Abdollah.saboori@polito.it (A. Saboori).

https://doi.org/10.1016/j.jeurceramsoc.2023.07.033
Received 17 January 2023; Received in revised form 9 May 2023; Accepted 16 July 2023
Available online 18 July 2023

Table 1
Various range of available materials for current AM systems.

Additive manufacturing materials		
Polymers	Metallic materials	Others
PVC, PS, PMMA, PE, PC, Epoxy, ABS, PU, PP, PLA, PES, Nylon, Elastomers	Cobalt and alloys, Gold, Molybdenum, Rhenium, Silicon, Tungsten, Vanadium, Titanium and alloys, Silver, Nickel and alloys, Manganese, Chrome, Aluminium and alloys, Steels, Copper and alloys	Cellulose, Green sand, Office paper, Starch, Wax, Wood, Plaster, MDF, Ceramics

ABS: Acrylonitrile butadiene styrene; **PC**: Polycarbonate; **PES**: Polysulfone; **PLA**: Polylactic acid; **PMMA**: Polymethyl methacrylate; **PP**: Polypropylene; **PS**: Polystyrene; **PU**: Polyurethane; **PVC**: Polyvinyl chloride; **MDF**: Medium-density fibreboard.

From the beginning of rapid prototyping at early stages, polymeric materials with very high processability have been used to produce 3D net shape parts. With technological developments, metallic materials with lower processability with respect to polymeric ones have also been processed using AM technologies [20]. However, due to the inherent properties of ceramic materials, this class of structural materials has not progressed to the same level as the other two classes. As a matter of fact, in polymeric and metallic materials, an AM process is mainly used as a manufacturing process. In this process, the consolidation process takes place together with shaping, whereas in the case of ceramic parts, AM processes, till now, have been used as a shaping process. In this case, the consolidation phase has been implemented through conventional sintering processes at high temperature in ovens. Nonetheless, several efforts have been undertaken to process ceramic materials through a single-step AM process in which the shaping and consolidation process take place simultaneously.

3. Additive manufacturing of ceramics

Ceramics offer excellent thermal insulation capability as well as high mechanical properties in an extensive range of temperatures. Moreover, they have been increasingly used in electronics manufacturing owing to their excellent electrical insulation properties. On the other hand, ceramic materials possess a low thermal expansion coefficient so that by varying temperatures, they expand negligibly and present a good shape consistency. Thus, in many industrial applications, such as aerospace, automotive, and machine tools, ceramics, owing to their excellent mechanical properties, including high corrosive resistance, high-temperature strength, high wear resistance, high degree of hardness, and good tribological features, attract lots of attention [21,22].

Nevertheless, the shaping process of ceramic materials cannot be performed using conventional forging and machining formation. To this aim, they are usually shaped through multi-step methods [23], including powder mixture (binder and stabilizers) and shape forming such as extrusion, slip casting, pressing, tape casting, gel casting and inkjet moulding. Thereafter, the green body that has been shaped should undergo a sintering process to perform the final consolidation. It is well reported that the traditional methods are rather expensive since they include moulding, heat treatment and, sometimes, post-sintering machining.

AM of ceramic has been extensively developed during the last years to overcome conventional manufacturing disadvantages, specifically concerning size shrinkage, generation of parts with complex structures, and high tool wear. AM of ceramics is mainly utilized in the aerospace, automotive, and healthcare sectors. Furthermore, 3D printing has been considered an essential method to print advanced ceramics for biomaterials and bone tissue engineering, e.g., scaffolds for bones and teeth. Compared to traditional methods like casting and sintering, 3D-printed ceramic scaffolds utilized in tissue engineering are more convenient and faster [24]. Ceramic AM is fundamentally different from conventional manufacturing methods. This process joins materials to each other layer by layer and includes four steps: model design and slicing, printing, and post-treatment [25]. Over the past years, AM of complex shapes ceramics has attracted lots of attention due to the expensive and time-consuming post-processing of sintered ceramic parts with desirable shapes. In addition, 3D printing of porous ceramics or lattice structures offers several advantages for developing advanced lightweight materials in various applications. However, it is well documented that due to the high melting temperature, various optical/thermal features, and low thermal shock resistance of ceramics, the processability of this class of material through the direct layer-by-layer AM techniques is very challenging.

According to the ASTM, complex shape ceramic part production using the AM techniques can be classified into two groups; direct or single-step and indirect process, also known as multi-step[23]. In the multi-step AM process, the manufactured green body requires post-processing steps such as debinding and sintering treatments to consolidate the green body. Sheet lamination [26], Materials Extrusion-based techniques (MEX) [27], Binder Jetting (BJT) [28], vat photopolymerization-based technologies (VPP) [29], Direct Inkjet Printing (DIP) [30], and indirect Selective Laser Sintering (SLS) are the most available indirect AM technologies. Whereas there are currently only 2 AM processes that can be used to produce complex shape advanced ceramic parts via directly shaping and consolidating the material in a single step; Laser Powder Bed Fusion (L-PBF) and Directed Energy Deposition (DED).

Another AM method to process ceramics is referred to as negative ceramic AM. In this method, sacrificial polymer moulds are shaped using AM technologies such as Fused Deposition Modeling (FDM) [31], Material Jetting (MJT) [32], SLS [33], and Stereolithography (SLA) [34]. Subsequently, polymer moulds are impregnated with a ceramic slurry by casting or gel casting that is then removed by dissolution or thermal burn-out [35]. Negative AM can shape polymers in an easier, more processable and cost-effective way compared to ceramics. In the next

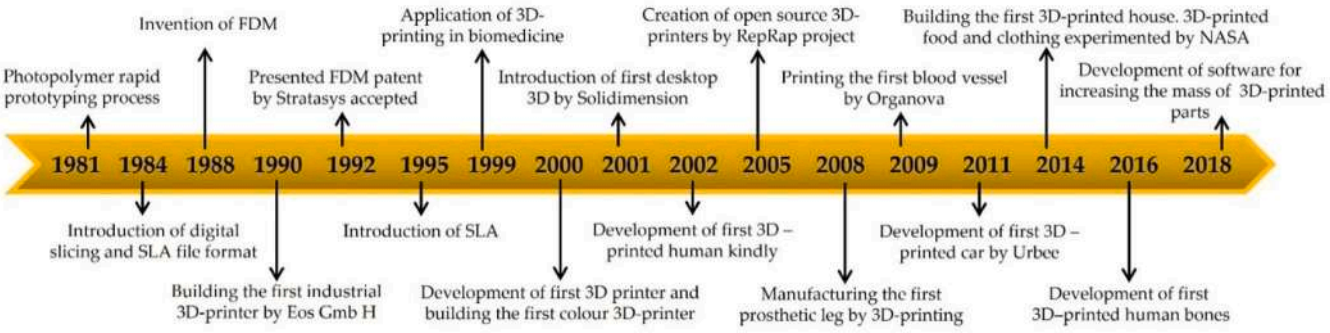

Fig. 1. Timeline of the significant discoveries in AM technology from the 1980 s to 2018. FDM: Fused deposition modelling; SLA: Stereolithography.

step, conventional colloidal casting processes shape ceramic components. Besides, where parts with complex internal geometries are needed, the design complexity can be reduced using negative AM. Nevertheless, this method does not control the material composition, such as material grading and multi-material fabrication, although all direct AM techniques do not possess this ability. In addition, manufacturing steps in negative AM are more than multi-step, and single-step AM, as shown in Fig. 2 [36]. This figure also demonstrates the potential of single-step ceramic AM to noticeably decrease the time of manufacturing by removing the steps for post-shaping. Instead, Fig. 3 compares the ceramic forming using conventional and AM methods [37]. In fact, as mentioned earlier, these AM technologies belong to the multi-step approaches that require further post heat treatment to achieve the final consolidation.

In recent years, AM technologies have been successfully employed to manufacture net shape ceramic components. As far as the kind of ceramic is concerned, it should be highlighted that the common AM manufactured ceramic materials are zirconia, alumina, silicon carbide, silicon nitride, biocompatible materials (i.e. bioglass, hydroxyapatite), and polymer-derived ceramics. Zirconia is widely processed using the ME-based AM, SLA, BJT, and inkjet 3D printing methods to produce customized parts such as dental products. Nevertheless, recently a novel 3D printing process which is called IntrinSIC® is developed by Schunk technical ceramics for serial production of high quality, complex shape ceramics [38]. Similarly, alumina has been extensively used as a structural ceramic owing to its high hardness, low cost, and heat resistance. Silicon carbide and silicon nitride have gained increased consideration as very hard materials, specifically in the aerospace industry, due to the requirements for fabricating dense products with excellent mechanical characteristics. In addition, AM techniques have also been used to generate medical implants using biocompatible ceramic materials like bioglasses and hydroxyapatite.

Table 2 lists structural and functional ceramic materials that have already been processed using AM technologies [22,39]. The shape and functional characteristics are simultaneously obtained in single-step AM techniques, such as DED, SLM, and SLS processes. In these processes, the ceramic particles are bonded together by chemical binding, solid-state sintering, and partial and full particle melting. Instead, in multi-step AM processes such as BJT, LOM, MEX, VPP, and MJT, the shaping step is followed by one or several consolidation steps. In these methods, a binder material is utilized for keeping the ceramic powders together (into a shape), which is followed by removing this binder through one or more “debinding” steps [40].

In AM of ceramics, cracks and large pores can be avoided in as-built

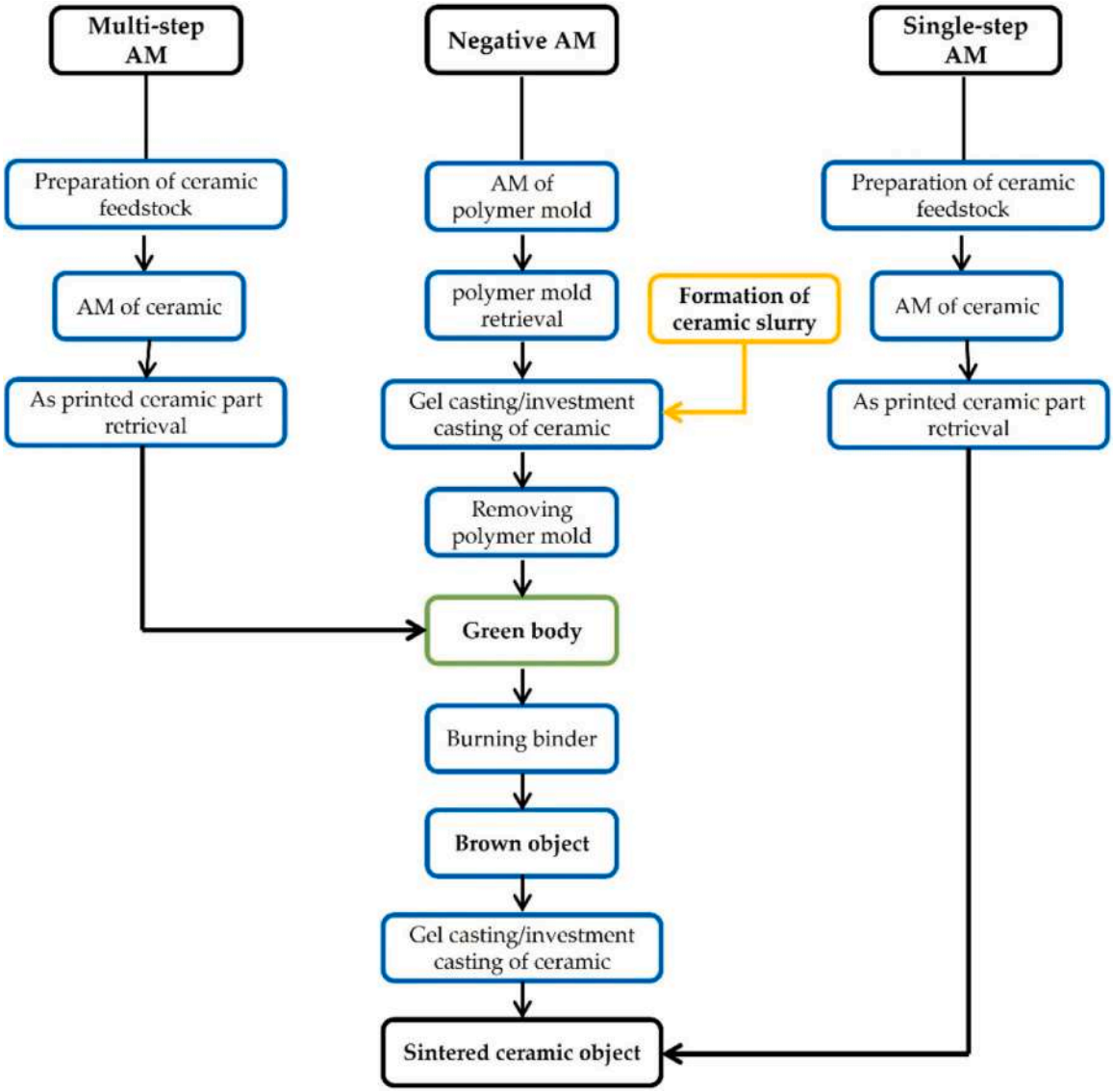

Fig. 2. Processing steps from feedstock to the sintered ceramic part using multi-step direct AM, single-step direct AM, and negative ceramic AM.

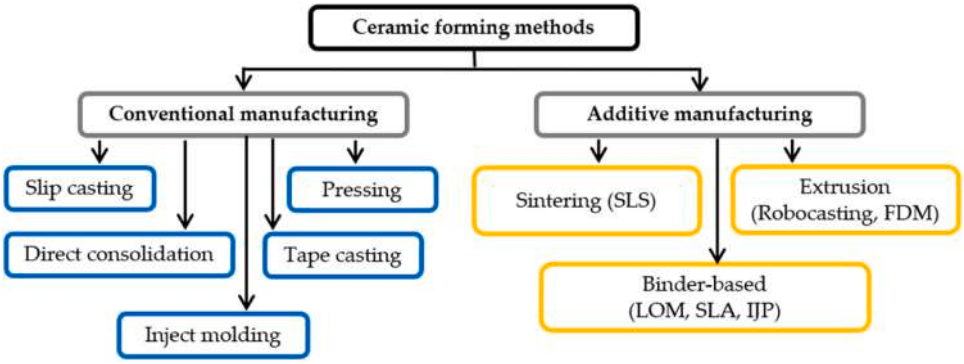

Fig. 3. A classification of forming techniques for ceramic materials.

Table 2
A summary of structural and functional ceramics fabricated by AM-based techniques.

Method	Structural ceramics	Functional ceramics	Features exhibited
3DP	ZrO_2, Al_2O_3, Ti_3SiC_2, Si_3N_4, TiC-TiO_2, SiC, $CaSiO_3$	$BaTiO_3$, PZT, TiO_2, YBCO, LSMO	Biocompatible, no cytotoxic effect, high porosity
SLS	ZrO_2, Al_2O_3, Al_2O_3-SiO_2, TiC-Al_2O_3, ZrB_2, SiC, (HA-TCP), (HA-PC)	$BaTiO_3$, PZT	Rough surface, low geometrical accuracy, macro-porous structure
SLA	Al_2O_3, Al_2O_3-SiO_2, Al_2O_3-ZrO_2, SiO_2, TiO_2, SiC, $ZrSiO_4$	SiCN, PZT, Fe_2O_3, $Fe(C_2O_4)$, $Bi(V_xNb_{1-x})O_4$, SiCN	High performance, versatile functionalities
FFF	Al_2O_3, ZrB_2, SiC, Si_3N_4, ZrO_2, WC-ZrO_2, ZrC, Al_2O_3-ZrO_2	$BaTiO_3$, PZT, PMN, $LiFePO_4$, $Li_4Ti_5O_{12}$, $BaZrO_3$, $SrTiO_3$, ZnO, TiO_2	
LOM	ZrO_2, Al_2O_3, SiC/C, Si_3N_4, SiO_2	SiO_2-Al_2O_3-RO-glass, LZSA, PZT	lightweight fabricated part
SLM	YSZ, Al_2O_3-$GdAlO_3$-ZrO_2		Limited to manufacture small objects, very fine resolution
LENS	ZrB_2, Al_2O_3-YAG-ZrO_2		
IJP	Si_3N_4 (aqueous ink)		Desirable mechanical strength
DLP	Al_2O_3	Bioactive glass	Excellent relative density, desirable mechanical strength

PZT: Lead zirconium titanate; **LSMO**: Lanthanum strontium manganite; **YBCO**: Yttrium barium copper oxide; **RO**: Alkaline oxide (R: Alkali); **PMN**: Lead magnesium niobate; **YSZ**: Yttria-stabilised Zirconia; **HA-TCP**: Hydroxyapatite–tricalcium phosphate; **HA-PC**: Hydroxyapatite polycarbonate; LOM: Laminated object manufacturing; **LENS**: Laser Engineered Net Shaping; **FFF**: Fused Filament Fabrication; **DLP**: Digital Light Processing; **IJP**: Inkjet Printing

parts by optimizing process parameters so that the mechanical characteristics of samples are comparable to conventionally manufactured ceramics [41]. Nevertheless, very small defects can grow after printing and during the heat treatment process of ceramics, significantly affecting final properties. Therefore, it is necessary to develop effective techniques to control these defects. Table 3 compares the mechanical properties of high-performance ceramic materials generated by conventional and AM technologies [42].

So far, several studies have been conducted on designing ceramics with enhanced mechanical characteristics. Nevertheless, there are many limitations in the structural complexity of ceramics, especially in high-performance sectors such as aerospace, defence, electronics, and

Table 3
Mechanical features of HPC materials generated by conventional and AM processes.

HCP Materials	Flexural Strength (MPa)		Fracture Toughness ($MPa*m^{1/2}$)		Ref
	Conventional	AM	Conventional	AM	
Al_2O_3	310 – 379	427	4.5	-	[43]
ZrO_2	900	731	13.0	-	[44]
B_4C	200	58 – 67	4.0	3.5	[45]
SiSiC	350	123 – 150	4.0	-	[26]
Si_3N_4	679 – 896	597 – 613	5.0 – 8.0	4.0 – 7.0	[46]

energy [47,48]. Production of complex ceramics by conventional forming methods such as dry pressing, isostatic pressing, etc., faces several challenges, notably in the mould manufacturing process, which is costly and time-consuming [49,50]. Besides, their hardness and brittleness made machining ceramic objects very challenging. Therefore, lots of attention has been paid to AM technologies to produce complex shape ceramic components by overcoming their inherent limitations, such as machinability and formability, by pre-processing raw materials before printing [39]. Despite the accurate printing, this technique is faced with challenges, including [25,51]:

- The limited available materials.
- Layer-by-layer appearance.

- Low build rate.
- Limitations in the part size.
- Fair printing quality due to the presence of defects leading to unstable bonding between lamination surfaces and non-uniformity of materials.

In order to comprehensively overview the correlation between the AM processes and materials characteristics, in the next section, all the available ceramic AM processes are described, and the achieved properties are discussed in detail.

4. Powder-based deposition technique

In powder-based ceramic AM technologies, a powder bed including loose ceramic particles as feedstock material is processed in each layer. These ceramic particles are bonded together using a spread of liquid binders or powder fusion through thermal energy provided by a laser beam. In the following section, different types of powder-based AM techniques are described, namely, binder jetting, selective laser sintering, and laser powder bed fusion.

4.1. Powder bed fusion (PBF)

As discussed earlier, PBF is classified into single and multiple steps based on selectively fused powder particles on the powder bed [52,53]. Table 4 provides the binding and powder deposition mechanisms for single- and multiple-step PBF [22].

In ceramic processing, three main powder bed-based technologies are typically applied: BJT, SLS, and L-PBF. Depending on the particle size, the thickness of the powder layer can be in the range of 20–200 μm. The fusion process or binding mechanism mainly includes four types: solid-state sintering, chemically induced binding, liquid-phase sintering (partial melting), and full-state melting [54].

4.1.1. Selective laser sintering (SLS)

SLS process, which is a PBF technology, was developed in the 1980 s as a manufacturing technique to produce near-net shape polymeric parts by fusing or sintering successive layers of powdered material using a carbon dioxide (CO_2) laser. In this process, the powder particles lie loosely in a bed, and a roller distributes the powder over the surface of a build chamber. Before sintering the particles, they are heated just under their melting point by tracing cross-sectional slices from the virtually designed CAD model. The fabrication piston is lowered by one layer thickness each time a layer is processed and bonds to the previous layer. These steps are repeated until the completion of the part. After the fabrication of the object, a post-processing step, such as sanding with high-pressure air and/or cleaning with pressurized air, is needed. In this technology, it is well documented that various cheap and environmentally materials can be processed to produce fully dense parts with very high accuracy.

However, it is reported that the SLS process can also be used for building crack-free dense ceramic components with extremely high melting points, low or no plasticity and poor thermal shock resistance compared to polymers and metals [55]. Fig. 4 demonstrates various stages in the SLS processing of ceramic parts, from the feedstock material to the final dense part [51]. As seen in this process chain, to increase the density of the as-built parts to achieve the desired strength and little geometrical distortion, some post-processing, such as infiltration or isostatic pressing, should be considered in assistance with SLS [56].

Feedstock preparation is one of the key steps in the processability of ceramics through the SLS process. In contrast to the L-PBF process, where the consolidation occurs through the melting and solidification, in the SLS process, the sintering of particles governs the densification. Nevertheless, fabrication of ceramic parts using the SLS approach is still challenging due to their high melting point (e.g. alumina and zirconia have a melting point of 2045 ℃ and 2715 ℃, respectively). Therefore, a common way to overcome this challenge is to coat or mix the matrix powder with materials having lower melting points, such as polymers [57–59]. Shi et al. [55,60,61] successfully prepared the Al_2O_3/Epoxy resin (E06), ZrO_2/E06, and SiC/E12 composites by the mechanical mixing method combined with the SLS process. They observed that composite powders prepared by mechanical mixing possess an excellent flowability and uniform composition. Shahzad et al. manufactured Al_2O_3–PA complex composite microspheres parts with an enhanced density up to 94% of the theoretical value using SLS assisted by Quasi-Isostatic Pressing (QIP) at elevated temperatures [62]. Moreover, they obtained Al_2O_3–PP (polypropylene) composite spheres after post-processing through pressure infiltration with 30 vol% Al_2O_3 powder-based ethanol suspension and Warm Isostatic Pressing (WIP, at 135 °C and 64 MPa) [63]. They reported that the green density increased from 34% to 83%, and the final density incremented from 64% to 88%. In the same method, the density of 3 mol% Y_2O_3-stabilised ZrO_2 (3YSZ) parts increased up to 92% of the theoretical density by SLS combined with warm isostatic pressing even though it caused a large linear shrinkage of $>$ 35% [64]. Fig. 5 displays scanning electron micrographs (SEM) of the as-printed SLS and WIPed SLS composites. The SLS material showed a non-homogenous microstructure consisting of joined starting powder micro-spheres. Nevertheless, the samples included the inter-agglomerate voids due to a limited or lack of plastic flow during the SLS process (Fig. 5a). Whereas after WIPing, samples showed a more homogeneous microstructure along with enhanced density owing to plastic deformation (Fig. 5b and c).

The microstructures of a sintered ZrO_2 are demonstrated in Fig. 6. The sintered SLS samples had a low density of 32%, and the micrograph of the sample still showed the layered structure (Fig. 6a). During sintering, the microspheres were fully densified; therefore, the intergranular voids in the deposited microsphere layers were the source of the porosity (Fig. 6b). As can be observed in Fig. 6c, the microstructure of sintered Pressure Infiltrated (PI) ZrO_2 was more homogenous with a higher density. Although a large crack was observed in the center of the sintered WIPed parts, the large intergranular pores were removed with a residual porosity of ~5 μm (Fig. 6e and f). The formation of this crack can be attributed to the high amount of shrinkage during WIPing, as sintered ZrO_2 samples exhibited a linear shrinkage of ~48% and 52% in the (X/Y) direction and building direction, respectively. The combined PI and WIPed samples showed a similar sintered microstructure as for WIPed samples (Fig. 6g and h), but without forming a large crack.

Generally, the SLS of ceramic parts could be obtained mainly by two methods, i.e., the direct SLS and the indirect SLS. The forming process is complicated in the direct SLS owing to the poor thermal shock resistance of ceramic materials. Furthermore, the sintered parts have approximately low density and poor mechanical properties [65,66]. Slocombe et al. [67] produced complex-shaped TiC–Al_2O_3 ceramics via the direct SLS combined with self-propagating high-temperature synthesis to overcome the defect of a low density of direct sintered samples. Nevertheless, it is difficult to avoid easy cracking in the direct SLS-manufactured parts because of the thermal stresses during the sintering process that cause poor mechanical features in the final products [55]. Thus, the indirect SLS method could be appropriate for forming crack-free specimens by sintering low-melting polymer binders in compositions. This step is followed by a binder removal process with a slow heating rate and then furnace sintering to increase the final density and avoid crack formation [55,68]. Different organic and inorganic binders have been developed so far for the fabrication of ceramic parts using the SLS process (Table 5) [23]. The inorganic binders used in this technique include long-chain fatty acids (e.g., stearic acid), waxes, thermosets, and thermoplastics [58]. Moreover, some studies used a combination of binders like a thermoset/semi-crystalline PA-11 or nylon 11 to produce graphite [69] and a wax/amorphous thermoplastic PMMA to fabricate the composite ceramic Al_2O_3-ZrO_2-TiC [70].

Despite the disadvantages of the SLS method to print ceramic parts, such as low resolution, poor surface finish, and high porosity content, this process is already adopted in various fields [56]. SLS is prevalent in the tomography-assisted fabrication of scaffolds for biomedical purposes [71,72]. There are many bone implants manufactured through the SLS process with the combination of hydroxyapatite with ceramic–polymer/glass mixtures [73], polycarbonate [72], and silica with polyamide [59]. For instance, Tang et al. [55] manufactured porous

Table 4
Binding and powder deposition mechanisms of single and multiple-step PBF.

PBF	Binding mechanism	Powder deposition mechanism
Single-step	Full melting	Conventional, slurry coater, aerosol-assisted spray deposition
	Partial melting	Conventional, slurry coater, slurry sprayer, ring blade, electrophoretic deposition
	Solid-state sintering	Conventional
	Chemically induced binding	Conventional, slurry coater, ring blade
Multiple-step	Partial melting	Conventional, slurry coater
	Gelling	Slurry coater

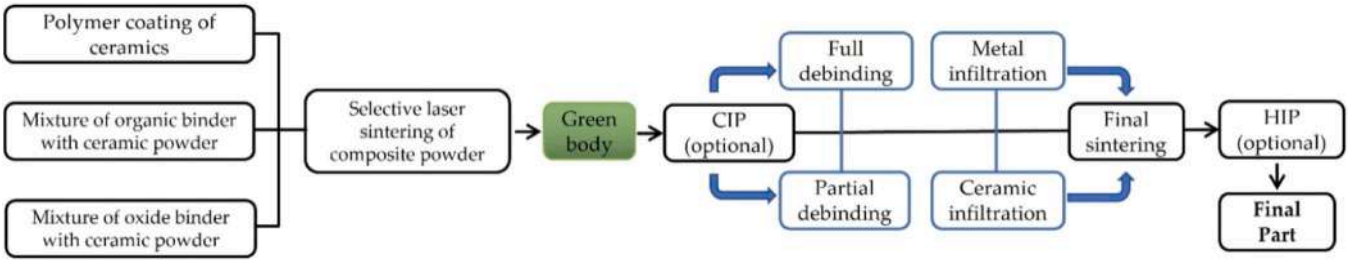

Fig. 4. SLS processing of ceramic parts, CIP: Cold isostatic pressing; HIP: Hot isostatic pressing [51].

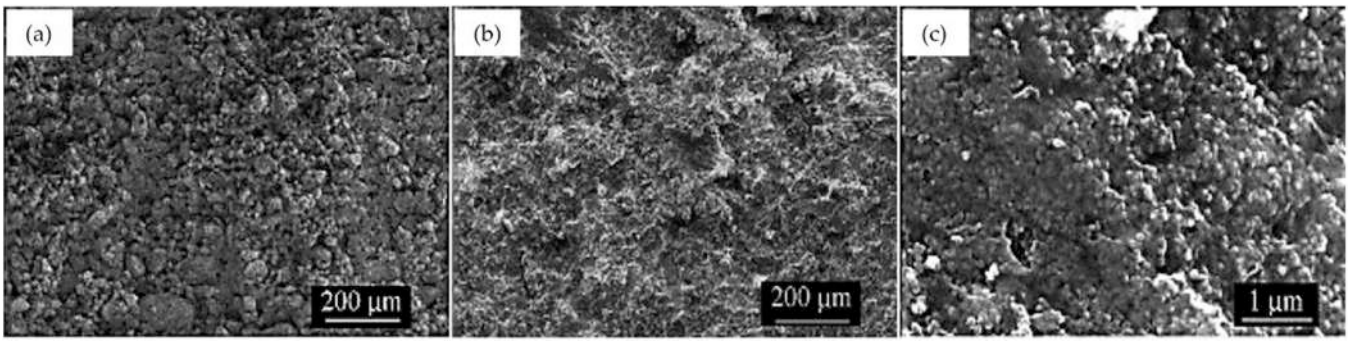

Fig. 5. Scanning electron micrographs of the green samples, (a) manufactured by SLS; (b and c) SLS + WIP [64].

ceramic components with 3D pore structures via the SLS. They fabricated porous cordierite ceramic parts in structures of a straight hole honeycomb and a gyroid cellular lattice with compressive strength and porosity of 8.92 MPa and 62.3%, respectively. Table 6 shows some reported results on the SLS-printed ceramics materials.

4.1.2. Laser powder bed fusion (L-PBF)

Over the past years, applying the L-PBF process to produce complex shape ceramic components attracted lots of attention. This technique is similar to the SLS one in using high-energy laser sources. However, L-PBF is a time-saving process that manufactures the parts by fully melting the powders, using higher energy density of laser sources, and needs no binder or post-sintering process for further consolidation. The L-PBF process is considered as the only 3D printing process to manufacture ready-to-use complex ceramic parts with higher purity, nearly full density, and high strength in a single step and less time. This can be explained by fully melting the powder into the liquid phase, ensuring fast densification instead of heating the powder at a particular point where the particles are partially melted and fused together in the SLS process. Hence, products with lower porosity, superior control over the crystal structure, and excellent final characteristics can be produced via the L-PBF process [56,83].

Nevertheless, the final properties of a ceramic part produced via the L-PBF process depend on several factors, such as feedstock properties, orientation and position of fabrication, and manufacturing parameters. Besides, the physical and chemical properties of the interaction between the material and source of energy and post-processing of the printed part play a significant role in determining the final features. One of the noticeable parameters is the layer thickness, which controls the production time and the part's surface quality. A smaller layer thickness leads to less surface roughness, even though it increases the build time. In contrast, a larger layer thickness may cause a significant stair-step effect on the component's surface [56].

Despite showing great potential, L-PBF of ceramics is complicated compared to metallic materials owing to some inherent problems related to the process; hence, their applications are still very limited. This limitation can be attributed to the formation of defects like porosity, rough surface finishes, low accuracy of dimension, and densification of the final product. These defects lead to the hard achievement of the isotropic ceramic body. In the L-PBF process, laser processing parameters are crucial factors influencing the quality of fabricated parts. The balling effect can happen when exposed to insufficient energy input, while excessive energy would result in powder spattering [84]. Nonetheless, direct melting consists of a high-temperature interaction between laser and powder during a short period, leading to large gradients of temperature within small volumes of material and thermal stress termed as the drastic heating and cooling rates upon each laser scan [85]. Since ceramics have limited thermal shock resistance; thus, cracks and distortions form in the sintered parts because of thermal stress [86,87]. For instance, Shishkovsky et al. [88] processed the ZrO_2 parts using the L-PBF process and found cracks and large open pores in the final parts. In another work, Mercelis et al. [85] experimentally studied the origin of the residual stresses in the L-PBF manufactured products. They developed a simple theoretical model to predict the existence of residual stress. They also found that the scanning strategy has a noticeable influence on the level of residual stresses. In addition, difficulty in keeping homogenous quality during printing and incomplete melting due to the short interaction time during laser scanning resulted in poor surface quality and large residual porosity in the as-built samples [89].

The alumina parts with only 85% relative density were produced by Deckers et al. [90] using the L-PBF process. The L-PBF of ZrO_2–Y_2O_3 powder was carried out by Bertrand et al. [91] with a final density of only 56%, which did not improve even after using heat treatment in a conventional furnace. However, the problems were mitigated in an Al_2O_3–ZrO_2 system by using bed preheating at above 1500 °C, employing a second laser before scanning across the bed, and melting in the defined areas of each layer [92]. It is well documented that a powder bed preheating with precise control of powder morphology can result in nearly fully dense parts. Spodumene glass-ceramic was produced by Gan et al. [93] using the L-PBF process. The spodumene-Al_2O_3 samples were classified into three different layer thicknesses, including 50 µm (LT50 series samples), 100 µm (LT100 series samples), and 150 µm (LT150 series samples), and at three different heating conditions, including as-printed, 850 °C, and 950 °C. MicroCT images of the produced

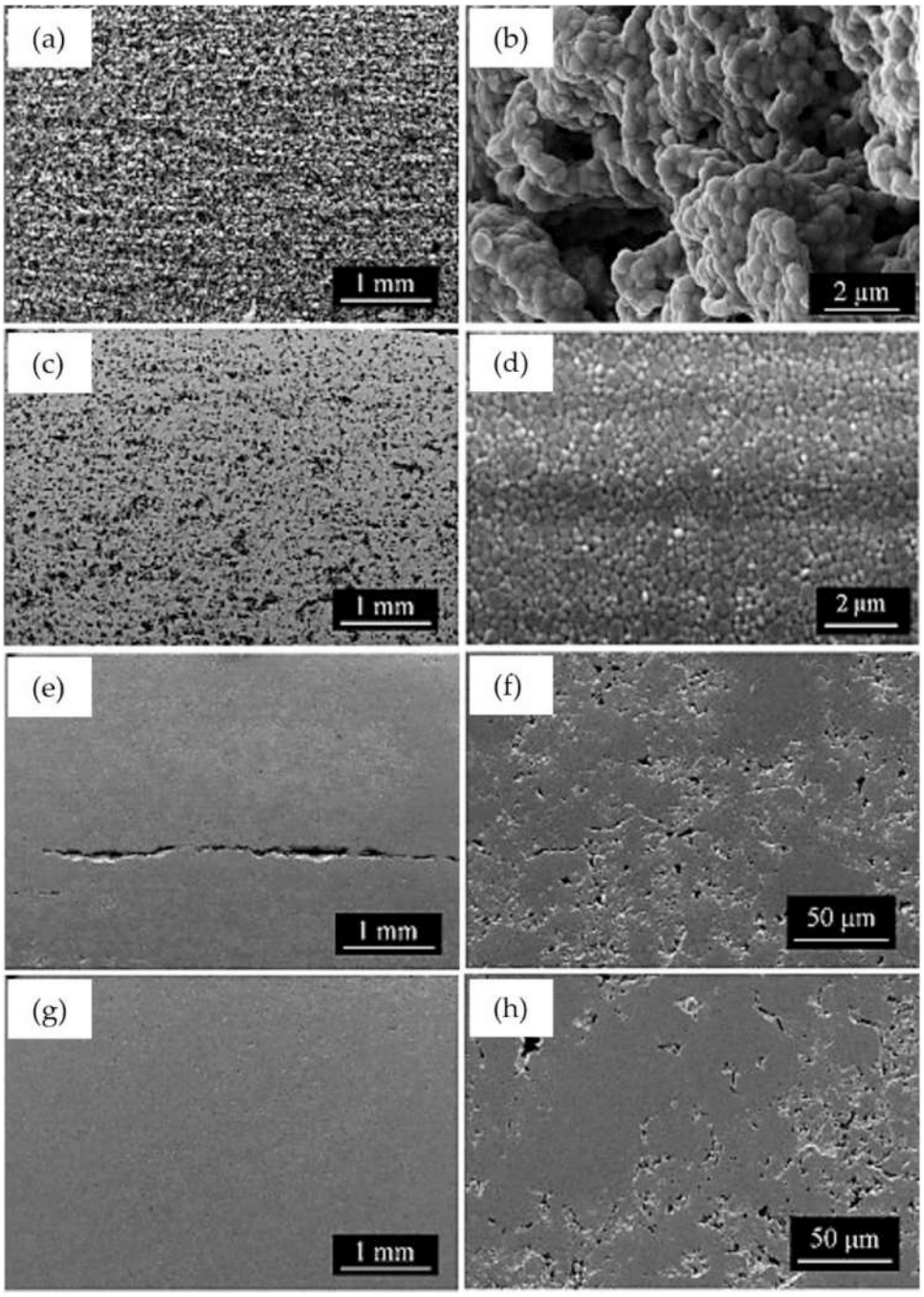

Fig. 6. Scanning electron micrographs of cross-sectioned sintered samples, (a and b) manufactured by SLS; (c) SLS + PI; (e and f) SLS + WIP; and (d, g, and h) SLS + PI + WIP [64].

samples at 950 °C with various layer thicknesses are displayed in (Fig. 7a-c). As can be seen, the pore size was reduced with the increase in layer thickness. Moreover, most of the closed pores were mainly formed near the external surfaces. Besides, the total porosity percentage of the glass-ceramic samples declined by increasing the layer thickness (Fig. 7d). These results presented negative correlations between layer thickness, pore sizes, and porosity content. In terms of mechanical characteristics, it is reported that the strength of the as-printed samples was initially reduced by increasing layer thickness (Fig. 7e). Then by heating the specimens at 850 °C, the printed samples at all three-layer thicknesses presented similar strengths of 2.18 MPa, 2.10 MPa, and 2.04 MPa for the LT50T850, LT100T850, and LT150T850, respectively. Nonetheless, higher strengths were obtained by heating the samples at 950 °C, especially for those with a layer thickness of 100 μm, increased up to 4.33 MPa.

Recently, Shen et al. [94] fabricated $Al_2O_3/GdAlO_3$ binary eutectic ceramics at different scanning rates (4 −60 mm/min) at a laser power of 200 W. It was revealed that the hardness gradually increased by increasing the scanning rate, whereas the fracture toughness first enhanced and then slowly declined (Fig. 8). The maximum average hardness and fracture toughness were obtained at the laser power of 200 W and scanning rate of 10 mm/min, with the values of 17.1 ± 0.2 GPa and 4.5 ± 0.1 MPa• $m^{1/2}$, respectively. Compared to prepared $Al_2O_3/GdAlO_3$ by floating zone melting [95], the L-PBF samples presented better mechanical behaviour, with an average hardness of 16.7 GPa and a fracture toughness of 4.08 MPa $m^{1/2}$.

Table 5
Organic and inorganic binders to produce various ceramic parts using a conventional SLS technique.

Inorganic binder	Organic binder			
	Acid	Wax	Thermoset	Thermoplastic
• HBO_2 (Al_2O_3-B_2O_3, Al_2O_3-glass-B_2O_3)	• Stearic acid (ZrB_2, Al_2O_3)	• Carnauba wax (Al_2O_3) • Unspecified (Al_2O_3-ZrO_2-TiC)	• Phenolic resin (Graphite, SiC) • Epoxy resin (K_2O-Al_2O_3-SiO_2)	• Nylon-12, polypropylene, polystyrene, PMMA (Al_2O_3) • PMMA (Al_2O_3-ZrO_2-TiC) • Acrylic (apatite-mullite) • Nylon 11 (Graphite) • Polypropylene (ZrO_2)

Table 6
Characteristics of manufactured ceramic parts by selective laser sintering.

Materials	Post-processing	Characteristics of printed parts	Ref
RB-SiC	-	• Flexural strength (MPa): 162 • Modulus (GPa): 285	[74]
	CIP+LSI	• Flexural strength (MPa): 348	[75]
	LSI	• Flexural strength (MPa): ~360	[76]
ZrO_2–PP	PI/debinding/ sintering	• Sintered density (%): 54 • Linear shrinkage (%): 30 (X and Y direction), 31% (Z)	[64]
	WIPing/ debinding/ sintering	• Relative density (%): 92 • Linear shrinkage (%): 48 (X and Y direction), 52% (Z)	
	PI/WIPing/ debinding/sintering	• Relative density (%): 85 • Linear shrinkage (%): 38 (X and Y direction), 42% (Z)	
SiC	PIP	• Relative density (%): 80.9 • Flexural strength (MPa): 220	[77]
Al_2O_3	Polymer debinding/ sintering	• Relative density (%): 85–92	[62]
	QIP	• Relative density (%): 94.1	
CF-SiC	LSI	• Flexural strength (MPa): 239	[78]
Al_2O_3	-	• Compressive strength (MPa): 4 • Porosity: 65% • Open pore size: 38.3 μm	[79]
Mullite	Debinding	• Compressive strength (MPa): 2.08 • Thermal conductivity (W/(m·K)): 0.18	[80]
Si_3N_4	-	• Compressive strength (MPa): 432 • Vickers hardness (GPa): 12	[81]
Yttria	-	• Porosity (%): 41 • Young's modulus (GPA): 2	[82]
	Post-SLS heat treatment	• Porosity (%): 31 • Young's modulus (GPA): 12	

CF: Carbon fiber; LSI: Liquid silicon infiltration; PIP: Polymer precursor infiltration; PI: Pressure infiltration; QIP: Quasi isostatic pressing.

Further developments introduced some modified 3D printing methods derived from the L-PBF process with the ability to manufacture complex shape ceramic parts, such as slurry-based L-PBF [96,97]. Other forms of powder packing have been developed instead of dry powder deposition to raise the sintered density and prevent crack formation in the L-PBF ceramics. The slurry form offers the benefits of a more homogeneous and highly packed nature. Gahler et al. [97] used stable slurries loaded with an alumina-silica powder mixture (up to 63 vol%) and water with high fluidity. Before drying, the materials are deposited layer by layer through a doctor blade system, as in tape casting. Due to the formation of liquid-phase SiO_2, the prepared products possessed a smooth surface with a high density of up to 92%. The properties of fabricated ceramics products using the L-PBF process are presented in Table 7 [98].

4.2. Binder jetting (BJT)

BJT which is considered an indirect 3D-printing, is defined by ISO/ASTM 52,900:2015 as an "AM process in which a liquid bonding agent is selectively deposited to join powder materials" [52]. In this process, a powder roller spreads a thin layer of powder on the building platform to form a powder bed. Then, the printhead applies an organic binder solution dropwise onto the selected regions of the powder bed surface defined by the CAD model. The binder helps the powder particles in the chosen areas to join together. The first layer is built in this way, and afterwards, the build platform is lowered by a defined height, and a new layer of powder is spread over the first layer. These steps are repeated in the same manner until the whole part is completed. The obtained part, referred to as the green part, then should be subjected to the post-processing steps, such as curing, debinding, and sintering. These post processings should be implemented in order to perform further consolidation and achieve the maximum possible density in the final product. Depending on the type of powder and system, various kinds of binders can be used, including carbohydrates (dextrin, maltodextrin, starch, etc.), polymers (polyvinyl alcohol, polyethylene glycol, polyvinylpyrrolidone, etc.), colloidal silica, phosphoric acid, isopropanol, acrylic acid, commercial Zp-7, commercial schelofix, and phenolic binder, etc. [104,105].

In particular, this technology is extensively used to produce ceramic components in various applications such as structural, biomedical, optical, and electronics [105–107]. Alumina was the first ceramic investigated by the inventors of binder jetting [108,109]. For instance, Mariani et al. [110] produced α-Al_2O_3 components by binder jetting technology. They reported that the fabricated objects possess high green relative density values of 61.2% and the highest final sintered density was 75.4% after the thermal treatment at 1750 ℃. Despite the relatively large residual internal porosity (~40%), materials presented good mechanical properties, including flexural strength and Vickers hardness of 56.1 MPa and 1.95 GPa, respectively. Kunchala et al. [111] assessed the effect of adding nanoparticle densifiers on printing liquid's manufacturability, density, porosity, and compressive strength of BJT-prepared ceramics. They have found that, by increasing the amount of densifier up to 15 wt%, the samples' relative density and compressive strength enhanced up to ~30% and 641 kPa, respectively. Manotham et al. [112] studied the shrinkage, density, porosity, microstructures, mechanical properties, and printing patterns of alumina samples. It was revealed that the full printing sample showed the shrinkage, density, flexural strength, and compressive strength of 11%, 39%, 1.04 MPa, and 1.78 MPa, respectively. They succeeded to minimize the crack formation in the manufacturing the large-sized part (60 mm in diameter and 30 mm in height) through the medium of checkerboard-patterned printing with 50% of the binder's quantity at core areas. Gaytan et al. [113] also used BJT technology to fabricate barium titanate (BTO) samples. After the sintering step, the final relative densities were 41.4%, 60.6%, and 65.2% for the sintered samples at 1260 °C, 1330 °C, and 1400 °C, respectively. Fig. 9(a and b) show powder agglomeration and lack of sintering in BTO samples after sintering at 1260 °C with an average grain size of 91 μm. After sintering at 1330 °C, the samples had an average grain size of 21 μm and presented irregular grain growth, demonstrating that sintering was still in progress. In addition, the space between grown grains was observed, and pores were irregular and interconnected at various dimensional planes (Fig. 9(c and d)). The sintered specimens at 1400 °C showed uniform grain growth with an average grain size of 44 μm (Fig. 9(e and f)). Similar to sintered samples at 1330 °C, there are pores and interconnected porosity in the samples after sintering at 1400 °C. Furthermore, the fabricated $BaTiO_3$ samples showed piezoelectric properties with a piezoelectric coefficient $d33$ which improved by increasing the sintering temperatures. It can be attributed to the improvement of density and grain size reduction. The piezoelectric properties of these samples make them an ideal candidate for sensor applications that can be utilized in power plants, gas turbines,

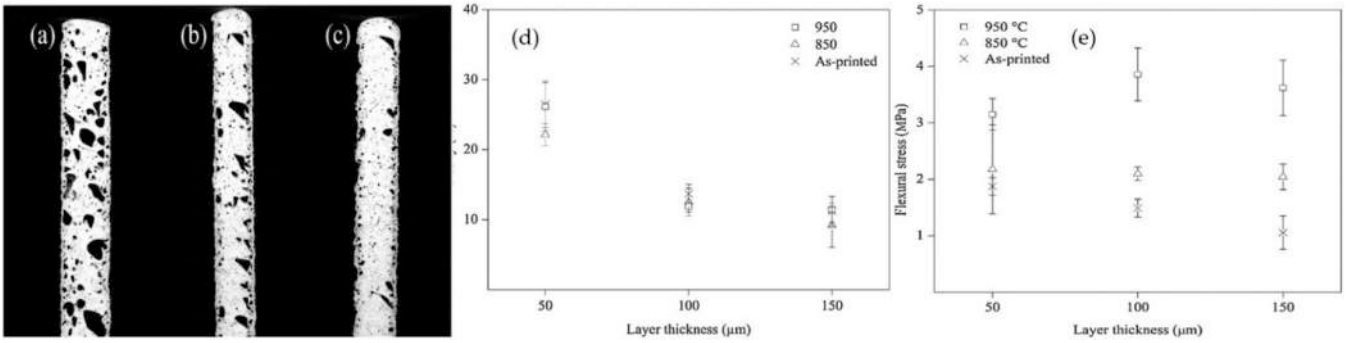

Fig. 7. MicroCT image of, (a) LT50T950; (b) LT100T950; (c) LT150T950; (d) percentage of porosity; (e) flexural strength of the L-PBF-printed spodumene-Al_2O_3 samples at different temperatures [93].

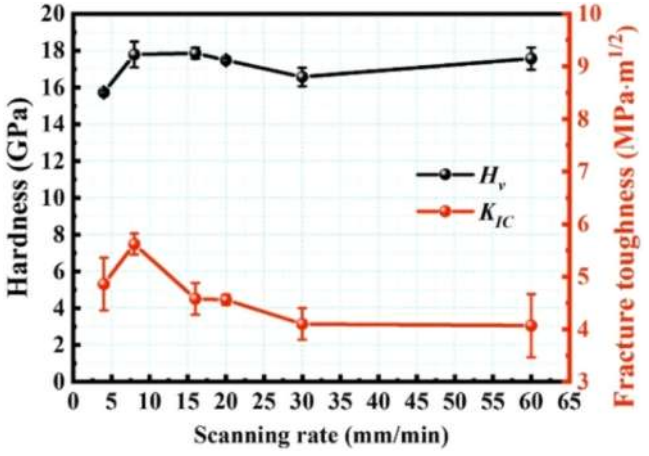

Fig. 8. Hardness and fracture toughness of the L-PBF Al_2O_3/$GdAlO_3$ ceramics at various scanning rates of 4–60 mm/min and the laser power of 200 W [94].

and oxy-fuel combustion, due to the ability to monitor pressure.

The BJT-manufactured ceramic materials and their applications are listed in Table 8.

Despite pure compound materials, numerous studies utilized composites to develop various characteristics. However, these materials can present improved features but sometimes lead to weaknesses in biocompatibility properties [134]. Although the produced ceramic part using BJT possesses high porosity, they offer some benefits like no need for support structures, a minimal amount of sacrificial materials, and high scalability [105]. Table 9 summarizes some reported works on BJT-manufactured ceramic products.

4.3. Directed energy deposition (DED)

Laser-based DED process, also known as Laser cladding (LC), Laser Energy Net Shaping (LENS), or Laser Metal Deposition (LMD), was firstly commercialized in the mid-1990 [139,140]. In this technique, feedstock materials delivered directly in a molten pool generated by a heat source like electron beam, laser or plasma arc [141,142]. In the DED process, ceramic materials with the melting point up to 3000 °C can be melted using a high-power laser beam. During the deposition, the already deposited layers were exposed to repeated thermal cycles and very high cooling rates. This thermal history in the as-built parts depends strongly on the process parameters [143,144]. As a matter of fact, these process parameters that can change the thermal history of components have remarkable influence on the microstructure, physical and mechanical characteristics of as-deposited materials[145,146]. These parameters are classified into three main categories, namely, system (specifications) dependent, feedstock (powder, in this example) dependent, and process (deposition) variables dependent (Table 10) [139].

So far, several efforts have been undertaken on the fabrication of different materials using the DED method, such as steels, titanium alloys, cobalt alloys, nickel alloys, aluminum alloys, high-entropy alloys, intermetallics, shape memory alloys (SMAs), composites, and functionally graded materials (FGMs)[144,147,148]. Besides, this technique has also been employed to build ceramic oxide parts such as alumina, zirconia, eutectic ceramic composites, zirconia-alumina ceramics, alumina/aluminum titanate ceramics, mullite ceramics, and magnesium aluminate spinel ceramics [149].

Recently, four different Al_2O_3-ZrO_2 functionally graded ceramic

Table 7
Process parameters of relevant publications through the L-PBF method.

Materials	Process parameters	Characteristics	Ref
(0.5 wt%)B_4C/Ti (1.0 wt%)B_4C/Ti	Laser Power (W): 95–260 Laser Spot Size (μm): 70 Scan speed (mm/s): 330–900 Hatch spacing (μm): 60 Layer thickness (μm): 40	• Nanohardness (GPa): 5.46 • Compressive strength (MPa): 1535 • Nanohardness (GPa): 6.11 • Compressive strength (MPa): 1747	[99]
Ti/(TiC+TiN)	Laser power (W): 250 Hatch spacing (μm): 50 Layer thickness (μm): 50 Scan speed (mm/s): 1000	• COF: 0.792 • Wear rate: 1.0×10^{-4} $mm^3/N^{-1}m^{-1}$	[100]
TiC/Ti	Spot size (μm): 70 Laser power (W): 90 Scan speed (mm/s): 300 Hatch spacing (μm): 50 Layer thickness (μm): 50	• Relative density (%): 98.3 • Microhardness ($HV_{0.2}$): 577 • Coefficient of friction: 0.19 • Wear rate: 2.3 × 10–16 m^3 $N^{-1}m^{-1}$ lap^{-1}	[101]
Al_2O_3/$GdAlO_3$/ZrO_2	Scan speed:12 mm/min Scan speed: 48 mm/min	• Relative density (%): 98.7 • Relative density (%):95.7	[102]
YSZ	Power (W): 100 maximum Wavelength (nm): 1060–1100 Spot size (μm): 34 Hatch spacing (μm): 80 Layer thickness (μm): 150	• Relative density (%): 88 • Microhardness (HV_{500}): 1.209 ± 262	[103]

COF: Coefficient of friction

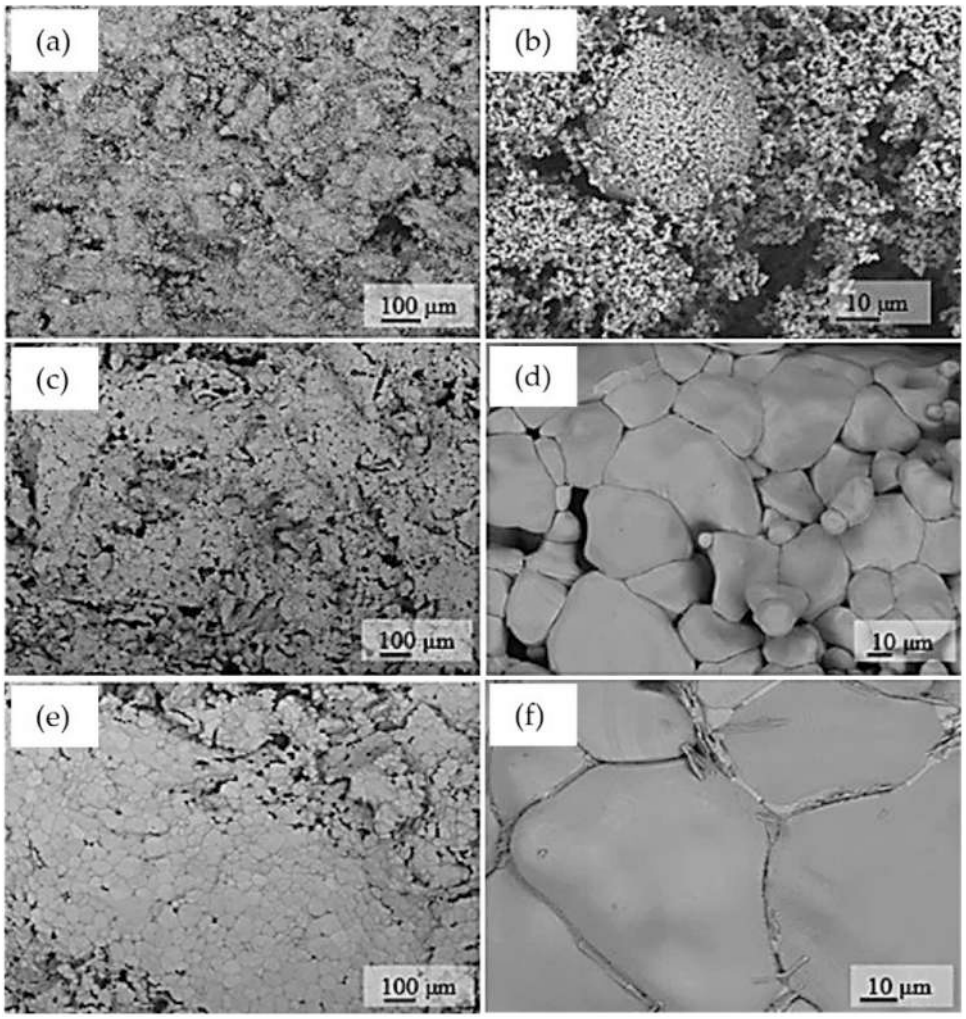

Fig. 9. SEM images of barium titanate samples after sintering at (a and b) 1260 °C; (c and d) 1330 °C; (e and f) 1400 °C for 4 h [113].

Table 8
Obtained ceramics by binder jetting and their applications.

Ceramics parts	Applications	Ref
Oxides, Carbides, and Nitrides such as Al_2O_3, AlN, Al_2O_3-Cu-Cu_2O, Al_2O_3-ZrO_2, B_4C-SiC, Sic-Si_3N_4-SiON, SiSiC, TiC, WC-Co, CaO-$CaZrO_3$, Al- Al_2O_3, Si_3N_4, TiO_2	Structural ceramics	[111, 114–119]
Calcium phosphate family (calcium polyphosphate, dicalcium phosphate, tricalcium phosphate), hydroxyapatite, Bioactive glass	Orthopaedics	[120–124]
Al_2O_3, Si_3N_4, $BaTiO_3$	Electronics functional ceramics	[104,125, 126]
Al_2O_3 +dental glass, Al_2O_3 +dental porcelain,	Dental part	[127,128]
SiO_2	Optical	[129]
$Ca_5(PO_4)_3(OH)$, Si/SiC, Bioactive glass, $Ca_3(PO_4)_2$	Bone tissue	[121, 130–133]

(FGC) samples were manufactured through the DED method [150]. It was found that the bonding strength was noticeably improved, and interface fracture of FGC samples altered to transgranular fracture. Moreover, the samples' microhardness and flexural strength reached 25 GPa and a maximum of 160.19 MPa, respectively. Highly dense (≥98%) Al_2O_3-YAG-ZrO_2 (AYZ) samples were successfully fabricated by Fan et al. [151] using the LENS technique. The LENSed AYZ specimens presented refined eutectic microstructures and almost isotropic features. Fig. 10(a and b) demonstrate the measured nano-hardness (H) and elastic modulus (*E*) of the sample as a function of the maximum load. As can be seen in these graphs there was no significant difference between these two section properties, and it implies that the as-built AYZ specimens had isotropic properties.

Mishra et al. [152] assessed the effect of various processing parameters such as laser power, thermo-physical properties, and scanning strategy, on the characteristics of the as-built Al_2O_3 samples produced via the DED process. They reported that alumina with a 3D structure could be prepared on Al_2O_3 and Ti–6Al–4 V substrates using laser power ~225 and ~300 W, respectively. The experimental results revealed that the as-built bulk alumina structures on a Ti–6Al–4 V substrate presented a lower porosity and crack content with a higher relative density of 85%. In contrast, the manufactured bulk alumina on the Al_2O_3 substrate showed a lower relative density of 70%. Moreover, they evaluated the effect of the scanning strategy on the shape, size, and distribution of pores that formed during the DED process. Niu et al. [153] investigated the microstructure, flexural and compressive strength of DED-manufactured alumina ceramics. The dominated phase in those samples with a relative density of 99.5% was high-temperature-stable α-Al_2O_3. They reported the average flexural and compressive strength of 210 MPa and 395 MPa, respectively, for the as-deposited alumina sample (Fig. 11). The fabricated samples had the maximum flexural and compressive strength of 350 MPa and 618 MPa, respectively. These results were comparable with prepared samples from the traditional sintering method with the maximum flexural strength and compressive

Table 9
Summary of the reported studies on binder jetting-manufactured ceramics parts.

Materials/ Test method	Post-processing	Characteristics	Ref
SiSic/ Weibull strength	LSI	• Weibull strength (MPa): 358–380 • Relative density (%):75–85	[118]
SiC/4-point flexural strength	CVI, CVD	• Weibull strength (MPa): ~135 • Relative density (%):85–87	[135]
$BaTiO_3$	Sintering (1260 ℃)	• Relative density (%): 41.4	[113]
	Sintering (1330 ℃)	• Relative density (%): 60.6	
	Sintering (1400 ℃)	• Relative density (%): 65.2	
3Y-TZP/3-point bending	Sintering (1400 ℃)	• Relative density (%): 86.8 • Average strength (σm) (MPa): 438	[136]
SiC-SiC/ 3-point flexural strength	CVI	• Weibull strength (MPa): ~ 200 • Relative density (%): 84 • Modulus (GPa): 458	[137]
3Y-TZP/3-point bending	Sintering	• Relative density (%): 65.1 • Average strength (σm) (MPa): 81	[138]
Al_2O_3/ Compression	Sintering (2 h)	• Compressive strength: 71.79 MPa • Young's modulus: 31.25 ± 8.43 GPa • Hardness: 240 ± 66 MPa	[125]
	Sintering (16 h)	• Compressive strength: 131.86 MPa • Young's modulus: 54.14 ± 14.54 GPa • Hardness: 1.51 ± 0.0967 MPa	

CVD: Chemical vapor deposition; LSI: Liquid silicon infiltration; CVI: Chemical vapor infiltration

Table 10
Directed energy deposition parameters.

System specifications	Feedstock parameters	Deposition variables
• Max. laser power • Laser wavelength • Laser spot size • Laser type (pulse duty cycle and pulse frequency)	• Material properties • Power porosity/ size • Power morphology • Power flowability/ reflectivity • Power impurity pick-up	• Laser scan speed • Laser power • Hatch spacing • Layer thickness • Working distance • Substrate materials • Scanning methodology • O_2 and H_2O content in the chamber

strength of 350 MPa and 625 MPa, respectively.

Table 11 shows the characteristics of various DED-manufactured ceramic parts.

DED has critical advantages over the PBF technique from materials design to applications: multi-material structures, coating, repairing, alloy design, and functionally gradient structure [139,165]. The porosities in the PBF process are more critical than in the DED process. Whereas, in the DED technique, samples with high density can be obtained by setting the process parameters with various lasers and several materials. DED enables the production of larger parts with better static and dynamic mechanical properties compared to the PBF techniques. Since larger powder particle sizes are used in the DED process, it offers both cost and safety advantages compared to PBF. Despite these benefits, it has a lower-dimensional resolution, lower powder efficiency/recyclability, and larger surface waviness (principally when printing a mixture of powders) concerning the PBF [139].

However, fast cooling rates and high thermal gradients (thermal conditions) in the DED process can cause some defects such as complex phase transformations and microstructural changes, non-uniform residual stresses, distortions, porosity, and cracking, which finally result in a fair corrosion resistance and mechanical behavior degradation, and premature failure. Besides, it often needs post-fabrication machining to achieve an appropriate surface quality [139,166,167].

5. Bulk solid-based deposition technologies

5.1. Sheet lamination (SHL)

In SHL, thin solid sheets of material are used to build parts layer by layer using additive and subtractive technologies. These layers are bonded together by the employment of heat and pressure with a thermal adhesive coating. A roller delivers the build materials, and then a sheet of material spreads across a movable build platform. Subsequently, a laser cuts the parts based on the designed digital CAD models to a single-layer thickness. After completing the process, the unwanted material can be easily collected from the rectangles. In the SHL process, the scrap material can play as support structures. The bonding between adjacent layers can be carried out when the heated roller compresses the sheets and activates a heat-sensitive adhesion. These steps are repeated until the end of the part production. In the final step, products with high density can be obtained after further removing the binder and high temperatures sintering. In this technique, paper foils are used as materials; so, resulting in products with properties similar to wood [4] and probably have to be moisture-protected by lacquer [168].

The post-processing of SHL parts strongly depends on the nature of each component. To improve the layer bonding for curved SHL parts, maybe it is necessary to undergo a curing process for the adhesive or compression step [40]. Moreover, a waste removal step, a coating step, and an additional downstream heat treatment may be needed. The heat treatment is of special interest for the SHL process of ceramic-based materials. SL ceramic products are built from paper or polymer sheets filled with ceramic particles [169–171]. Therefore, a heat treatment at temperatures below 600 ℃ is required to remove any organic components from these parts. Additionally, the green products are exposed to debinding in an oxygenated atmosphere and less pressure sintering to densify the parts [40]. The residual porosities can be filled by infiltration methods to raise the final products' strength.

Several ceramic materials have been produced via this process, such as monolithic silicon carbide, SiSiC composites, and aluminum nitride [42]. Besides, through the SHL technique it is possible to fabricate a dense ceramic-metal composite [172,173].

Griffin et al. first reported the SHL technique's manufacturing of ceramic in 1994 [174,175] based on tape casting of Al_2O_3 and ZrO_2 green sheets. Thereafter, other structural ceramics such as silicon carbide, Si/silicon carbide composite [176], zirconia and alumina/zirconia composite, titanium carbide/nickel composite [177], glass-ceramic composite [178] and functional ceramics like PZT for functional telescoping actuators [179] and hydroxyapatite for bone implant were successfully manufactured using the SL process.

Moreover, some efforts have been focused on the SHL manufacturing of lightweight ceramic parts based on pre-ceramic papers filled with ceramic powders [170,180]. For instance, Rodrigues et al. [181] produced silicon nitride components with 40% average volume shrinkage and a final relative density of 97% after sintering. Penas et al. [182] investigated the microstructure and mechanical characteristics of SHL-fabricated Si_3N_4, such as Young's modulus, flexural strength, and fracture toughness. They reported that the properties of SHL- Si_3N_4 samples were comparable with conventionally manufactured Si_3N_4 using reaction-bonding, slip casting, and pressure-less sintering. Gomes et al. [178] produced LiO_2–ZrO_2-SiO_2-Al_2O_3 (LZSA) glass-ceramics with high flexural strength at high porosities compared to the same

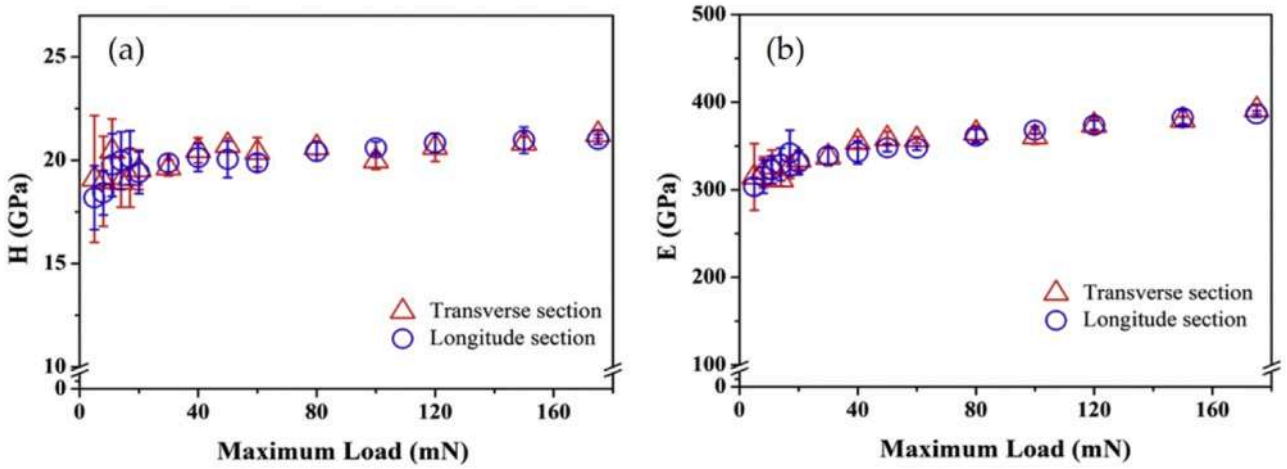

Fig. 10. Mechanical properties of the LENSed AYZ specimens in transverse and longitude sections, (a) Hardness; (b) elastic modulus, as a function of indentation load [151].

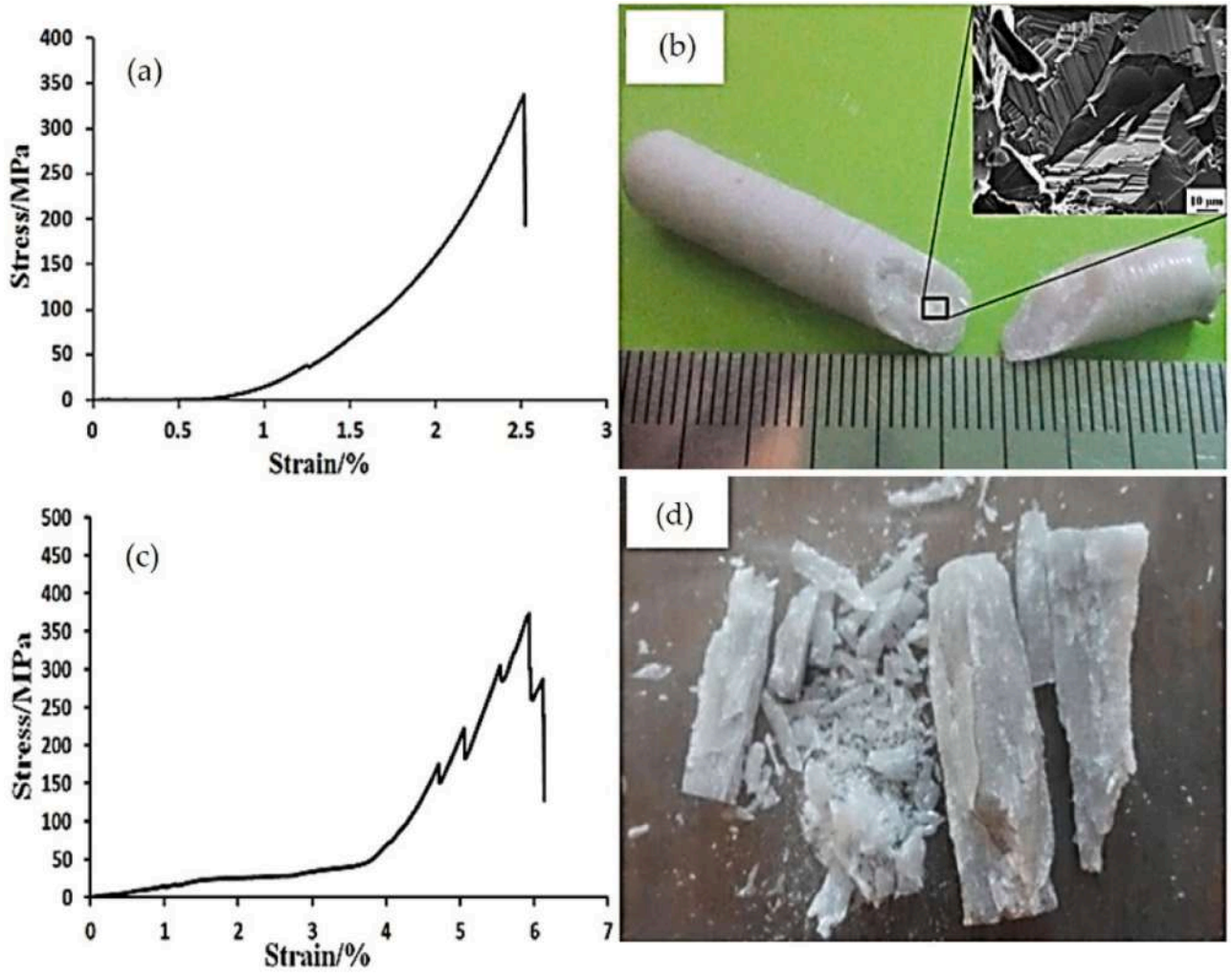

Fig. 11. Flexural strength test, (a) stress-strain curve; (b) fracture sample, Compressive strength test: (c) stress-strain curve; (d) fracture sample [153].

glass-ceramic material produced by traditional methods.

SHL utilization is limited to laminated sheets and the production of parts with rather simple internal geometries [65,178]. SHL offers relatively lower dimensional accuracy than stereolithography, DED, and SLS techniques [183]. It is low-cost and produces large products that are relatively temperature resistant and strong. The elimination of deformation and distortion can also be considered the advantage of this technique due to the low thermal stress induced in the preparation process [184] (Table 12).

Table 11
Characteristics of the as-built ceramic parts produced via the DED technique.

Materials	Porosity/ Cracks	Characteristics	Ref
ZrO_2-Al_2O_3	6.5% /Yes	• Flexural strength (MPa): 208	[154,155]
Al_2O_3-SiO_2, Mullite	2.2% /Yes	• Flexural strength (MPa): 62.8	[156]
- Al_2O_3 - Al_2O_3/Y_2O_3 - Al_2O_3/YSZ	Only for Al_2O_3– YSZ	• Vickers microhardness (GPa): > 14.71	[157]
ZrO_2-Al_2O_3	Yes	• Compressive strength (MPa): 450	[158]
Al_2O_3-TiO_2	1% /No	• Flexural strength (MPa): 212	[159–161]
Yttria stabilized zirconia	1.3% /Yes	• Hardness (GPa): 19.8 • Elastic modulus (GPa): 236.1	[162]
Al_2O_3–$Y_3Al_5O_{12}$ (YAG)	1.4%/-	• Microhardness (GPa): 17.35 • Fracture toughness (MPa $m^{1/2}$): 3.14	[163]
Al_2O_3–ZrO_2 (Y_2O_3)	-	• Microhardness (GPa): 17.15 • Fracture toughness (MPa $m^{1/2}$): 4.79	[164]

Table 12
Mechanical characteristics of manufactured ceramic samples using SLH.

Materials	Characteristics	Ref
Biomorphous SiSiC ceramic (41 vol% SiC, 33 vol% Si, 26 vol % C)	• Flexural strength (MPa): 130 ± 10	[176]
LiO_2-ZrO_2-SiO_2-Al_2O_3 (LZSA)	• Relative density (%): 88.55 • Flexural strength (MPa): 127 ± 6	[185]
5 wt% $ZrSiO_4$ added LiO_2-ZrO_2-SiO_2-Al_2O_3 (LZSA5Zr)	• Relative density (%): 88.87 • Flexural strength (MPa): 96 ± 5	[178]
Si_3N_4	• Relative density (%): 97 • Flexural strength (MPa): 918 • Fracture toughness (MPa $m^{1/2}$): 7.45 • Elastic modulus (GPa): 307 • Vickers hardness (Kgf/mm^2): 1457	[186]
Al_2O_3	• Relative density: 97.1 • Hardness (HV): 391 • Flexural strength (MPa): 228 (perpendicular to stacks) • Flexural strength (MPa): 145 (parallel to layers)	[187]

5.2. Material Extrusion Process (MEX)

MEX is an AM process where ceramic materials in the form of paste, filament, or a preceramic polymer filament are extruded via a nozzle and then deposited onto a platform layer-by-layer to form a 3D structure. This process includes various technologies to shape advanced ceramics, (i) wax-based extrusion processes, and (ii) water-based extrusion processes, which are summarized in Table 13 [36]. The successful operation of all MEX techniques is based on the accurate control of the rheological features of the extruded paste or filament. Feedstocks should include a high solid loading of well-dispersed ceramic particles to avoid the formation of porosity and cracks and minimize shrinkage during heat treatments (debinding and sintering). Ceramic solids loading and adding a binder/viscosifier such as polyvinylpyrrolidone, polyethyleneimine, pluronic F-127, and methylcellulose increase the yield stress. A suitable paste for the MEX technique should have yield stress values between 100 and 1000 Pa [188,189].

5.2.1. Fused deposition modelling (FDM)

FDM is one of the most commonly used 3D printing methods, which was firstly developed by Crump et al., with a patent filed in 1989 [200]. Later, in 1990, it was commercialized by Stratasys Inc. [201]. In this method, inexpensive and environmentally safe feedstocks are used, categorized into fused and non-fused materials. In non-fused materials such as ceramic and concrete, there is no change in the state of materials during the process, and the flowing of viscous paste accomplishes through external pressure. The fabricated material is heated up to 0.5 °C higher than its melting point so that it immediately solidifies during post-extrusion for only one second. After the formation of the first layer, the build platform is lowered, and successive layers are deposited by the nozzle head that fused to the last layer. This process continues until the manufacturing of the complete object [42]. In contrast, during the process of fused-type materials, the state of the materials changes from solid to viscous paste and then again to solid. The solid materials melt into a viscous paste using a heater. Then it is extruded via the nuzzle, which moves both horizontally (x/y-axis) and vertically (z-axis) by a numerically controlled mechanism [4]. The surrounding environment of the extruded paste leads to its cooling down and immediately solidifying.

In this technology there are some print heads that allow co-printing of support structures for samples with complex geometry, and print samples with multiple materials [202]. In addition, the FDM system can print colorful products using different materials without blending them together. In this technology, a binder system develops with high strength, low viscosity, high strain and modulus, and easy burnout [203]. The binder includes 55 vol% of the ceramic powders, such as titanium dioxide, mullite, and fused silica. It should be underlined that, brittle ceramics that cannot be shaped into flexible and windable wires as feedstocks, should be embedded up to 60 vol% into thermoplastic binders and then deposited through the nozzle [204]. After printing, the manufactured ceramic parts should be subjected to a binder removal and sintering treatment for a further consolidation.

Similar to the FDM-produced plastic materials [205], the quality of the printed-ceramic parts, including surface roughness, mechanical features, dimensional accuracy, and homogeneity, strongly depends on the process parameters such as layer thickness, raster angle, building orientation, and rod width of fused ceramic/polymer filament, etc. Printed ceramic parts are characterized by high stability without the requirement of a post-processing step. However, they suffer from low surface quality due to the filament thickness; thus, finishing the fabricated objects is needed to obtain a smooth surface. Moreover, the staircase effect is another significant problem found in produced ceramic parts. The size of the extruded filament predetermines this phenomena, resulting in limited control in the z-direction [206]. Furthermore, FDM takes several days to print large and complex parts [12,207]. Some pros and cons of the FDM technique are summarized in Fig. 12 [15].

FDM can be used in different fields such as sensors and shielding, drug delivery, rapid tooling, architecture, fashion, education, aerospace, automotive, microfluidic, four-dimensional (4D) printing, prosthetics, and orthosis [208]. The first FDM-generated ceramic was reported in 1995 by Danforth [209] using Al_2O_3 and Si_3N_4-filled binder systems. They reported final sintering densities of 75–90% due to some defects in the sintered parts, such as voids, although no delamination was detected. A new biphasic calcium phosphate (BCP) scaffold reinforced with ZrO_2 (BCP/ZrO_2 scaffold) was fabricated using the FDM process for bone tissue engineering [210]. The morphology of the sintered BCP/ZrO_2 scaffold was investigated with SEM (Fig. 13). The FDM-printed scaffold had an overall size of 6.0 × 6.0 × 3.0 mm^3, with a pore size of approximately 350 μm and printed lattice width of 500 μm (Fig. 13a).

Mechanical testing of the scaffolds (Fig. 14) demonstrated that the compressive strength of the printed scaffold increased from 0.1 MPa to 0.5 MPa for pure BCP and BCP-10 wt% zirconia, respectively. The increase of compressive strength of the BCP scaffold was approximately

Table 13
Various material extrusion technologies for the manufacturing of advanced ceramics [36].

ME Process	Technique	Feedstock	Mechanism of solidification	Ref
Water-based extrusion	3DGP	Highly loaded aqueous ceramic slurry with gelling agent	Thermoplastic 3D Printing	[190]
	RC	Highly loaded aqueous ceramic slurry with low	Evaporation of the solvent to induce dilatancy of the slurry or Coagulation by	[191]
	DIW		controlled flocculation.	[192]
	CODE	amounts of organic additives (< 5 vol%)	Partial drying using an infrared lamp, with a liquid oil surrounding the part to prevent non-uniform evaporation from the sides	[193]
	FEF	Highly loaded aqueous paste with low	Crystallization of the aqueous liquid phase	[194]
	ABEF	amounts of organics	Glass transition of the polymer binder upon cooling	[195]
Wax-based extrusion	EFF	Highly loaded filament made of ceramic		[196]
	FDC	particles suspended in a thermoplastic polymer or wax.		[197]
	T3DP	Highly loaded liquid suspension of ceramic particles in a thermoplastic polymer.		[190]
	MJS	Mixture of ceramic and thermoplastic binder powders or pellets		[198]
	PHASE	Medium solids loading photocurable ceramic suspension	Photo-induced polymerization of the UV curable binder resin.	[199]

3DGP: 3D Gel Printing; RC: Robocasting; CODE: Ceramic On-Demand Extrusion; DIW: Direct ink writing; FEF: Freeze-Form Extrusion Fabrication; ABEF: Aqueous Based Extrusion Fabrication; EFF: Extrusion Freeform Fabrication; FDC: Fused Deposition of Ceramics; T3DP: Thermoplastic 3D Printing; MJS: Multiphase Jet Solidification; PHASE: Extrusion-Based AM Using Photoinitiated Polymerization

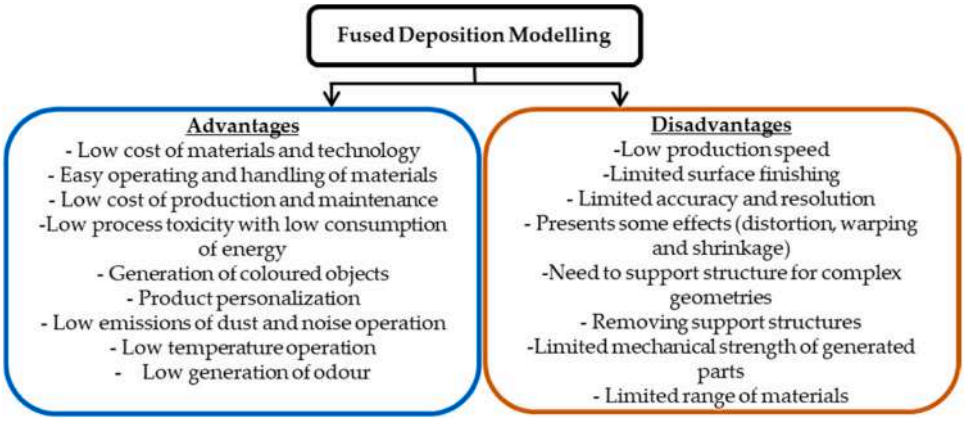

Fig. 12. Advantages and disadvantages of the FDM process.

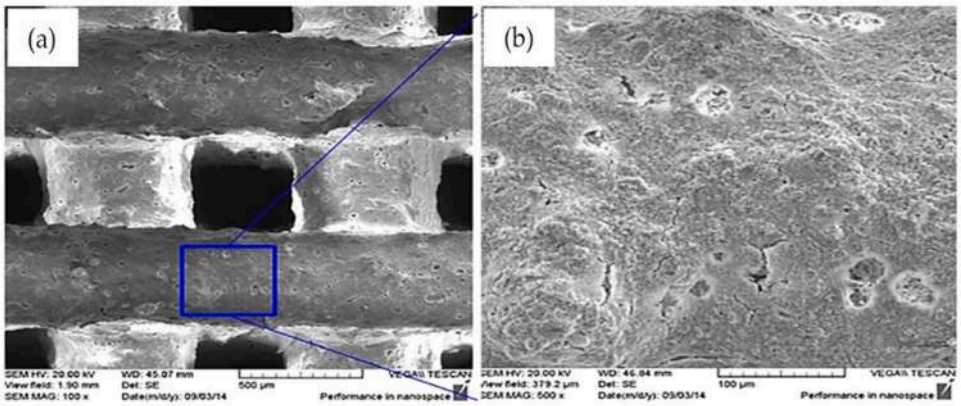

Fig. 13. SEM images of BCP/ZrO_2 scaffold, (a) pore size of about 350 μm and printed lattice width of 500 μm; (b) a granular surface of the FDM-manufactured scaffold after printing and sintering [210].

linear with cracking. On the contrary, BCP/ZrO2 scaffold exhibited apparent transgranular fracture owing to the addition of 10 wt% zirconia powder. It was found that incorporating ZrO_2 powders greatly enhanced the mechanical properties of the biphasic calcium phosphate scaffold.

Gorjan et al. [211] produced mullite ceramic components from a polymethyl siloxane ceramic precursor, γ-Al_2O_3 powder, ethylene-vinyl acetate (EVA), and an elastomeric binder using the FDM process. They

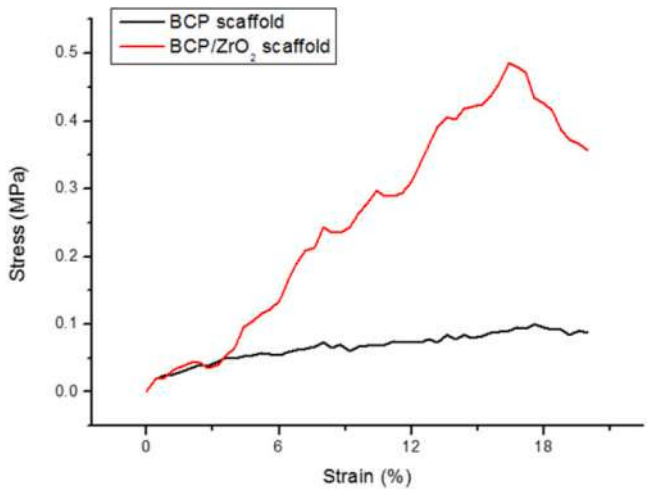

Fig. 14. Stress-strain curves of BCP and BCP/ZrO_2 scaffolds [210].

found that FDM could shape the preceramic polymers to fabricate large scale complex shape objects. In this process, the siloxane produced highly reactive silica during the firing, allowing the in-situ formation of silicate ceramic phases, such as mullite. Allahverdi et al. [212] successfully fabricated various shapes of functional electronic components such as transducers with polymers/piezoelectric ceramics such as lead-zirconate-titanate (PZT) and lead-magnesium-niobate (PMN) composites as feedstocks. Jafari et al. [213] utilized four extruders to fabricate multilayer PZT sensor components using soft and hard PZT ceramics in one layer. In recent years, recycling packaging materials such as polyethylene (LDPE) with low density, low mechanical strength, and thermal degradation into valuable products is a challenging task. Therefore, some investigations have been conducted to improve these features using ceramic/metallic reinforcements. Singh et al. [214] prepared SiC/Al_2O_3 reinforced LDPE using the FDM process as a novel method for the development of FGM for investment casting application. The SEM image confirmed the presence and dispersion of reinforced Al_2O_3 and SiC particles in the LDPE base composite (Fig. 15b). In addition, the optical micrograph and the SEM image of the final part generated with the help of FDM are demonstrated in Fig. 15(c and d). It revealed that the Al_2O_3 and SiC reinforcement particles in waste LDPE were in the final FGM so that will contribute to the improvement of wear properties and other surface features of the FGM.

In addition, several investigations have been conducted on the FDM method to fabricate a 3D model of a biomedical scaffold from materials such as alumina, calcium phosphates, hydroxyapatite (HAp), and beta-tricalcium phosphate (β-TCP). To this aim, thermoplastic polymers are blended with ceramics to obtain excellent characteristics of a 3D printed scaffold (Table 14) [215–217]. Conzelmann et al. [218] prepared complex alumina parts with tetrahedron structures. The generated structures contained dense parts printed from multiple contiguous layers comparable to the open structure scaffolds.

6. Liquid/Slurry- based deposition technique

The slurry-based 3D printing of ceramics generally includes the dispersion of ceramic particles as feedstock in a liquid or semi-liquid system, either in inks or pastes, which depend on the viscosity and solid loading of the system. This slurry can be printed using photo-polymerization, inkjet printing, or extrusion.

6.1. Material jetting (MJT) or multi-jet modelling (MJM)

MJT is a process that utilizes inkjet technologies through thousands of micro-size nozzles for 3D-printing products [202,224]. In this process, droplets of the built material are selectively deposited on a surface to form filament-like structures [225]. The molten thermoplastic suspension or wax injects along with the structural material as a support structure which can be easily removed by heating or washing at the end of the fabrication process [226]. The printer software mixes the thermo-polymer material cartilages, then moves the inkjet nozzles along the x/y-axis. The build materials are agglomerated by the deposited

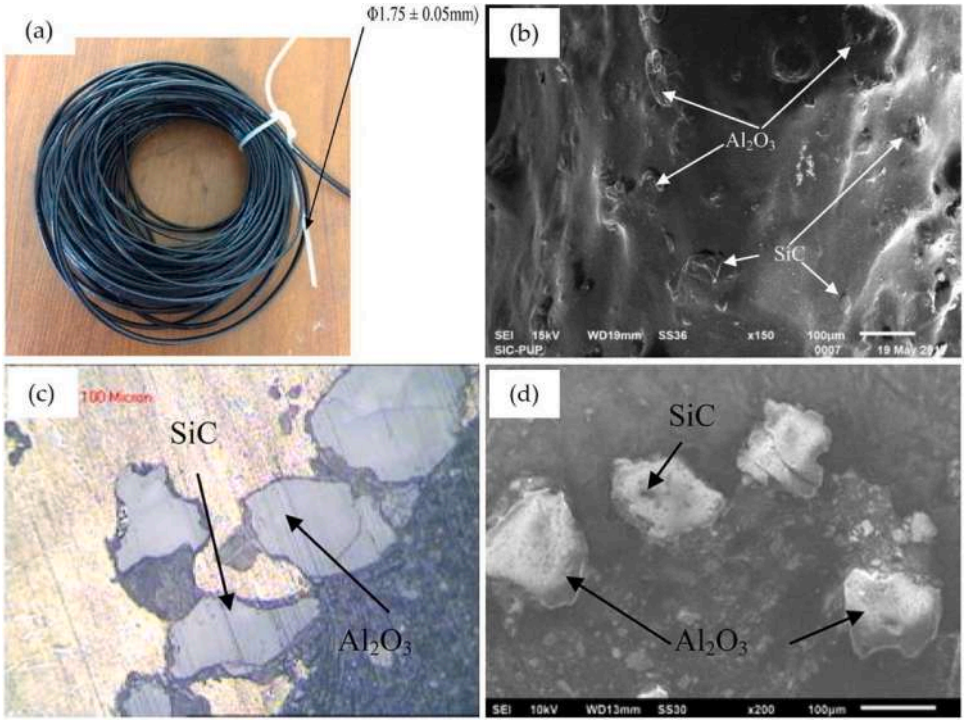

Fig. 15. (a) Prepared filament wire with reinforced LDPE waste; (b) SEM image of reinforced LDPE wire; (c) optical micrograph of prepared FGM by using FDM assisted investment casting respectively; (d) SEM image of prepared FGM respectively [214].

Table 14
FDM-manufactured composite filaments for biomedical applications.

Materials	Properties	Applications	Ref
BCPs/PLA	• Nontoxic, well cell proliferation	Scaffolds (bone substitutes/tissue engineering)	[219]
PA/HAp/ZrO_2	• Tensile strength (MPa): 22.78	Filaments	[220]
PA/β-TCP/ZrO_2	• Tensile strength (MPa): 24.25 • Flexural strength (MPa): 29.06		[221]
PCL/HAp	• Compressive modulus (MPa): 338	Bone scaffolds	[222]
PCL/TCP	• Compressive modulus (MPa): 253		
PCL/DCB	• Compressive modulus (MPa): 241		
Al_2O_3 (50 vol%) sintered at 1150 °C La-based glass frits infiltrated into Al_2O_3 (50 vol%) at 1120 °C	• Porosity (%): 34 • Pore size (μm): 0.2 • Porosity (%): 3.5 • Pore size (μm): 26.7 • Flexural strength (MPa): 238 ± 40	Dental restoration	[223]
Al_2O_3 (57 vol%) sintered at 1150 °C La-based glass frits infiltrated into (57 vol %) at 1120 °C	• Porosity (%): 35 • Pore size (μm): 0.2 • Porosity (%): 3 • Pore size (μm): 54.3 • Flexural strength (MPa): 264 ± 11		

droplets and solidify when subjected to an external light source (UV lamp) or cooling. Subsequently, the build platform is lowered along the z-axis by one layer thickness, and the second layer is built upon the first layer and continues until the part is constructed completely [12].

Among current available AM techniques for fabricating ceramic components, the conventional material jetting method can generate parts with high complex geometries, high resolution, low thickness (less than 20 μm), dense green bodies, good surface finish, homogeneous mechanical properties, and high dimensional accuracy [227,228]. In this method, increasing the surface inclination of the printing area leads to decreasing the surface roughness, which is not present in other AM technologies [229,230]. The combination of two materials together consisting of different colors can be performed by this technology [231,232]. MJM technique is inexpensive, time-effective, and office-friendly, but manufactured parts have lower strength. Besides, material jetting is greatly restricted to mostly less than 25 vol% solid loading and low viscous ceramic inks, often in the range of 20–40 $mPas^{-1}$, which causes the limitation of the widespread adoption of this method [233].

Extensive studies have focused on producing ceramic parts using inkjet technology with thermal drop-on-demand material jetting (DODMJ) that is also accessible via piezoelectric technology for manufacturing 3D structures [234,235]. This method can generate high-performance ceramics such as alumina, zirconia, and silicon-based ceramic materials. For example, Willems et al. [236] manufactured zirconia stabilized with 3 mol% yttria (3Y-TZP) by MJ technique and investigated the microstructure and mechanical behavior of the sintered printed objects. The printed parts using layer thickness of 10.5 μm had a high green density of 58%, and approximately fully dense sintered ceramics of 99.7%. Moreover, they reported the hardness and toughness of 12.5–12.8 GPa and 3.8–3.9 MPa $m^{1/2}$, respectively, independent of the printing direction. Mummareddy et al. [237] produced material jetted zirconia with complex geometries with an average shrinkage of 17%. They assessed the sintering process and print orientations for solid ceramic samples and lattice structures. Printed samples in zero direction displayed a relatively higher strength than all the sintering profiles under compression and flexural conditions. In addition, sintered zirconia parts showed an excellent averaged strength for a longer time and a slower ramp than those sintered for a short sintering profile. Table 15 presents the properties of MJ-printed zirconia objects found in the literature.

With attention to the advantages presented by material jetting, it is an appropriate technique for tooling purposes and rapid prototype manufacturing. This process can overcome challenges when a part is generated using conventional manufacturing methods like waterjet cutting, EDM, laser cutting, casting, etc. [241]. Furthermore, the MJT process has several applications in electronics (production of capacitors [242]), dental prostheses, medical industry (tissue engineering applications [243]), etc.

6.2. Vat photopolymerization (VPP)

VPP is one of the most popular AM processing for manufacturing ceramics materials, which uses photo-curable inks to facilitate the printing process [244]. Most of the attention has been paid to this process in both academic and industrial fields due to its benefits such as high surface smoothness, high speed, perfect dimensional accuracy, and a wide range of applications in functional devices, ceramics, biomedical, etc. [245]. However, a large volume of sacrificial binder is essential in this technique. In the VPP process, ceramic powder is suspended in a monomer(s)/oligomer(s) doped with a photoinitiator. A UV 6 light illuminates the suspension leading to the polymerization and hardening of the monomer(s)/oligomer(s) [245]. This green body exposes debinding followed by sintering at high temperatures to obtain the final ceramic component. It should be mentioned that the binding and used structure materials can affect the debinding and the sintering temperatures, respectively. For example, for alumina and zirconia materials, the sintering temperature can be increased up to 1600 °C [42]. In addition, ceramic parts should be sintering under a controlled temperature to reduce the thermal stresses and avoid cracks formation. After sintering, the obtained samples offer high density and complex features [42]. Table 16 provides some monomers used in the production of ceramic parts through the vat photopolymerization process with their density and viscosity.

A highly loaded ceramic slurry (typically 45–55% by volume) with a printable viscosity in the range of 3000–5000 mPa.s is a key parameter

Table 15
Overview of reported MJT-printed ceramics materials.

Materials/ Test method	Characteristics of sintered parts	Ref
8Y-TPZ	• Hardness (HV): 1516 • Fracture toughness (MPa/ $m^{0.5}$): 5.62	[233]
3Y-TZP/4-point bending	• Relative density (%): 96.9 • Weibull modulus(m): 3.5 (X direction)	[238]
3Y-TZP/Biaxial	• Relative density (%): ~100 • Weibull modulus (m): 10.4 (X direction)	[239]
3Y-TZP/4-point bending	• Relative density (%): 99.7 • Weibull modulus (m): 5.9 (X direction), 4.1 (Z direction) • Average bending strength (σ_m)(MPa): 748 ± 148 (X direction), 331 ± 83 (Z direction)	[236]
3Y-TZP/Biaxial	• Relative density (%): 99.7 • Weibull modulus (m): 8.5 (X direction), 2.0 (Z direction) • Average bending strength (σ_m)(MPa): 1004 ± 138 (X direction), 367 ± 135 (Z direction)	
3Y-TZP/4-point bending	• Relative density (%): 96.2 • Weibull modulus (m): 3.6 (X direction) • Average bending strength (σ_m)(MPa): 759 ± 233 (X direction)	[240]

8Y-TPZ: 8 wt% yttria-stabilized zirconia; X: Fabricating direction is perpendicular to applied forces; Z = fabricating direction is parallel to applied forces.

Table 16
Reported monomers used in ceramic vat photopolymerization.

Monomer	Density g. cm^{-3}	Viscosity (mPa.s)	Ref
Acrylamide (AM)	1.32	Solid	[248, 249]
2-Hydroxyethyl acrylate (2HEA)	1.01	8–10	[250, 251]
4-Acryloylmorpholine (AGMO)	1.12	12–15	[252, 253]
Isobornyl acrylate (IBOA)	0.98–0.99	2–9	[254, 255]
2-Phenoxiethyl acrylate (PHEA)	1.10	5–15	[256]
1,4-Butanediol diacrylate (BDDA)	1.05	8	[255]
Di(ethylene glycol) diacrylate (DEGDA)	1.12	12	
1,6-Hexanediol ethoxylate (2) ($HDEODA^{+}$)	1.01–1.05	10–30	[257]
Dipentaerythritol penta-/hexa-acrylate (DPHA)	1.16	4000–7000	

in VPP techniques [246]. However, slightly higher viscous systems (up to 8940 mPa.s) were reported to be effective too in commercial porcelain-based resins [247].

It should be highlighted that, Stereolithography (SLA) and Digital Light Processing (DLP) attract more attention in industries as two significant AM technologies that apply inks for processing ceramic materials.

6.2.1. Stereolithography (SLA)

SLA technique was the first commercially available process introduced to the market, owing to the highest levels of accuracy, smooth surface finish, and good chemical bonding between the layers [258, 259]. This method is based on the "top-down" approach. It can manufacture several small samples simultaneously because the prepared specimens are oriented next to each other in the same build platform. SLA contains a liquid resin vat, a model-building platform, and an ultraviolet (UV) laser. The ceramic components are generated by laser vat-polymerizing successive layers based on liquid resins. These resins include organic molecules, monomers, oligomers or prepolymers, photoinitiators, and other additives that are added to impart different functionality. The resin is cured and solidified through a chemical reaction using a light source (laser or LEDs) in the wavelength of UV light to form a highly cross-linked polymer network. The UV-laser is focused onto the surface of a vat filled with liquid photopolymer, and highly exothermic polymerization of resin carry out for each cross-section. The polymerization spontaneously continues until the monomers remain to react or any other terminating reaction occurs. When the first layer is completely polymerized based on the CAD model, a resin-filled blade sweeps across the object's cross-section, re-coating it with a one-layer thickness of fresh resin. Subsequently, the build platform is lowered in the z-direction and polymerizes the subsequent layer. These steps are repeated until the sample is entirely built. The size and number of produced objects affect their speed. The SLA approach needs less resin; the excess resin can be drained and reused after creating the sample [4, 83].

The ceramic products possess fewer porosities and high manufacturing accuracy [260]. They are cleaned and post-cured in an alcohol bath and ultraviolet oven to polymerize the unreacted resin groups and strengthen the products [12]. The final products of SLA-fabricated ceramics can be solid or porous, depending on the solid loading of ceramic-resin slurry and post-processing steps such as de-bonding and sintering [261].

Since 1994, Halloran et al. extensively studied the SLA technique, starting with the utilization of highly concentrated ceramic suspensions up to 65 vol%, including silica, alumina, and silicon nitride [262–266]. Defect-free multi-ceramic triangles with tunable thermal expansion were produced by Zhang et al. [267] based on ZrO_2 and Al_2O_3 using the SLA method. The thermal expansion behavior of the manufactured structures was characterized based on a non-contact digital image correlation (DIC) technology. In the structures with a β value of 66.5°, the thermal strain decreased with the temperature, indicating the Negative Thermal Expansion (NTE) behavior (Fig. 16). For the structures with a β value of 53.23°, there was only a slight change in the measured thermal strain with raising the temperature, indicating zero (or approximately zero) thermal expansion behavior (Fig. 16). By increasing the temperature and finally increasing the measured thermal strain in structures with a β value of 37.0°, the positive thermal expansion (PTE) behaviour was obtained (Fig. 16). The experimentally measured equivalent thermal expansion (α_{equ}) of the ceramic structures were -15.8×10^{-6} /°C, 0.7×10^{-6} /°C, and 16.2×10^{-6} /°C for negative, zero, and positive thermal expansion in the height direction, respectively. All the errors between the theoretically designed α_{equ} and experimentally measured α_{equ} were below 1.0×10^{-6} / °C showing the great agreement between the experimental testing values and the designed values.

Li et al. [268] used the micro SLA technique to produce a hydroxyapatite/tricalcium phosphate (HA/TCP) bone scaffold. They determined that the printed HA/TCP scaffolds have hierarchical porous properties with microscale pores (~20–1000 μm) and interconnected tiny pores (less than 5 μm) induced by burning the polymer and post-processing. Wu et al. [249] produced Zirconia-Toughened Alumina (ZTA) ceramics with nearly full density and an average size of 0.35 μm. The generated samples offered a hardness of 17.7 GPa with a fracture toughness and flexural strength of 5.7 MPa $m^{1/2}$ and 530.3 MPa, respectively. Camargo et al. [269] conducted experiments to determine the rheological behavior of ceramic suspensions and the influence of the suspension formulation, such as solid loading, ceramic particle size, size distribution, and monomers for vat photopolymerization. They obtained low viscosity of < 3 Pa.s and high solid loading of > 40 vol%. Surface quality and mechanical properties of stereolithography printed and sintered zirconia ceramic components evaluated by Xing et al. [270]. They reported that the 3D printed ZrO_2 had the anisotropic characteristics of surface quality due to the various scanning paths. Fig. 17 shows the surface roughness and mechanical properties of printed sample bars with different printed dimensions. The surface roughness of the horizontal surface reached below 0.41 μm while it increased to 1.07 μm along the fabrication direction on the vertical surface Fig. 17(a). Furthermore, the fracture toughness, the hardness, and the flexural strength of ZrO_2 ceramics reached 6.37 ± 0.25 MPa.$m^{1/2}$, 13.90 ± 0.62 GPa, and 1154 ± 182 MPa, respectively, with the density up to

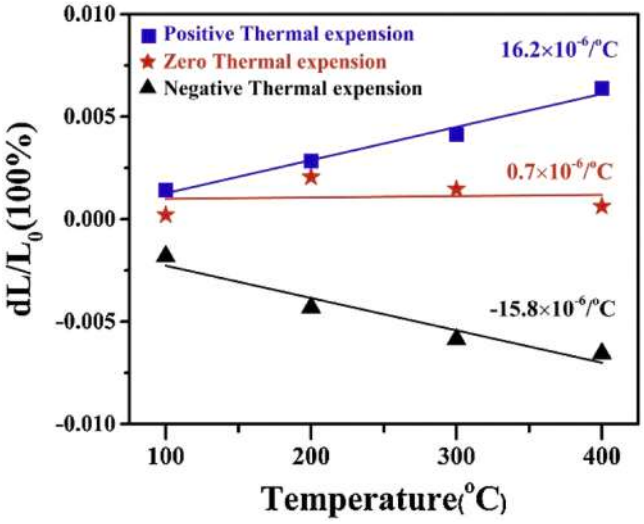

Fig. 16. Experimentally measurement of thermal strain in height direction for the multi-ceramic structures [267].

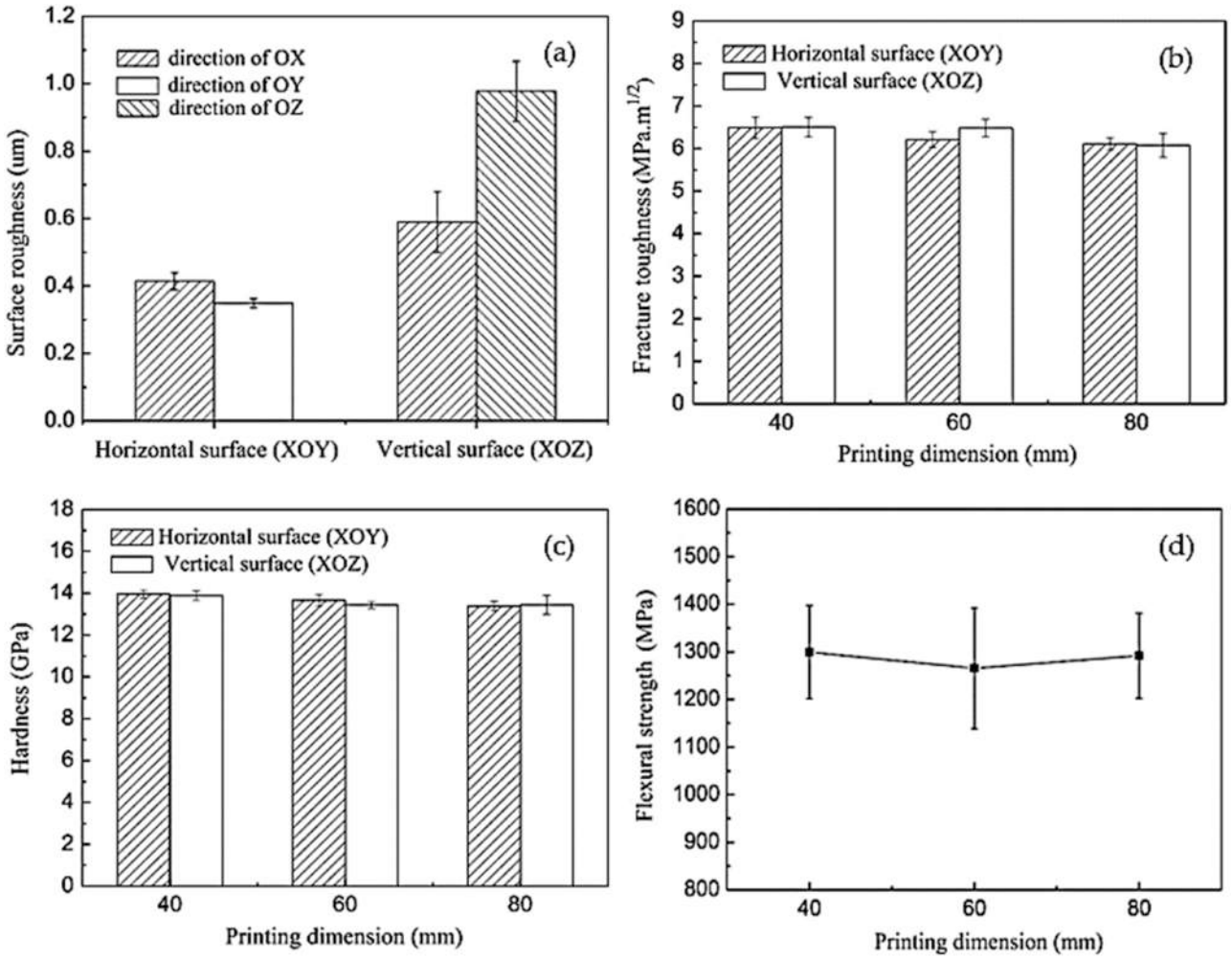

Fig. 17. 3D manufactured and sintered zirconia bars with various printed dimensions, (a) surface roughness along the three directions on the (XOY) and (XOZ) surfaces of samples; (b) Fracture toughness; (c) hardness; (d) flexural strength [270].

99.3%.

Table 17 shows an overview of the stereolithography AM of ceramics.

Stereolithography-printed ceramic parts have been extensively developed and applied for the fabrication of dense/cellular ceramic components with complex structures such as integrally cored casting molds [276,277], microelectronic components like sensors [278,279], photonic crystals [280], biomedical implants such as bone scaffolds [281] and dental components [271]. There are reported remarkable advancements in the stereolithography process in terms of minimizing the content of remaining monomer, segregation of ceramic particles, curing plan, and debinding [266,282,283].

Table 17
Overview of reported SLA-manufactured ceramics materials.

Materials	Characteristics of sintered parts	Ref
ZrO_2	• Relative density (%): 98.58 • Surface Vickers hardness (HV): 1398 • Surface roughness (μm): 2.06	[271]
3 mol% Y_2O_3- ZrO_2	• Relative density (%): 99.3 • Bending strength (σ_m)(MPa): 200	
3 mol% Y_2O_3- ZrO_2	• Relative density (%): 97 • Bending strength (σ_m)(MPa): 1044	[272]
Al_2O_3	• Relative density (%): 99.3 • Vickers hardness (GPa): 17.5	[273]
Al_2O_3-ZrO_2	• Density (g/cm^3): 4.27 • Fracture toughness (MPa.m$^{1/2}$): 5.2 • Vickers hardness (GPa): 17.6	[274]
Hydroxyapatite	• Compressive strength (MPa): 37	[248]
Al_2O_3 toughened ZrO_2	• Relative density (%): 99.5 • Bending strength (σ_m)(MPa): 530 ± 30 • Relative density (%): 88.3 • Bending strength (σ_m)(MPa): 175	[249] [275]

6.2.2. *Digital light processing (DLP)*

DLP is considered as a subcategory of the vat-polymerization approach, as both utilize light as the polymerizing agent [203]. DLP is mask-based stereolithography so that an integral image is transferred to the photopolymerisable liquid surface by exposing the light source via a patterned mask. It was first proposed by Nakamoto and Yamaguchi [292] with physical masks. In 1997, Bertsch et al. [284] developed and improved the DLP using a liquid crystal display (LCD) as the dynamic mask generator. Since 2001, LCDs have been replaced with Digital Micromirror Devices (DMDs) due to their competitive fill factor and reflectivity, which cause higher resolution and contrast in the light display [285–287].

DLP technique is able to print small complex geometries products with high accuracy with liquid photopolymers as the construction material. A transparent vat is filled by the photopolymer laying above a projector which applies a high-power LED source. This projector is based on a micro-electro-mechanical system (MEMS) using a Digital Mirror Device (DMD). DMD contains individually moving micro-mirrors for controlling the path reflection of the UV light. During the fabrication process, the build platform (on the x-y axis) is dipped into the resin vat

with one layer thickness. Subsequently, one-layer forms based on the CAD model through the reflection of the UV light by the DMD to the surface of the resin vat [288]. After building a layer, the build platform is moved to the z-axis (upwards) by one layer thickness. These steps are repeated to complete the product [289,290]. A manual post-processing step is needed in the DLP technique, and polymerization shrinkage affects printed parts. Compared to SLA, printed products with DLP possess good accuracy, affordable cost, perfect feature resolution (several micrometers), and smooth surfaces. Furthermore, faster light switching and image projection decrease the manufacturing time in the DLP process concerning SLA. Therefore, most of the industry's attention has been paid to this technique [291,292].

The DLP process can produce zirconia and alumina structural components with an almost full density of 97–99% and a Vickers hardness of 13.1 and 17.5 GPa, respectively. These results are comparable with the produced parts using the traditional methods [273,293]. Alumina and bioactive glass with complex structures and suitable characteristics printed using DLP. The printed products presented high density (above 90%) with comparable mechanical strength [294–296]. In addition, ceramic structures with unique properties and characteristics can be produced by DLP, such as honeycomb catalyst supports, heat exchangers, and negative Poisson's ratio metamaterial [297,298]. The porous scaffolds of ZrO_2/HA composite with different HA additions were printed using the DLP technology [261]. All the printed scaffolds, including 0 wt% HA (ZH0), 10 wt% HA (ZH10), 20 wt% HA (ZH20), and 30 wt% HA (ZH30), had similar microstructures (Fig. 18). It was found that the incorporation of HA positively affected cell proliferation and differentiation.

In addition, the composite scaffold with 10 wt% HA presented the highest compressive strength (Fig. 19a), which can be explained by the pinning and bridging effect of a small amount of HA grains (Fig. 19b and c). By soaking the scaffolds in the Simulated Body Fluid (SBF), the compressive strengths of the composite scaffolds gradually decreased and increased after 14 and 28 days, respectively, due to the degradation of calcium phosphate components and the deposition of apatite (Fig. 19d). The compressive strengths of all the printed scaffolds were enhanced up to 20 MPa after 28 days of soaking, comparable with the compressive strengths of the zirconia scaffolds (25 MPa) in the same period. The results showed that all scaffolds had the required compressive strengths with respect to the cancellous bone with the potential application value in bone repair.

Rauchenecker et al. [299] successfully printed aluminum nitride parts and sintered them at 1700 C. Depending on the sample orientations concerning the building direction, the flexural strength of AM samples varied in the range of 320 and 498 MPa. Moreover, the printed parts showed high thermal conductivity of 160 W m^{-1} K^{-1}. Guo et al. [300] produced fine lattice structural titanium dioxide ceramics by DLP process for bone tissue engineering, filters, and radiators. The fabricated ceramic specimens were rutile phase TiO_2 with porosity from 50% to 80%. By controlling process parameters such as debinding and sintering, ceramic cracking and collapse caused by resin volatilization were effectively avoided. The SEM images showed that TiO_2 structural ceramics have regular and complete porous structures with a strut diameter of about 200 μm (Fig. 20). TiO_2 specimens were composed of uniform layers with an interlayer thickness of about 0.01 mm. Moreover, the SEM image on the outer side of the strut demonstrated some holes in the surface of the samples (Fig. 20b), which were mainly concentrated in the layer-to-layer joint. The formation of these holes was due to the principle of DLP 3D printing layer-by-layer exposure molding. Nevertheless, in the TiO_2 samples produced under the non-optimal parameters, there were cracks (Fig. 20e) and some holes (Fig. 20f) on the sample surface, specifically at the interlaminar junction (Fig. 20e and f).

They also found that by decreasing the porosity from 80% to 50%, the compressive strength of lattice ceramics enhanced from 1.13 MPa to 1.50 MPa (Fig. 21).

Nevertheless, it should be pointed out that production of ceramic objects using the DLP process is more expensive with respect to the FDM process in terms of running costs. Table 18 shows the properties of some DLP-printed ceramic parts.

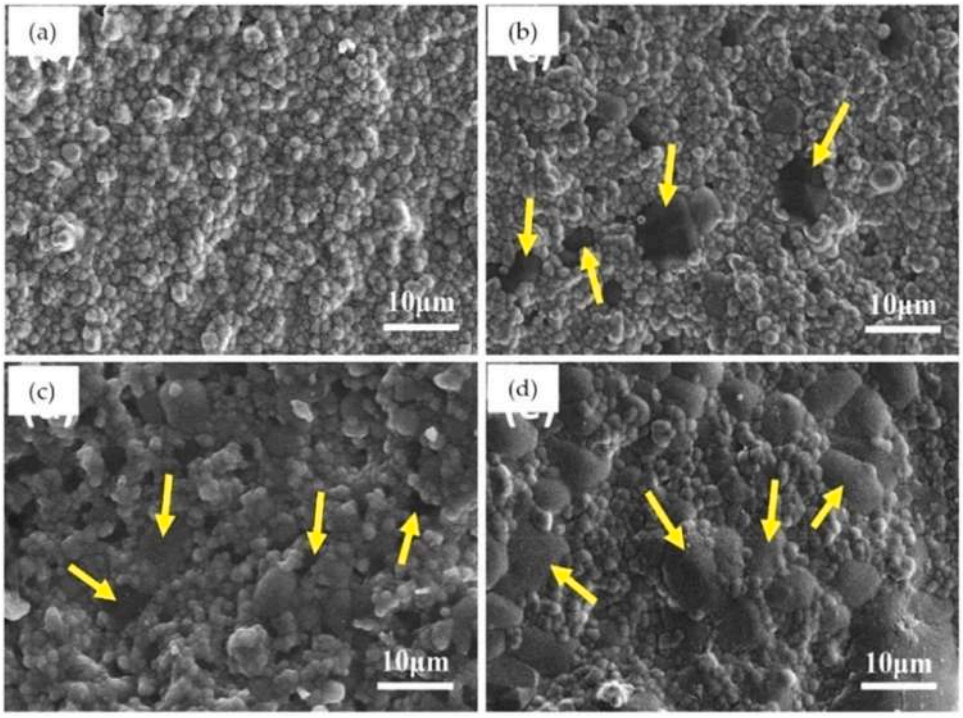

Fig. 18. SEM micrographs of, (a) ZH0; (b) ZH10; (c) ZH20; (d) ZH30 scaffolds. Yellow arrows show the dark grains of various sizes embedded in the ZrO_2 grains [261].

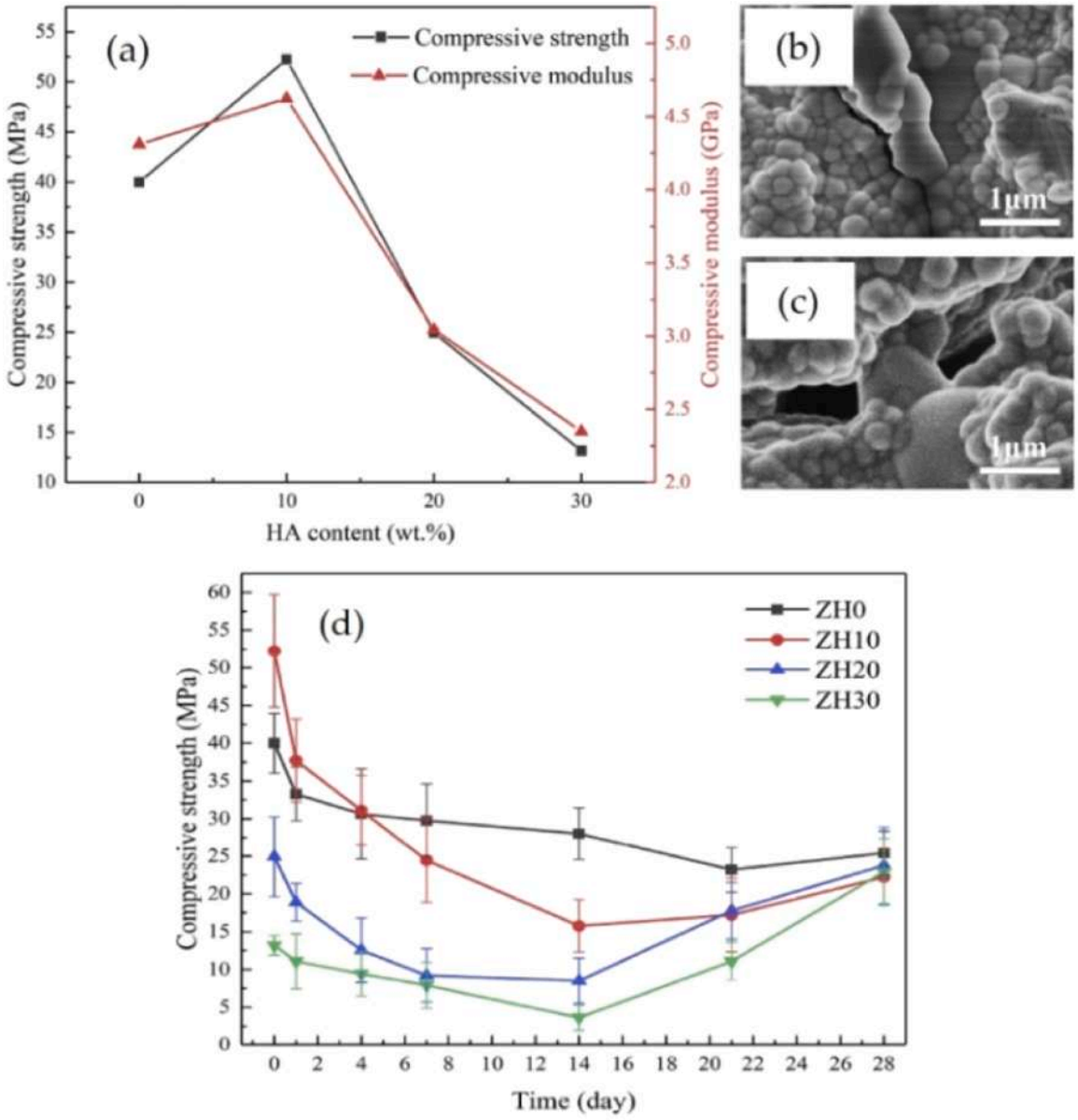

Fig. 19. (a) Compressive strength of printed scaffolds as a function of HA content; SEM image of (b) crack deflection; (c) bridge on the ZH10 scaffold; (d) compressive strengths of the scaffolds after soaking in SBF for different periods [261].

7. A comparison of AM techniques

All the AM technologies are based on a similar concept so that they share several mutual benefits such as mass production, reducing the fabrication time, and raw material wastage [312]. They print small to large complex structures from 3D models with good resolution, improved mechanical properties, and noticeably lower defect rates. The AM process uses different techniques to create parts by layer-by-layer material addition principle; SLA, SLS, MJ, BJT, FDM, and SL are well-enacted methods, whereas other AM techniques are limited. These processes are selected according to the feedstocks and applications. Table 19 provides information about the main commercial AM systems used to produce ceramic materials [13,65,313–317].

In many AM approaches, heating and cooling are essential steps. Fig. 22 compares the fabrication speed, achieved resolution, and the special energy needed in seven main AM processes as defined by ISO/ASTM 17296 [318]. Many AM technologies like BJT use various binders for producing using relatively lower heat. Although it is a good idea, the selection of a proper binder, its durability, and its applications can be challenging. Despite utilizing similar heat input, the non-equilibrium heat transfer during cooling can result in microstructural differences [319]. The DED process uses the maximum energy in the fabrication of ceramic components with the highest speed, while the generation of ceramic parts using BJT needs the minimum energy (Fig. 22) [41].

Generally, a versatile range of feedstocks can be processed by SL techniques such as fiberglass or ceramic fillers. In contrast, other AM approaches use powdery or liquid raw materials. Within the AM techniques, the SL process can accelerate the large-scale production of parts [282,320]. Even though SHL is under-represented by industrial standards, it offers substantial benefits concerning other AM techniques. By comparing the characteristic values for the printing resolution from various AM methods, SHL possesses a printing resolution compatible with all other AM approaches (Fig. 22).

There are two main methodologies for evaluating the environmental impact: the analysis of life cycle and the assessment of environmental impact (Life Cycle Assessment, LCA, approach). Nevertheless, these techniques cannot directly measure ecological impacts and predict the results [321]. Table 20 provides the environmental and health effects of

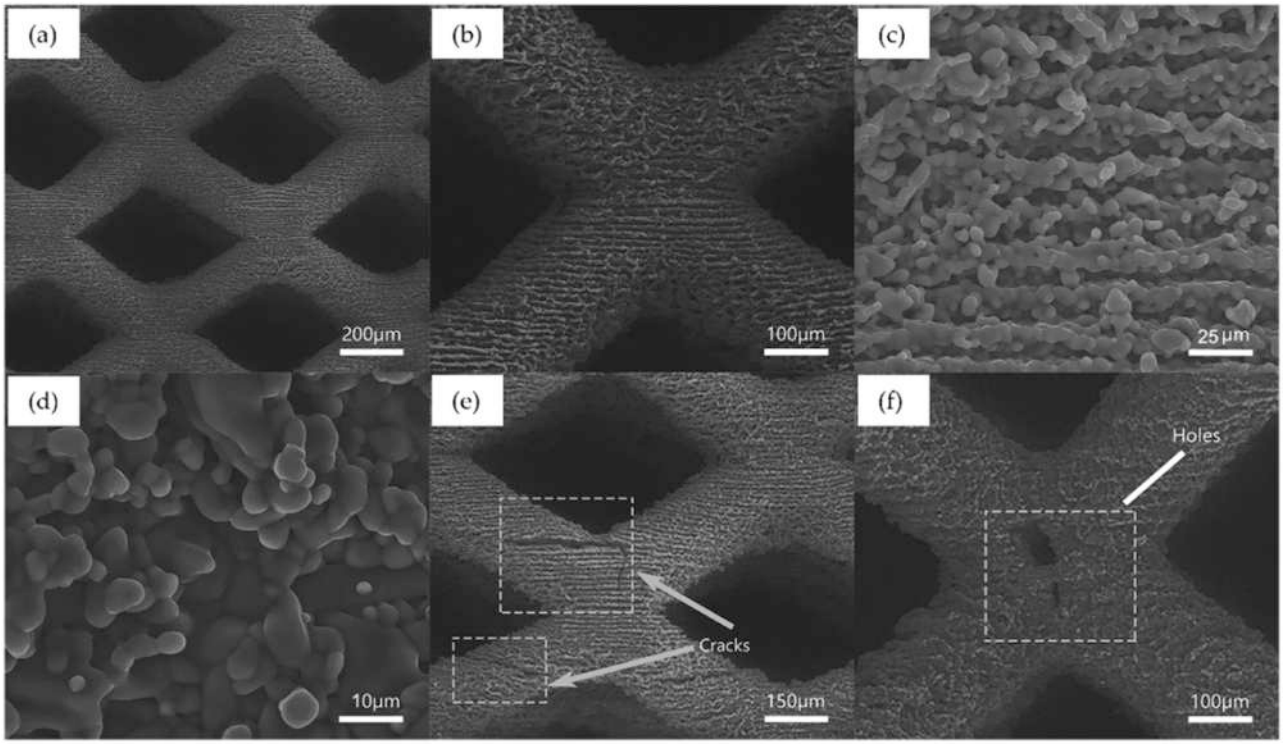

Fig. 20. SEM images of the titanium dioxide lattice structure [300].

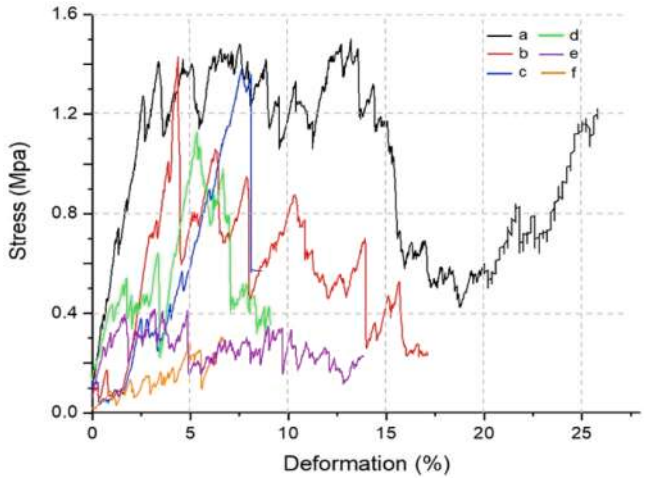

Fig. 21. The stress-strain curves of lattice structural titanium dioxide including different porosity, (a) 50% porosity; (b) 60% porosity; (c) 70% porosity; (d) 80% porosity; (e) 70% porosity (with cracks); (f) 70% porosity (with holes) [300].

various traditional and AM technologies [14]. Compared with AM technologies, conventional methods lead to serious health effects and greenhouse gas emissions such as carbon dioxide, methane, nitrous oxide, fluorinated gases, sulfur hexafluoride (SF_6), and nitrogen trifluoride.

For creating a 3D component, the power range, wavelength of the laser, the flexibility of the laser point, and repetition rate should be considered. Due to the poor thermal conductivity of ceramic materials, a relatively lower power laser can be applied for the manufacturing of components, but it is essential to avoid any thermal shock. Generally, laser power is in the range from 0.1 W to 10 kW. Moreover, depending on the technique, material, and type of product, laser wavelength can be

Table 18
Overview of reported vat-polymerization-printed ceramics materials.

Materials	Characteristics of sintered parts	Ref
5 mol% Y_2O_3- ZrO_2	• Relative density (%): 99.3 • Weibull modulus (m): 9.8 (X direction), 8.4 (Z direction) • Average bending strength (σ_m)(MPa): 657 ± 84 (X direction), 126 ± 18 (Z direction)	[301]
3 mol% Y_2O_3- ZrO_2	• Relative density (%): 98.7 • Weibull modulus (m): 8.2 • Average bending strength (σ_m)(MPa): 320 ± 41	[302]
	• Relative density (%): 99.5 • Weibull modulus (m): 9.3 • Average bending strength (σ_m)(MPa): 1013 ± 126	[303]
	• Relative density (%): 94.7 • Average bending strength (σ_m)(MPa): 595	[304]
	• Relative density (%): 99.5 • Average bending strength (σ_m)(MPa): 425 (X direction), 576 (Z direction)	[305]
3 mol% Y_2O_3- ZrO_2	• Relative density (%): 99.1 • Weibull modulus (m): 11.4	[306]
Silica	• Density (g/cm^3): 1.42 • Flexural Strength (MPa): 13.31	[307]
45S5 Bioglass®	• Biaxial strength (MPa): 40 • Compressive strength (MPa): 0.33	[295]
Al_2O_3 toughened ZrO_2	• Relative density (%): 98.4 • Average bending strength (σ_m)(MPa): 430 ± 60	[308]
HA	• Compressive strength (MPa): average 11.8 (X direction), average 5.1 (Y direction)	[309]
Al_2O_3 toughened ZrO_2	• Relative density (%): 99.4 • Average bending strength (σ_m)(MPa): 517	[310]
11 mol% CeO_2-stabilized ZrO_2/16 vol% Al_2O_3	• Relative density (%): 99.4	[311]

X: Fabricating direction is perpendicular to applied forces; Z = fabricating direction is parallel to applied forces

Table 19
A summary of the main AM techniques for manufacturing ceramics, merits, demerits, and applications.

AM technology	Merits	Demerits	Applications
Materials extrusion (FDM, FFF)	Fast, low cost, material agnostic, low waste, high density	Rough surface, stresses in debinding and sintering, low accuracy, interfacial porosity	Medical, electronics, composites, construction, prototyping, toys, architectural design, casting patterns
Material jetting	Smooth surface, high resolution, multiple materials possible, material agnostic	Need cleanout of support material, particle size < 1 μm, limited part size	Medical, technical ceramics
Binder jetting	No required support, porous green body for fast debinding, material agnostic, several materials and colors can be printed, high scalability	Particle size> 5 μm, weak green body, some roughness, may need supports for sintering, Excess powder clean-up, longer postprocessing times, high porosity	Medical, fast prototyping, niche-technical, sand-casting molds
Sheet lamination	High speed, material agnostic, no required support	Limitation of geometry, rough surface, non-recyclable waste, low resolution, delamination, interfacial porosity	Heat exchangers, composites, technical ceramics, paper, and foundry industries
Vat polymerization (SLA, DLP, LCM)	Smooth surface, high resolution, can be used for complex geometric and pre-ceramics, high density, excellent accuracy, no required support	Slow, expensive, more complex rheology compared with polymers AM, weak UV absorbing materials, high porosity, limited part size	Technical ceramics, medical, cores, molds, biomedical, prototyping
Powder bed fusion (L-PBF)	can be used for complex geometries, without debinding or sintering, strong as-printed product, no required support	Slow, residual porosity, excess powder clean-up, some roughness, high temperature, cracking, high porosity	Optics, medical, lighting, art, and design, dental bridges and crowns, car seats, plants, watches, jewelry, gearbox housing
Directed energy deposition	Less heat and waste compared with L-PBF, curved surface, without debinding or sintering, enclosed structures, high density	Need of strong cooling, rough surface, limited geometries, high-temperature gradients, thermal cracks	Optics, lighting, art, design

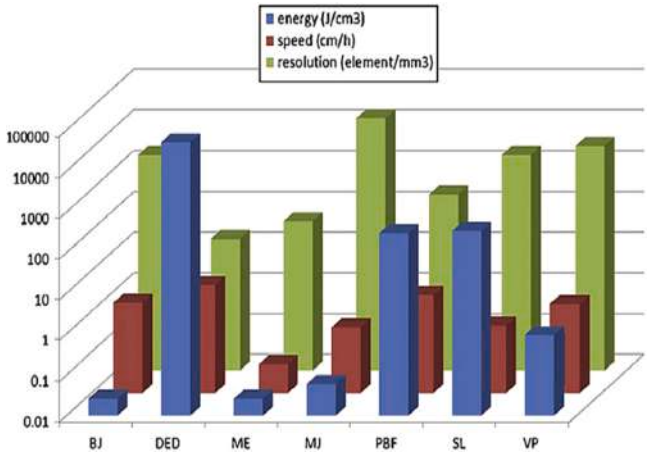

Fig. 22. Comparing the applied relative energy, AM process speed, and resolution of manufactured parts using seven main categories of AM techniques [41].

in the range of ultraviolet (UV) to mid-infra-red (IR) [41].

Furthermore, Table 21 distinctly compares the properties of the main available AM methods [41,42]. Low-cost feedstock are materials which are commercially available at low cost. At the same time, the fabrication cost includes operation, processing, post-processing, and capital expenses. In other words, AM is economical for mass customization and fabrication of a certain number of products. The raw materials and process costs for FDM and SL methods are suitable.

In contrast, SLS and L-PBF methods can produce larger volume parts with higher mechanical strengths and costs. Larger build volumes fabricate using BJT with lower mechanical strengths and relatively reduced costs. Although AM processes can create bigger build volumes, fabrication of a large part with no cracks or deformation is still challenging. On the contrary, multiple smaller components are printed by AM methods in one batch, which makes AM methods suitable for batch production.

8. Challenge of ceramic AM

Additive manufacturing of ceramic parts is relatively more challenging with respect to polymer and metallic parts, owing to their high melting temperatures and inherent brittleness. For instance, the melting points of alumina and tungsten carbide are 2050 °C and 2870 °C, respectively. For this reason, most of ceramic parts are produced using indirect AM processes that need post-processing steps such as debinding and sintering for further consolidation. Although in SLS, L-PBF, and DED processes, ceramics are directly sintered or melted, high thermal stress generally causes crack formation in printed parts. Compared with these methods, SLA is more famous for creating ceramic components in an indirect way. Still, the material selection, post-processing, and controlling processing parameters are more critical. Besides, due to ceramic materials' low thermal expansion coefficient and inherent brittleness, the full-scale industrial AM techniques for mass production and printing large parts are still challenging. Even though AM technologies of ceramic materials offer several advantages, they pose several problems such as restriction of part size, generation of overhang structures,

Table 20
A comparison of conventional and commonly utilized AM methods.

Process	Utilized material	Utilized energy	Utilized chemical materials	Gas emission	Impacts
SLS	Polymers, ceramics, composites, metals, hybrid	High power laser beam	Polyamide resin	CO_2	-
SHL	Polymers, metals, ceramics, hybrids	High power laser beam, heat	Solvent	VOCs	-
FDM	Polymers, ceramics, composites	Heat	Propylene glycol, monomethyl ether	CO_2, NO_x, SO_x, CO	burning eyes, throat, and skin, dizziness, headache, etc.
SLA	Polymers, ceramics	UV laser beam	Propylene carbonate	CO_2, SO_x, CO	Less toxic
Machining	Metals and alloys	Mechanical energy	Cutting fluid	GHGs	Serious effect on health

GHGs: Greenhouse gases; NO_x: Nitrogen oxides; SO_x: Sulfur oxides.

Table 21
Comparison of various 3D printing technology for manufacturing ceramics [42,56,322–325].

Process	Layer formation technique	Accuracy/ Resolution (μm)	Layer thickness (μm)/ Temperature process	Surface finish/ Support structure	Build size	Feedstock cost/ Process cost
SLA	Photopolymerization	High (25–150)/10	< 10 /very low	Good/required	Extra small small Medium	Low/ Medium
FDM	Extrusion	Good / 50–200	100–250 /low	Good/ required	Medium large Extra large	Low/ Low
SLS	Powder fusion	Low (>100)/80–250	25–92 /low	Limited/not required	Medium Large	Low/High
SLM		< 20/ 80–250	75–150 /high	High/required		
LOM	Sheet lamination	Medium (c.a. 50) / -	100/low	Poor/required	Medium Large	Low/ Low
BJT	Binder bonding	High (30–50 μm) / < 50 μm	30–200/Low	High/-	Medium large Extra large	Low/Medium
DED	Material deposition	Very low (<1 mm) / -	500–1000/high	Poor/-	Versatile	Low/High

< 1 mm: Extra small; 1–10 mm: Small; 10 mm–0.1 m: Medium; 0.1–1 m: Large; > 1 m: Extra large.

warpage, bonding layer to layer, poor accuracy, misalignment, and inconsistent material under-extrusion [326].

One of the main concerns of using these AM processes is printing large ceramic objects. Indeed, 3D printing of large parts is not direct; they are cut into smaller pieces and assembled later. Nevertheless, the produced parts often lack strength. Furthermore, large ceramic parts possess problems during binder removal and sintering, which can be attributed to significant variations in sectional thickness and differences in thermal features and shrinkage. Another major challenge is the formation of porosity and voids between the layers or/and beads. These defects have a severe effect on ceramic materials [327]. Depending on the AM process, the amount of voids in the printed part is different, which can lead to delamination of parts in extreme cases. Produced ceramic objects using extrusion-based AM processes are prone to such limitations [328]. These defects can be minimized by loading high solid in the feedstock, accurate control of the feedstock viscosity, temperature of the built environment, and changing the nozzle design [329]. The same inconvenient and solutions to limit them can be reported for DLP, with the exception of the nozzle design.

In all the parts produced via single step AM processes, anisotropy in mechanical properties and microstructure is intrinsic. By producing parts layer by layer, when high thermal gradients and repeated heating/ cooling cycles are generated, they result in microstructure variation and anisotropic mechanical features in various directions [330]. The anisotropy property can be addressed by applying proper post-printing techniques such as sintering and hot isostatic pressing of printed ceramic parts. Fused deposition-created objects have the required strength for many ceramic engineering applications. Whereas, due to the poor mechanical properties, the produced parts using SLS, L-PBF, and SHL are handicapped. Other than the fused deposition, all other AM technologies are restricted by the volume of specimens and printing speed. Meanwhile, SHL and the fused deposition are not able to produce complex products with high resolution [331].

9. Conclusion

Recent trends in AM technologies successfully employed to produce net shape ceramic components were illustrated in this work. Many research demonstrated the versatility of the presented techniques towards the development of either fully dense ceramics with complex-shapes, and porous materials with controlled porosity features.

AM is economical for mass customization and manufacturing of a certain number of products. The raw materials and process costs for FDM and SL methods are suitable. On the contrary, SLS and L-PBF methods can produce larger volume parts with higher mechanical strengths but also at higher costs. While larger build volumes fabricated using BJT present lower mechanical strengths and relatively reduced costs. Although AM processes can create bigger build parts, the fabrication of a large component with no cracks or deformation is still challenging. In addition, during binder removal and sintering, large ceramic parts show problems which can be attributed to significant variations in sectional thickness and differences in thermal features and shrinkage. However, multiple smaller components can be printed by AM methods in one batch, which makes AM methods suitable for batch production.

Another major challenge is the formation of porosity and voids between the layers or/and beads. These defects have a deleterious effect on ceramic materials. Depending on the AM process, the quantity of voids in the printed part is different, which can lead to delamination of parts during the debinding or the sintering step in extreme cases. Produced ceramic objects using extrusion-based AM processes are prone to such limitations, as well as with DLP. Nonetheless, these defects can be minimized by a high solid loading in the feedstock, an accurate control of the feedstock viscosity and of the temperature of the built environment, and by changing the nozzle design in the extrusion techniques.

It is well documented that the conventional manufacturing methods lead to more greenhouse gas emissions compared to AM technologies and for this reason several efforts have been undertaken to adopt the AM technologies of the production complex shape ceramic components.

To conclude, the different techniques are not mature for mass production and are still actually limited to prototypes or to small batches production.

Declaration of Competing Interest

The authors declare that they have no known competing financial interests or personal relationships that could have appeared to influence the work reported in this paper.

References

[1] M. Revilla-León, M. Sadeghpour, M. Özcan, An update on applications of 3d printing technologies used for processing polymers used in implant dentistry, Odontology 108 (2020) 331–338, https://doi.org/10.1007/s10266-019-00441-7.
[2] M. Dadkhah, M.H. Mosallanejad, L. Iuliano, A. Saboori, A comprehensive overview on the latest progress in the additive manufacturing of metal matrix composites: potential, challenges, and feasible solutions, Acta Metall. Sin. (Engl. Lett. 34 (2021) 1173–1200, https://doi.org/10.1007/s40195-021-01249-7.
[3] C.K. Chua, K.F. Leong, J. An, Introduction to Rapid Prototyping of Biomaterials, in: R. Narayan (Ed.), Rapid Prototyping of Biomaterials, Woodhead Publishing, 2014, pp. 1–15. ISBN 978-0-85709-599-2.
[4] John C. Amirah Alammar, Marta Kois, Revilla-León, M.D. Wael Att, Additive manufacturing technologies: current status and future perspectives, J. Prosthodont. 31 (2022) 4–12.
[5] M.H. Mosallanejad, B. Niroumand, C. Ghibaudo, S. Biamino, A. Salmi, P. Fino, A. Saboori, In-situ alloying of a fine grained fully equiaxed ti-based alloy via

electron beam powder bed fusion additive manufacturing process, Addit. Manuf. 56 (2022), 102878, https://doi.org/10.1016/j.addma.2022.102878.
[6] S. Saleh Alghamdi, S. John, N. Roy Choudhury, N.K. Dutta, Additive manufacturing of polymer materials: progress, promise and challenges, Polym. (Basel) (2021) *13*, https://doi.org/10.3390/polym13050753.
[7] C.L. Ventola, Medical applications for 3D printing: current and projected uses, P T 39 (2014) 704–711.
[8] V. Viale, J. Stavridis, A. Salmi, F. Bondioli, A. Saboori, Optimisation of Downskin Parameters to Produce Metallic Parts via Laser Powder Bed Fusion Process: An Overview, Int. J. Adv. Manuf. Technol. 123 (2022) 2159–2182, https://doi.org/10.1007/s00170-022-10314-z.
[9] O. Keles, C.W. Blevins, and B.K. Effect of Build Orientation on the Mechanical Reliability of 3D Printed ABS, Rapid Prototyp. J. (2017) *23*.
[10] G. Del Guercio, M. Galati, A. Saboori, Innovative approach to evaluate the mechanical performance of Ti–6Al–4V lattice structures produced by electron beam melting process, Met. Mater. Int. 27 (2021) 55–67, https://doi.org/10.1007/s12540-020-00745-2.
[11] U. Scheithauer, E. Schwarzer, T. Moritz, A. Michaelis, Additive manufacturing of ceramic heat exchanger: opportunities and limits of the lithography-based ceramic manufacturing (LCM), J. Mater. Eng. Perform. 27 (2018) 14–20, https://doi.org/10.1007/s11665-017-2843-z.
[12] J.W. Stansbury, M.J. Idacavage, 3D printing with polymers: challenges among expanding options and opportunities, Dent. Mater. 32 (2016) 54–64, https://doi.org/10.1016/j.dental.2015.09.018.
[13] A.J. Allen, I. Levin, S.E. Witt, Materials research & measurement needs for ceramics additive manufacturing, J. Am. Ceram. Soc. 103 (2020) 6055–6069, https://doi.org/10.1111/jace.17369.
[14] R. Kumar, M. Kumar, J.S. Chohan, Material-specific properties and applications of additive manufacturing techniques: a comprehensive review, Bull. Mater. Sci. 44 (2021) 181, https://doi.org/10.1007/s12034-021-02364-y.
[15] H.I. Medellin-Castillo, J. Zaragoza-Siqueiros, Design and manufacturing strategies for fused deposition modelling in additive manufacturing: a review, Chin. J. Mech. Eng. 32 (2019) 53, https://doi.org/10.1186/s10033-019-0368-0.
[16] J. Kotlinski, Mechanical properties of commercial rapid prototyping materials, Rapid Prototyp. J. 20 (2014) 499–510.
[17] M.H. Mosallanejad, B. Niroumand, A. Aversa, D. Manfredi, A. Saboori, Laser Powder Bed Fusion In-Situ Alloying of Ti-5%Cu Alloy: Process-Structure Relationships, J. Alloy. Compd. (2020), 157558, https://doi.org/10.1016/j.jallcom.2020.157558.
[18] CW, H. Apparatus for Production of Three-Dimensional Objects by Stereolithography.
[19] C.W. Hull, S.T. Spence, D.J. Albert, D.R. Smalley, R.H. Method and Apparatus for Production of Three-Dimensional Objects by Stereolithography.
[20] M.H. Mosallanejad, S. Sanaei, M. Atapour, B. Niroumand, L. Iuliano, A. Saboori, Microstructure and Corrosion Properties of CP-Ti Processed by Laser Powder Bed Fusion under Similar Energy Densities, Acta Metall. Sin. (Engl. Lett. (2022), https://doi.org/10.1007/s40195-022-01376-9.
[21] A. Peigney, Tougher ceramics with nanotubes, Nat. Mater. 2 (2003) 15–16, https://doi.org/10.1038/nmat794.
[22] M. Saha, M. Mallik, Additive manufacturing of ceramics and cermets: present status and future perspectives, Sādhanā 46 (2021) 162, https://doi.org/10.1007/s12046-021-01685-2.
[23] Jan Deckers, Jef Vleugels, J.-P. Kruth, Additive manufacturing of ceramics: a review, J. Ceram. Sci. Technol. 5 (2014) 245–260.
[24] Y. Wen, S. Xun, M. Haoye, S. Baichuan, C. Peng, L. Xuejian, Z. Kaihong, Y. Xuan, P. Jiang, L. Shibi, 3D printed porous ceramic scaffolds for bone tissue engineering: a review, Biomater. Sci. 5 (2017) 1690–1698, https://doi.org/10.1039/c7bm00315c.
[25] S. Jang, S. Park, C. Bae, Development of ceramic additive manufacturing: process and materials technology, Biomed. Eng. Lett. 10 (2020) 493–503, https://doi.org/10.1007/s13534-020-00175-4.
[26] H. Windsheimer, N. Travitzky, A. Hofenauer, P. Greil, Laminated object manufacturing of preceramic-paper-derived SiSiC composites, Adv. Mater. 19 (2007) 4515–4519, https://doi.org/10.1002/adma.200700789.
[27] S. Onagoruwa, S. Bose, A. Bandyopadhyay, Fused Depos. Ceram. (FDC) Compos. (2001) 224–231.
[28] B. Leukers, H. Gülkan, S.H. Irsen, S. Milz, C. Tille, H. Seitz, M. Schieker, Biocompatibility of ceramic scaffolds for bone replacement made by 3D printing, Materwiss. Werksttech. 36 (2005) 781–787, https://doi.org/10.1002/mawe.200500968.
[29] Z.C. Eckel, C. Zhou, J.H. Martin, A.J. Jacobsen, W.B. Carter, T.A. Schaedler, Additive manufacturing of polymer-derived ceramics, Sci. (80-.) 351 (2016) 58–62, https://doi.org/10.1126/science.aad2688.
[30] A.M. Wätjen, P. Gingter, M. Kramer, R. Telle, Novel prospects and possibilities in additive manufacturing of ceramics by means of direct inkjet printing, Adv. Mech. Eng. 6 (2014), 141346, https://doi.org/10.1155/2014/141346.
[31] G. Franchin, P. Colombo, Porous Geopolymer Components through Inverse Replica of 3D Printed Sacrificial Templates, J. Ceram. Sci. Technol. 6 (2015) 105–112, https://doi.org/10.4416/JCST2014-00057.
[32] A. Ortona, C. D'Angelo, S. Gianella, D. Gaia, Cellular ceramics produced by rapid prototyping and replication, Mater. Lett. 80 (2012) 95–98, https://doi.org/10.1016/j.matlet.2012.04.050.
[33] D. Guo, L. Li, K. Cai, Z. Gui, C. Nan, Rapid prototyping of piezoelectric ceramics via selective laser sintering and gelcasting, J. Am. Ceram. Soc. 87 (2004) 17–22, https://doi.org/10.1111/j.1151-2916.2004.tb19938.x.
[34] A. Woesz, M. Rumpler, J. Stampfl, F. Varga, N. Fratzl-Zelman, P. Roschger, K. Klaushofer, P. Fratzl, Towards bone replacement materials from calcium phosphates via rapid prototyping and ceramic gelcasting, Mater. Sci. Eng. C. 25 (2005) 181–186, https://doi.org/10.1016/j.msec.2005.01.014.
[35] R. Lu, S. Chandrasekaran, W.L. Du Frane, R.L. Landingham, M.A. Worsley, J. D. Kuntz, Complex shaped boron carbides from negative additive manufacturing, Mater. Des. 148 (2018) 8–16, https://doi.org/10.1016/j.matdes.2018.03.026.
[36] Y. Lakhdar, C. Tuck, J. Binner, A. Terry, R. Goodridge, Additive manufacturing of advanced ceramic materials, Prog. Mater. Sci. 116 (2021), 100736, https://doi.org/10.1016/j.pmatsci.2020.100736.
[37] Shishkovsky, I. *Additive Manufacturing of High-Performance Metals and Alloys: Modeling and Optimization*; IntechOpen, 2018; ISBN 9781789233889.
[38] Schunk Technical Ceramics Ceramic 3D Printing with IntrinSiC® Available online: ⟨https://www.schunk-group.com/technical-ceramics/en⟩.
[39] N. Sangeetha, P. Monish, V.M. Brathikan, Review on various materials used in additive manufacturing, {IOP} Conf. Ser. Mater. Sci. Eng. 1228 (2022) 12015, https://doi.org/10.1088/1757-899x/1228/1/012015.
[40] H.-H. Tang, H.-C. Yen, Slurry-based additive manufacturing of ceramic parts by selective laser burn-out, J. Eur. Ceram. Soc. 35 (2015) 981–987, https://doi.org/10.1016/j.jeurceramsoc.2014.10.019.
[41] S.A.M. Tofail, E.P. Koumoulos, A. Bandyopadhyay, S. Bose, L. O'Donoghue, C. Charitidis, Additive manufacturing: scientific and technological challenges, market uptake and opportunities, Mater. Today 21 (2018) 22–37, https://doi.org/10.1016/j.mattod.2017.07.001.
[42] J.-C. Wang, H. Dommati, S.-J. Hsieh, Review of additive manufacturing methods for high-performance ceramic materials, Int. J. Adv. Manuf. Technol. 103 (2019) 2627–2647, https://doi.org/10.1007/s00170-019-03669-3.
[43] M. Schwentenwein, J. Homa, Additive manufacturing of dense alumina ceramics, Int. J. Appl. Ceram. Technol. 12 (2015) 1–7, https://doi.org/10.1111/ijac.12319.
[44] J.-C. Wang, H. Dommati, Fabrication of zirconia ceramic parts by using solvent-based slurry stereolithography and sintering, Int. J. Adv. Manuf. Technol. 98 (2018) 1537–1546, https://doi.org/10.1007/s00170-018-2349-3.
[45] THORNTON, A.S. FREEZE-FORM EXTRUSION FABRICATION OF BORON CARBIDE, issouri University of Science and Technology ProQuest Dissertations Publishing, 2015.
[46] R. Vaidyanathan, J. Walish, J.L. Lombardi, S. Kasichainula, P. Calvert, K. C. Cooper, The extrusion freeforming of functional ceramic prototypes, JOM 52 (2000) 34–37, https://doi.org/10.1007/s11837-000-0066-4.
[47] E.P. Simonenko, D.V. Sevast'yanov, N.P. Simonenko, V.G. Sevast'yanov, N. T. Kuznetsov, Promising ultra-high-temperature ceramic materials for aerospace applications, Russ. J. Inorg. Chem. 58 (2013) 1669–1693, https://doi.org/10.1134/S0036023613140039.
[48] M.T. Sebastian, R. Ubic, H. Jantunen, Low-loss dielectric ceramic materials and their properties, Int. Mater. Rev. 60 (2015) 392–412, https://doi.org/10.1179/1743280415Y.0000000007.
[49] M. Trunec, J. Klimke, Z.J. Shen, Transparent alumina ceramics densified by a combinational approach of spark plasma sintering and hot isostatic pressing, J. Eur. Ceram. Soc. 36 (2016) 4333–4337, https://doi.org/10.1016/j.jeurceramsoc.2016.06.004.
[50] M. Jabbari, R. Bulatova, A.I.Y. Tok, C.R.H. Bahl, E. Mitsoulis, J.H. Hattel, Ceramic tape casting: a review of current methods and trends with emphasis on rheological behaviour and flow analysis, Mater. Sci. Eng. B 212 (2016) 39–61, https://doi.org/10.1016/j.mseb.2016.07.011.
[51] L. Jiang, X. Peng, D. Walczyk, 3D printing of biofiber-reinforced composites and their mechanical properties: a review, Rapid Prototyp. J. 26 (2020) 1113–1129, https://doi.org/10.1108/RPJ-08-2019-0214.
[52] A. Standard, 2012). *Procedia Eng*, F2792-12a: Standard Terminology for Additive Manufacturing Technologies, 63, ASTM International,, West Conshohocken, PA, 2013, pp. 4–11, 2012). *Procedia Eng*.
[53] R. Barros, F.J.G. Silva, R.M. Gouveia, A. Saboori, G. Marchese, S. Biamino, A. Salmi, E. Atzeni, Laser Powder Bed Fusion of Inconel 718: Residual Stress Analysis before and after Heat Treatment, Met. (Basel) (2019) *9*, https://doi.org/10.3390/met9121290.
[54] J. Kruth, P. Mercelis, J. Van Vaerenbergh, L. Froyen, M. Rombouts, Binding Mechanisms in Selective Laser Sintering and Selective Laser Melting, Rapid Prototyp. J. 11 (2005) 26–36, https://doi.org/10.1108/13552540510573365.
[55] A.-N. Chen, J.-M. Wu, K. Liu, J.-Y. Chen, H. Xiao, P. Chen, C.-H. Li, Y.-S. Shi, High-performance ceramic parts with complex shape prepared by selective laser sintering: a review, Adv. Appl. Ceram. 117 (2018) 100–117, https://doi.org/10.1080/17436753.2017.1379586.
[56] Z. Chen, Z. Li, J. Li, C. Liu, C. Lao, Y. Fu, C. Liu, Y. Li, P. Wang, Y. He, 3D printing of ceramics: a review, J. Eur. Ceram. Soc. 39 (2019) 661–687, https://doi.org/10.1016/j.jeurceramsoc.2018.11.013.
[57] J. Deckers, J.-P. Kruth, K. Shahzad, J. Vleugels, Density Improvement of Alumina Parts Produced through Selective Laser Sintering of Alumina-Polyamide Composite Powder, CIRP Ann. 61 (2012) 211–214, https://doi.org/10.1016/j.cirp.2012.03.032.
[58] J.P. Deckers, K. Shahzad, L. Cardon, M. Rombouts, J. Vleugels, J.-P. Kruth, Shaping ceramics through indirect selective laser sintering, Rapid Prototyp. J. 22 (2016) 544–558, https://doi.org/10.1108/RPJ-10-2014-0143.
[59] H. Chung, S. Das, Functionally graded nylon-11/silica nanocomposites produced by selective laser sintering, Mater. Sci. Eng. A 487 (2008) 251–257, https://doi.org/10.1016/j.msea.2007.10.082.
[60] Z. Wang, Y. Shi, W. He, K. Liu, Y. Zhang, Compound process of selective laser processed alumina parts densified by cold isostatic pressing and solid state sintering: experiments, full process simulation and parameter optimization,

Ceram. Int. 41 (2015) 3245–3253, https://doi.org/10.1016/j.ceramint.2014.11.014.
[61] M.Y. Liu, J.M. Wu, A. Chen, The Fabrication and Properties of SiC Composite Powders for Selective Laser Sintering (and others), Aerosp. Shanghai 33 (2016) 125–131.
[62] J. Deckers, K. Shahzad, J. Vleugels, J.-P. K, Isostatic pressing assisted indirect selective laser sintering of alumina components, Rapid Prototyp. J. 18 (2012) 409–419.
[63] K. Shahzad, J. Deckers, J.-P. Kruth, J. Vleugels, Additive manufacturing of alumina parts by indirect selective laser sintering and post processing, J. Mater. Process. Technol. 213 (2013) 1484–1494, https://doi.org/10.1016/j.jmatprotec.2013.03.014.
[64] K. Shahzad, J. Deckers, Z. Zhang, J.-P. Kruth, J. Vleugels, Additive manufacturing of zirconia parts by indirect selective laser sintering, J. Eur. Ceram. Soc. 34 (2014) 81–89, https://doi.org/10.1016/j.jeurceramsoc.2013.07.023.
[65] A. Zocca, P. Colombo, C.M. Gomes, J. Günster, Additive manufacturing of ceramics: issues, potentialities, and opportunities, J. Am. Ceram. Soc. 98 (2015) 1983–2001, https://doi.org/10.1111/jace.13700.
[66] E. Juste, F. Petit, V. Lardot, F. Cambier, Shaping of ceramic parts by selective laser melting of powder bed, J. Mater. Res. 29 (2014) 2086–2094, https://doi.org/10.1557/jmr.2014.127.
[67] A. Slocombe, L. Li, Selective Laser Sintering of TiC–Al2O3 Composite with Self-Propagating High-Temperature Synthesis, J. Mater. Process. Technol. 118 (2001) 173–178, https://doi.org/10.1016/S0924-0136(01)00905-0.
[68] A. Ma, F. Roters, D. Raabe, Studying the effect of grain boundaries in dislocation density based crystal-plasticity finite element simulations, Int. J. Solids Struct. 43 (2006) 7287–7303, https://doi.org/10.1016/j.ijsolstr.2006.07.006.
[69] Chakravarthy, K.M. and Bourell, D.L. Binder Development for Indirect SLS of Non Metallics.; roceedings of the SFF Symposium: Austin, TX, 2010.
[70] Pei-Kang Bai, Jun Cheng, B. Liu, Selective Laser Sintering of Polymer-Coated Al2O3/ZrO2/TiC Ceramic Powder, Trans. Nonferrous Met. Soc. China 15 (2005) 261–265.
[71] C. Shuai, P. Feng, C. Cao, S. Peng, Processing and characterization of laser sintered hydroxyapatite scaffold for tissue engineering, Biotechnol. Bioprocess Eng. 18 (2013) 520–527, https://doi.org/10.1007/s12257-012-0508-1.
[72] S. XiaoHui, L. Wei, S. PingHui, S. QingYong, W. QingSong, S. YuSheng, L. Kai, L. WenGuang, Selective laser sintering of aliphatic-polycarbonate/hydroxyapatite composite scaffolds for medical applications, Int. J. Adv. Manuf. Technol. 81 (2015) 15–25, https://doi.org/10.1007/s00170-015-7135-x.
[73] C. Gao, B. Yang, H. Hu, J. Liu, C. Shuai, S. Peng, Enhanced sintering ability of biphasic calcium phosphate by polymers used for bone scaffold fabrication, Mater. Sci. Eng. C. 33 (2013) 3802–3810, https://doi.org/10.1016/j.msec.2013.05.017.
[74] S. Meyers, L. De Leersnijder, J. Vleugels, J.-P. Kruth, Direct laser sintering of reaction bonded silicon carbide with low residual silicon content, J. Eur. Ceram. Soc. 38 (2018) 3709–3717, https://doi.org/10.1016/j.jeurceramsoc.2018.04.055.
[75] K. Liu, T. Wu, D.L. Bourell, Y. Tan, J. Wang, M. He, H. Sun, Y. Shi, J. Chen, Laser additive manufacturing and homogeneous densification of complicated shape SiC ceramic parts, Ceram. Int. 44 (2018) 21067–21075, https://doi.org/10.1016/j.ceramint.2018.08.143.
[76] S. Song, Z. Gao, B. Lu, C. Bao, B. Zheng, L. Wang, Performance Optimization of Complicated Structural SiC/Si Composite Ceramics Prepared by Selective Laser Sintering, Ceram. Int. 46 (2020) 568–575, https://doi.org/10.1016/j.ceramint.2019.09.004.
[77] T.-T. Xu, S. Cheng, L.-Z. Jin, K. Zhang, T. Zeng, High-Temperature Flexural Strength of SiC Ceramics Prepared by Additive Manufacturing, Int. J. Appl. Ceram. Technol. 17 (2020) 438–448, https://doi.org/10.1111/ijac.13454.
[78] H. Fu, W. Zhu, Z. Xu, P. Chen, C. Yan, K. Zhou, Y. Shi, Effect of Silicon Addition on the Microstructure, Mechanical and Thermal Properties of Cf/SiC Composite Prepared via Selective Laser Sintering, J. Alloy. Compd. 792 (2019) 1045–1053, https://doi.org/10.1016/j.jallcom.2019.04.129.
[79] J.-M. Wu, M. Li, S.-S. Liu, Y.-S. Shi, C.-H. Li, W. Wang, Selective Laser Sintering of Porous Al2O3-Based Ceramics Using Both Al2O3 and SiO2 Poly-Hollow Microspheres as Raw Materials, Ceram. Int. 47 (2021) 15313–15318, https://doi.org/10.1016/j.ceramint.2021.02.096.
[80] M. Li, A.-N. Chen, X. Lin, J.-M. Wu, S. Chen, L.-J. Cheng, Y. Chen, S.-F. Wen, C.-H. Li, Y.-S. Shi, Lightweight Mullite Ceramics with Controlled Porosity and Enhanced Properties Prepared by SLS Using Mechanical Mixed FAHSs/Polyamide12 Composites, Ceram. Int. 45 (2019) 20803–20809, https://doi.org/10.1016/j.ceramint.2019.07.067.
[81] T. Minasyan, L. Liu, M. Aghayan, L. Kollo, N. Kamboj, S. Aydinyan, I. Hussainova, A novel approach to fabricate Si3N4 by selective laser melting, Ceram. Int. 44 (2018) 13689–13694, https://doi.org/10.1016/j.ceramint.2018.04.208.
[82] A. Ratsimba, A. Zerrouki, N. Tessier-Doyen, B. Nait-Ali, D. André, P. Duport, A. Neveu, N. Tripathi, F. Francqui, G. Delaizir, Densification Behaviour and Three-Dimensional Printing of Y2O3 Ceramic Powder by Selective Laser Sintering, Ceram. Int. 47 (2021) 7465–7474, https://doi.org/10.1016/j.ceramint.2020.11.087.
[83] P. Datta, V.K. Balla, Ceramics processing by additive manufacturing, Trans. Indian Natl. Acad. Eng. 6 (2021) 879–893, https://doi.org/10.1007/s41403-021-00225-y.
[84] L. Hao, S. Dadbakhsh, O. Seaman, M. Felstead, Selective laser melting of a stainless steel and hydroxyapatite composite for load-bearing implant development, J. Mater. Process. Technol. 209 (2009) 5793–5801, https://doi.org/10.1016/j.jmatprotec.2009.06.012.
[85] P. Mercelis, J. Kruth, Residual stresses in selective laser sintering and selective laser melting, Rapid Prototyp. J. 12 (2006) 254–265, https://doi.org/10.1108/13552540610707013.
[86] Evren Yasa, J.-P. Kruth, Application of Laser Re-Melting on Selective Laser Melting Parts, Adv. Prod. Eng. Manag. 6 (2011) 259–270.
[87] M.F. Zaeh, G. Branner, Investigations on residual stresses and deformations in selective laser melting, Prod. Eng. 4 (2010) 35–45, https://doi.org/10.1007/s11740-009-0192-y.
[88] I. Shishkovsky, I. Yadroitsev, P. Bertrand, I. Smurov, Alumina–zirconium ceramics synthesis by selective laser sintering/melting, Appl. Surf. Sci. 254 (2007) 966–970, https://doi.org/10.1016/j.apsusc.2007.09.001.
[89] O. Abdulhameed, A. Al-Ahmari, W. Ameen, S.H. Mian, Additive manufacturing: challenges, trends, and applications, Adv. Mech. Eng. (2019) *11*, https://doi.org/10.1177/1687814018822880.
[90] J. Deckers, S. Meyers, J.P. Kruth, J. Vleugels, Direct selective laser sintering/melting of high density alumina powder layers at elevated temperatures, Phys. Procedia 56 (2014) 117–124, https://doi.org/10.1016/j.phpro.2014.08.154.
[91] P. Bertrand, F. Bayle, C. Combe, P. Goeuriot, I. Smurov, Ceramic components manufacturing by selective laser sintering, Appl. Surf. Sci. 254 (2007) 989–992, https://doi.org/10.1016/j.apsusc.2007.08.085.
[92] J. Wilkes, Y. Hagedorn, W. Meiners, K. Wissenbach, Additive Manufacturing of ZrO2-Al2O3 Ceramic Components by Selective Laser Melting, Rapid Prototyp. J. 19 (2013) 51–57, https://doi.org/10.1108/13552541311292736.
[93] M.X. Gan, C.H. Wong, Properties of selective laser melted spodumene glass-ceramic, J. Eur. Ceram. Soc. 37 (2017) 4147–4154, https://doi.org/10.1016/j.jeurceramsoc.2017.04.060.
[94] Z. Shen, H. Su, H. Liu, D. Zhao, Y. Liu, Y. Guo, G. Fan, M. Yu, J. Chen, M. Guo, et al., Directly Fabricated Al2O3/GdAlO3 Eutectic Ceramic with Large Smooth Surface by Selective Laser Melting: Rapid Solidification Behavior and Thermal Field Simulation, J. Eur. Ceram. Soc. 42 (2022) 1088–1101, https://doi.org/10.1016/j.jeurceramsoc.2021.11.003.
[95] H. Su, Q. Ren, J. Zhang, K. Wei, B. Yao, W. Ma, G. Fan, M. Guo, L. Liu, H. Bai, et al., Microstructures and Mechanical Properties of Directionally Solidified Al2O3/GdAlO3 Eutectic Ceramic by Laser Floating Zone Melting with High Temperature Gradient, J. Eur. Ceram. Soc. 37 (2017) 1617–1626, https://doi.org/10.1016/j.jeurceramsoc.2016.11.041.
[96] T. Mühler, C.M. Gomes, J. Heinrich, J. Günster, Slurry-based additive manufacturing of ceramics, Int. J. Appl. Ceram. Technol. 12 (2015) 18–25, https://doi.org/10.1111/ijac.12113.
[97] A. Gahler, J.G. Heinrich, J. Günster, Direct Laser Sintering of Al2O3–SiO2 Dental Ceramic Components by Layer-Wise Slurry Deposition, J. Am. Ceram. Soc. 89 (2006) 3076–3080, https://doi.org/10.1111/j.1551-2916.2006.01217.x.
[98] S. Pfeiffer, K. Florio, D. Puccio, M. Grasso, B.M. Colosimo, C.G. Aneziris, K. Wegener, T. Graule, Direct Laser Additive Manufacturing of High Performance Oxide Ceramics: A State-of-the-Art Review, J. Eur. Ceram. Soc. 41 (2021) 6087–6114, https://doi.org/10.1016/j.jeurceramsoc.2021.05.035.
[99] H. Li, Z. Yang, D. Cai, D. Jia, Y. Zhou, Microstructure evolution and mechanical properties of selective laser melted bulk-form titanium matrix nanocomposites with minor B4C additions, Mater. Des. 185 (2020), 108245, https://doi.org/10.1016/j.matdes.2019.108245.
[100] L. Xi, K. Ding, D. Gu, S. Guo, M. Cao, J. Zhuang, K. Lin, I. Okulov, B. Sarac, J. Eckert, et al., Interfacial Structure and Wear Properties of Selective Laser Melted Ti/(TiC+TiN) Composites with High Content of Reinforcements, J. Alloy. Compd. 870 (2021), 159436, https://doi.org/10.1016/j.jallcom.2021.159436.
[101] Dongdong Gu, Guangbin Meng, Chuang Li, W. M, R. P, Selective Laser Melting of TiC/Ti Bulk Nanocomposites: Influence of Nanoscale Reinforcement, Scr. Mater. 67 (2012) 185–188.
[102] H. Liu, H. Su, Z. Shen, D. Zhao, Y. Liu, M. Guo, Y. Guo, J. Zhang, L. Liu, H. Fu, Effect of scanning speed on the solidification process of Al2O3/GdAlO3/ZrO2 eutectic ceramics in a single track by selective laser melting, Ceram. Int. 45 (2019) 17252–17257, https://doi.org/10.1016/j.ceramint.2019.05.281.
[103] Q. Liu, B. Song, H. Liao, Microstructure study on selective laser melting yttria stabilized zirconia ceramic with near IR fiber laser, Rapid Prototyp. J. 20 (2014) 346–354, https://doi.org/10.1108/RPJ-12-2012-0113.
[104] Wenchao Du, Xiaorui Ren, Chao Ma, Z.P. BINDER JETTING ADDITIVE MANUFACTURING OF CERAMICS: A LITERATURE REVIEW. In Proceedings of the Proceedings of the ASME 2017 International Mechanical Engineering Congress and Exposition IMECE2017; Florida, USA, 2017.
[105] W. Du, X. Ren, Z. Pei, C. Ma, Ceramic binder jetting additive manufacturing: a literature review on density, J. Manuf. Sci. Eng. (2020) *142*, https://doi.org/10.1115/1.4046248.
[106] S. Huang, C. Ye, H. Zhao, Z. Fan, Additive manufacturing of thin alumina ceramic cores using binder-jetting, Addit. Manuf. 29 (2019), 100802, https://doi.org/10.1016/j.addma.2019.100802.
[107] W. Du, M. Singh, D. Singh, Binder jetting additive manufacturing of silicon carbide ceramics: development of bimodal powder feedstocks by modeling and experimental methods, Ceram. Int. 46 (2020) 19701–19707, https://doi.org/10.1016/j.ceramint.2020.04.098.
[108] Cima, Michael and Sachs, Emanuel and Fan, Tailin and Bredt, James F. and Michaels, Steven P. and Khanuja, Satbir and Lauder, Alan and Lee, Sang-Joon J. and Brancazio, David and Curodeau, A. and others Three-Dimensional Printing Techniques 1995.
[109] Sachs, Emanuel and Cima, Michael and Cornie, J. Three Dimensional Printing: Rapid Tooling and Prototypes Directly from CAD Representation. In 1990 International Solid Freeform Fabrication Symposium; 1990.

[110] M. Mariani, R. Beltrami, P. Brusa, C. Galassi, R. Ardito, N. Lecis, 3D printing of fine alumina powders by binder jetting, J. Eur. Ceram. Soc. 41 (2021) 5307–5315, https://doi.org/10.1016/j.jeurceramsoc.2021.04.006.
[111] P. Kunchala, K. Kappagantula, 3D printing high density ceramics using binder jetting with nanoparticle densifiers, Mater. Des. 155 (2018) 443–450, https://doi.org/10.1016/j.matdes.2018.06.009.
[112] S. Manotham, S. Channasanon, P. Nanthananon, S. Tanodekaew, P. Tesavibul, Photosensitive binder jetting technique for the fabrication of alumina ceramic, J. Manuf. Process. 62 (2021) 313–322, https://doi.org/10.1016/j.jmapro.2020.12.011.
[113] S.M. Gaytan, M.A. Cadena, H. Karim, D. Delfin, Y. Lin, D. Espalin, E. MacDonald, R.B. Wicker, Fabrication of barium titanate by binder jetting additive manufacturing technology, Ceram. Int. 41 (2015) 6610–6619, https://doi.org/10.1016/j.ceramint.2015.01.108.
[114] C.A. Díaz-Moreno, Y. Lin, A. Hurtado-Macías, D. Espalin, C.A. Terrazas, L.E. Murr, R.B. Wicker, Binder jetting additive manufacturing of aluminum nitride components, Ceram. Int. 45 (2019) 13620–13627, https://doi.org/10.1016/j.ceramint.2019.03.187.
[115] D.M. Solis, A.V. Silva, N. Volpato, L.F. Berti, Reaction-bonding of aluminum oxide processed by binder jetting, J. Manuf. Process. 41 (2019) 267–272, https://doi.org/10.1016/j.jmapro.2019.04.008.
[116] R. Hamano, T. Ikoma, Preparation of α-Alumina Powder and Binder For 3D Printer, MRS Adv. 3 (2018) 969–975, https://doi.org/10.1557/adv.2018.300.
[117] A. Fleisher, D. Zolotaryov, A. Kovalevsky, G. Muller-Kamskii, E. Eshed, M. Kazakin, V. Popov, V Reaction Bonding of Silicon Carbides by Binder Jet 3D-Printing, Phenolic Resin Binder Impregnation and Capillary Liquid Silicon Infiltration, Ceram. Int. 45 (2019) 18023–18029, https://doi.org/10.1016/j.ceramint.2019.06.021.
[118] A. Zocca, P. Lima, S. Diener, N. Katsikis, J. Günster, Additive Manufacturing of SiSiC by Layerwise Slurry Deposition and Binder Jetting (LSD-Print), J. Eur. Ceram. Soc. 39 (2019) 3527–3533, https://doi.org/10.1016/j.jeurceramsoc.2019.05.009.
[119] R.K. Enneti, K.C. Prough, T.A. Wolfe, A. Klein, N. Studley, J.L. Trasorras, Sintering of WC-12%Co Processed by Binder Jet 3D Printing (BJ3DP) Technology, Int. J. Refract. Met. Hard Mater. 71 (2018) 28–35, https://doi.org/10.1016/j.ijrmhm.2017.10.023.
[120] E. Mancuso, N. Alharbi, O.A. Bretcanu, M. Marshall, M.A. Birch, A.W. McCaskie, K.W. Dalgarno, Three-Dimensional Printing of Porous Load-Bearing Bioceramic Scaffolds, Proc. Inst. Mech. Eng. Part H. J. Eng. Med. 231 (2017) 575–585, https://doi.org/10.1177/0954411916682984.
[121] C. Sun, X. Tian, L. Wang, Y. Liu, C.M. Wirth, J. Günster, D. Li, Z. Jin, Effect of particle size gradation on the performance of glass-ceramic 3D printing process, Ceram. Int. 43 (2017) 578–584, https://doi.org/10.1016/j.ceramint.2016.09.197.
[122] M. Seidenstuecker, L. Kerr, A. Bernstein, H.O. Mayr, N.P. Suedkamp, R. Gadow, P. Krieg, S. Hernandez Latorre, R. Thomann, F. Syrowatka, et al., 3D Powder Printed Bioglass and β-Tricalcium Phosphate Bone Scaffolds, Mater. (Basel) (2018) *11*, https://doi.org/10.3390/ma11010013.
[123] E. Sheydaeian, M. Vlasea, A. Woo, R. Pilliar, E. Hu, E. Toyserkani, Effect of glycerol concentrations on the mechanical properties of additive manufactured porous calcium polyphosphate structures for bone substitute applications, J. Biomed. Mater. Res. Part B Appl. Biomater. 105 (2017) 828–835, https://doi.org/10.1002/jbm.b.33616.
[124] S. Bose, S. Tarafder, A. Bandyopadhyay, Effect of chemistry on osteogenesis and angiogenesis towards bone tissue engineering using 3D printed scaffolds, Ann. Biomed. Eng. 45 (2017) 261–272, https://doi.org/10.1007/s10439-016-1646-y.
[125] J.A. Gonzalez, J. Mireles, Y. Lin, R.B. Wicker, Characterization of ceramic components fabricated using binder jetting additive manufacturing technology, Ceram. Int. 42 (2016) 10559–10564, https://doi.org/10.1016/j.ceramint.2016.03.079.
[126] Gaytan, Sara M. and Cadena, Monica and Aldaz, Mayela and Herderick, Edward and Medina, Francisco and Wicker, R. Analysis of Ferroelectric Ceramic Fabricated by Binder Jetting Technology. In *2013 International Solid Freeform Fabrication Symposium*; University of Texas: Austin, TX, 2013.
[127] H. Miyanaji, S. Zhang, A. Lassell, A. Zandinejad, L. Yang, Process development of porcelain ceramic material with binder jetting process for dental applications, JOM 68 (2016) 831–841, https://doi.org/10.1007/s11837-015-1771-3.
[128] H. Miyanaji, S. Zhang, A. Lassell, A.A. Zandinejad, L. Yang, Optimal process parameters for 3D printing of porcelain structures, Procedia Manuf. 5 (2016) 870–887, https://doi.org/10.1016/j.promfg.2016.08.074.
[129] H.-R. Wang, M.J. Cima, E.M. Sachs, Three-Dimensional Printing (3DP™) of Gradient-Index (GRIN) Lenses. Innovative Processing and Synthesis of Ceramics, Glasses, and Composites VI, John Wiley & Sons, Ltd,, 2006, pp. 189–201. ISBN 9781118380826.
[130] J. Suwanprateeb, R. Sanngam, W. Suvannapruk, T. Panyathanmaporn, Mechanical and in Vitro Performance of Apatite–Wollastonite Glass Ceramic Reinforced Hydroxyapatite Composite Fabricated by 3D-Printing, J. Mater. Sci. Mater. Med. 20 (2009) 1281, https://doi.org/10.1007/s10856-009-3697-1.
[131] E.M. Gonçalves, F.J. Oliveira, R.F. Silva, M.A. Neto, M.H. Fernandes, M. Amaral, M. Vallet-Regí, M. Vila, Three-Dimensional Printed PCL-Hydroxyapatite Scaffolds Filled with CNTs for Bone Cell Growth Stimulation, J. Biomed. Mater. Res. Part B Appl. Biomater. 104 (2016) 1210–1219, https://doi.org/10.1002/jbm.b.33432.
[132] A. Kumar, K.C. Nune, R.D.K. Misra, Biological functionality of extracellular matrix-ornamented three-dimensional printed hydroxyapatite Scaffolds, J. Biomed. Mater. Res. Part A 104 (2016) 1343–1351, https://doi.org/10.1002/jbm.a.35664.
[133] Z. Zhou, F. Buchanan, C. Mitchell, N. Dunne, Printability of calcium phosphate: calcium sulfate powders for the application of tissue engineered bone scaffolds using the 3D printing technique, Mater. Sci. Eng. C. 38 (2014) 1–10, https://doi.org/10.1016/j.msec.2014.01.027.
[134] W. Du, X. Ren, C. Ma, Z. Pei, Bind. Jet. Addit. Manuf. Ceram.: A Lit. Rev. Vol. Volume 14 (2017).
[135] A. Baux, A. Goillot, S. Jacques, C. Heisel, D. Rochais, L. Charpentier, P. David, T. Piquero, T. Chartier, G. Chollon, Synthesis and Properties of Macroporous SiC Ceramics Synthesized by 3D Printing and Chemical Vapor Infiltration/Deposition, J. Eur. Ceram. Soc. 40 (2020) 2834–2854, https://doi.org/10.1016/j.jeurceramsoc.2020.03.001.
[136] Huoping Zhao, Chunsheng Ye, Zitian Fan, Y. Shi, 3D printing of ZrO2 ceramic using nano-zirconia suspension as a binder, Proc. 2015 4th Int. Conf. Sens., Meas. Intell. Mater. (2016) 654–657.
[137] X. Lv, F. Ye, L. Cheng, S. Fan, Y. Liu, Fabrication of SiC Whisker-Reinforced SiC Ceramic Matrix Composites Based on 3D Printing and Chemical Vapor Infiltration Technology, J. Eur. Ceram. Soc. 39 (2019) 3380–3386, https://doi.org/10.1016/j.jeurceramsoc.2019.04.043.
[138] S. Huang, C. Ye, H. Zhao, Z. Fan, Q. Wei, Binder jetting yttria stabilised zirconia ceramic with inorganic colloid as a binder, Adv. Appl. Ceram. 118 (2019) 458–465, https://doi.org/10.1080/17436753.2019.1666593.
[139] D. Svetlizky, M. Das, B. Zheng, A.L. Vyatskikh, S. Bose, A. Bandyopadhyay, J. M. Schoenung, E.J. Lavernia, N. Eliaz, Directed Energy Deposition (DED) Additive Manufacturing: Physical Characteristics, Defects, Challenges and Applications, Mater. Today 49 (2021) 271–295, https://doi.org/10.1016/j.mattod.2021.03.020.
[140] A. Saboori, A. Aversa, F. Bosio, E. Bassini, E. Librera, M. Chirico, De, S. Biamino, D. Ugues, P. Fino, M. Lombardi, An Investigation on the Effect of Powder Recycling on the Microstructure and Mechanical Properties of AISI 316L Produced by Directed Energy Deposition, Mater. Sci. Eng. A (2019), 138360, https://doi.org/10.1016/j.msea.2019.138360.
[141] A. Aversa, A. Saboori, E. Librera, M. [de Chirico], S. Biamino, M. Lombardi, P. Fino, The role of directed energy deposition atmosphere mode on the microstructure and mechanical properties of 316L samples, Addit. Manuf. (2020), 101274, https://doi.org/10.1016/j.addma.2020.101274.
[142] A. Saboori, A. Aversa, G. Marchese, S. Biamino, M. Lombardi, P. Fino, Microstructure and Mechanical Properties of AISI 316L Produced by Directed Energy Deposition-Based Additive Manufacturing: A Review, Appl. Sci. (2020) *10*, https://doi.org/10.3390/app10093310.
[143] A. Saboori, G. Piscopo, M. Lai, A. Salmi, S. Biamino, An investigation on the effect of deposition pattern on the microstructure, mechanical properties and residual stress of 316L produced by directed energy deposition, Mater. Sci. Eng. A 780 (2020), 139179, https://doi.org/10.1016/j.msea.2020.139179.
[144] A. Saboori, D. Gallo, S. Biamino, P. Fino, M. Lombardi, An overview of additive manufacturing of titanium components by directed energy deposition: microstructure and mechanical properties, Appl. Sci. (2017) *7*, https://doi.org/10.3390/app7090883.
[145] A. Saboori, S. Biamino, M. Lombardi, S. Tusacciu, M. Busatto, M. Lai, P. Fino, How the nozzle position affects the geometry of the melt pool in directed energy deposition process, Powder Met. 62 (2019) 213–217, https://doi.org/10.1080/00325899.2019.1627490.
[146] S.K. Moheimani, L. Iuliano, A. Saboori, The Role of Substrate Preheating on the Microstructure, Roughness, and Mechanical Performance of AISI 316L Produced by Directed Energy Deposition Additive Manufacturing, Int. J. Adv. Manuf. Technol. (2022), https://doi.org/10.1007/s00170-021-08564-4.
[147] A. Saboori, M. Toushekhah, A. Aversa, M. Lai, M. Lombardi, S. Biamino, P. Fino, Critical Features in the Microstructural Analysis of AISI 316L Produced By Metal Additive Manufacturing, Metallogr. Microstruct. Anal. 9 (2020) 92–96, https://doi.org/10.1007/s13632-019-00604-6.
[148] S.H. Nedjad, M. Yildiz, A. Saboori, Solidification behaviour of austenitic stainless steels during welding and directed energy deposition, Sci. Technol. Weld. Join. 0 (2022) 1–17, https://doi.org/10.1080/13621718.2022.2115664.
[149] W.E. Frazier, Metal additive manufacturing: a review, J. Mater. Eng. Perform. 23 (2014) 1917–1928, https://doi.org/10.1007/s11665-014-0958-z.
[150] D. Wu, J. Shi, F. Niu, G. Ma, C. Zhou, B. Zhang, Direct Additive Manufacturing of Melt Growth Al2O3-ZrO2 Functionally Graded Ceramics by Laser Directed Energy Deposition, J. Eur. Ceram. Soc. 42 (2022) 2957–2973, https://doi.org/10.1016/j.jeurceramsoc.2022.01.034.
[151] Z. Fan, Y. Zhao, Q. Tan, N. Mo, M.-X. Zhang, M. Lu, H. Huang, Nanostructured Al2O3-YAG-ZrO2 Ternary Eutectic Components Prepared by Laser Engineered Net Shaping, Acta Mater. 170 (2019) 24–37, https://doi.org/10.1016/j.actamat.2019.03.020.
[152] G.K. Mishra, C.P. Paul, A.K. Rai, A.K. Agrawal, S.K. Rai, K.S. Bindra, Experimental Investigation on Laser Directed Energy Deposition Based Additive Manufacturing of Al2O3 Bulk Structures, Ceram. Int. 47 (2021) 5708–5720, https://doi.org/10.1016/j.ceramint.2020.10.157.
[153] F. Niu, D. Wu, F. Lu, G. Liu, G. Ma, Z. Jia, Microstructure and macro properties of Al2O3 ceramics prepared by laser engineered net shaping, Ceram. Int. 44 (2018) 14303–14310, https://doi.org/10.1016/j.ceramint.2018.05.036.
[154] A.R. Thakur, J.M. Pappas, X. Dong, Fabrication and characterization of high-purity alumina ceramics doped with zirconia via laser direct deposition, JOM 72 (2020) 1299–1306, https://doi.org/10.1007/s11837-019-03969-9.
[155] J.M. Pappas, A.R. Thakur, X. Dong, Effects of Zirconia Doping on Additively Manufactured Alumina Ceramics by Laser Direct Deposition, Mater. Des. 192 (2020), 108711, https://doi.org/10.1016/j.matdes.2020.108711.

[156] D. Wu, D. Zhao, F. Niu, Y. Huang, J. Zhu, G. Ma, In Situ Synthesis of Melt-Grown Mullite Ceramics Using Directed Laser Deposition, J. Mater. Sci. 55 (2020) 12761–12775, https://doi.org/10.1007/s10853-020-04938-3.
[157] F. Niu, D. Wu, G. Ma, S. Zhou, B. Zhang, Effect of second-phase doping on laser deposited AlO ceramics, Rapid Prototyp. J. 21 (2015) 201–206, https://doi.org/10.1108/RPJ-12-2014-0167.
[158] Y. Hu, H. Wang, W. Cong, B. Zhao, Directed energy deposition of zirconia-toughened alumina ceramic: novel microstructure formation and mechanical performance, J. Manuf. Sci. Eng. (2019) *142*, https://doi.org/10.1115/1.4045626.
[159] F. Niu, D. Wu, Y. Huang, S. Yan, G. Ma, C. Li, J. Ding, Direct Additive Manufacturing of Large-Sized Crack-Free Alumina/Aluminum Titanate Composite Ceramics by Directed Laser Deposition, Rapid Prototyp. J. 25 (2019) 1370–1378, https://doi.org/10.1108/RPJ-08-2018-0215.
[160] D. Wu, Y. Huang, F. Niu, G. Ma, S. Yan, C. Li, J. Ding, Effects of TiO2 doping on microstructure and properties of directed laser deposition alumina/aluminum titanate composites, Virtual Phys. Prototyp. 14 (2019) 371–381, https://doi.org/10.1080/17452759.2019.1622987.
[161] Y. Huang, D. Wu, D. Zhao, F. Niu, H. Zhang, S. Yan, G. Ma, Process optimization of melt growth alumina/aluminum titanate composites directed energy deposition: effects of scanning speed, Addit. Manuf. 35 (2020), 101210, https://doi.org/10.1016/j.addma.2020.101210.
[162] Z. Fan, Y. Zhao, M. Lu, H. Huang, Yttria stabilized zirconia (YSZ) thin wall structures fabricated using laser engineered net shaping (LENS), Int. J. Adv. Manuf. Technol. 105 (2019) 4491–4498, https://doi.org/10.1007/s00170-019-03322-z.
[163] F. Niu, D. Wu, G. Ma, J. Wang, J. Zhuang, Z. Jin, Rapid fabrication of eutectic ceramic structures by laser engineered net shaping, Procedia CIRP 42 (2016) 91–95, https://doi.org/10.1016/j.procir.2016.02.196.
[164] F. Niu, D. Wu, G. Ma, J. Wang, M. Guo, B. Zhang, Nanosized Microstructure of Al2O3–ZrO2 (Y2O3) Eutectics Fabricated by Laser Engineered Net Shaping, Scr. Mater. 95 (2015) 39–41, https://doi.org/10.1016/j.scriptamat.2014.09.026.
[165] A. Saboori, A. Aversa, G. Marchese, S. Biamino, M. Lombardi, P. Fino, Application of directed energy deposition-based additive manufacturing in repair, Appl. Sci. (2019) *9*, https://doi.org/10.3390/app9163316.
[166] N. Eliaz, N. Foucks, D. Geva, S. Oren, N. Shriki, D. Vaknin, D. Fishman, O. Levi, Comparative Quality Control of Titanium Alloy Ti–6Al–4V, 17–4 PH Stainless Steel, and Aluminum Alloy 4047 Either Manufactured or Repaired by Laser Engineered Net Shaping (LENS), Mater. (Basel) (2020) *13*, https://doi.org/10.3390/ma13184171.
[167] Jonathan Edgar, S. Tint, Additive Manufacturing Technologies: 3D Printing, Rapid Prototyping, and Direct Digital Manufacturing", 2nd Edition, Johns. Matthey Technol. Rev. 59 (2015) 193–198.
[168] Y. Zhang, H. Liu, Application of rapid prototyping technology in die making of diesel engine, Tsinghua Sci. Technol. 14 (2009) 127–131, https://doi.org/10.1016/S1007-0214(09)70079-3.
[169] Paolo Colombo, Johanna Schmidt, Giorgia Franchin, Andrea Zocca, J. Gunster, Additive manufacturing techniques for fabricating complex ceramic components from preceramic polymers, Am. Ceram. Soc. Bull. 96 (2017) 16–23.
[170] N. Travitzky, H. Windsheimer, T. Fey, P. Greil, Preceramic paper-derived ceramics, J. Am. Ceram. Soc. 91 (2008) 3477–3492, https://doi.org/10.1111/j.1551-2916.2008.02752.x.
[171] B. Dermeik, H. Lorenz, A. Bonet, N. Travitzky, Highly filled papers, on their manufacturing, processing, and applications, Adv. Eng. Mater. 21 (2019) 1900180, https://doi.org/10.1002/adem.201900180.
[172] X. Yin, N. Travitzky, P. Greil, Near-net-shape fabrication of Ti3AlC2-based composites, Int. J. Appl. Ceram. Technol. 4 (2007) 184–190, https://doi.org/10.1111/j.1744-7402.2007.02123.x.
[173] D. Horvitz, I. Gotman, E.Y. Gutmanas, N. Claussen, In Situ Processing of Dense Al2O3–Ti Aluminide Interpenetrating Phase Composites, J. Eur. Ceram. Soc. 22 (2002) 947–954, https://doi.org/10.1016/S0955-2219(01)00396-X.
[174] Curtis Griffin, Jo.Dee Daufenbach, and McMillin, S. Desktop Manufacturing: LOM vs. Pressing, Am. Ceram. Soc. Bull. 73 (1994) 109–113.
[175] Griffin, Curtis and Daufenbach, Jo.Dee and McMillin, S. Solid Freeform Fabrication of Functional Ceramic Components Using a Laminated Object Manufacturing Technique. In 1994 International Solid Freeform Fabrication Symposium; 1994.
[176] L. Weisensel, N. Travitzky, H. Sieber, P. Greil, Laminated object manufacturing (LOM) of SiSiC composites, Adv. Eng. Mater. 6 (2004) 899–903, https://doi.org/10.1002/adem.200400112.
[177] Y. Zhang, J. Han, X. Zhang, X. He, Z. Li, S. Du, Rapid Prototyping and Combustion Synthesis of TiC/Ni Functionally Gradient Materials, Mater. Sci. Eng. A 299 (2001) 218–224, https://doi.org/10.1016/S0921-5093(00)01377-0.
[178] C. Gomes, N. Travitzky, P. Greil, W. Acchar, H. Birol, A. Pedro Novaes de Oliveira, D. Hotza, Laminated Object Manufacturing of LZSA Glass-ceramics, Rapid Prototyp. J. 17 (2011) 424–428, https://doi.org/10.1108/13552541111184152.
[179] M.-J. Pan, A. Leung, C.C.M. Wu, B.A. Bender, R.J. Rayne, Optimizing the performance of telescoping actuators through rapid prototyping and finite element modeling, Ceram. Trans. 150 (2004) 53–62.
[180] C.M. Gomes, B. Gutbrod, N. Travitzky, T. Fey, P. Greil, Priceramic Paper Derived Fibrillar Ceramics. Ceramic Materials and Components for Energy and Environmental Applications, John Wiley & Sons, Ltd,, 2010, pp. 421–427. ISBN 9780470640845.
[181] Rodrigues, S.J. and Chartoff, R.P. and Klosterman, D.A. and Agarwala, M. and Hecht, N. Solid Freeform Fabrication of Functional Silicon Nitride Ceramics by Laminated Object Manufacturing 1. In *International Solid Freeform Fabrication Symposium*; 2000.
[182] O. Penas, R. Zenati, J. Dubois, G. Fantozzi, Processing, Microstructure, Mechanical Properties of Si3N4 Obtained by Slip Casting and Pressureless Sintering, Ceram. Int. 27 (2001) 591–596, https://doi.org/10.1016/S0272-8842(01)00006-2.
[183] Brooke Mansfield, Sabrina Torres, Tianyu Yu, D W. A Review on Additive Manufacturing of Ceramics. In Proceedings of the Proceedings of the ASME 2019 14th International Manufacturing Science and Engineering Conference MSEC2019; Erie, PA, USA, 2019.
[184] N. Travitzky, A. Bonet, B. Dermeik, T. Fey, I. Filbert-Demut, L. Schlier, T. Schlordt, P. Greil, Additive manufacturing of ceramic-based materials, Adv. Eng. Mater. 16 (2014) 729–754, https://doi.org/10.1002/adem.201400097.
[185] C.M. Gomes, C.R. Rambo, A.P.N. De Oliveira, D. Hotza, D. Gouvêa, N. Travitzky, P. Greil, Colloidal processing of glass–ceramics for laminated object manufacturing, J. Am. Ceram. Soc. 92 (2009) 1186–1191, https://doi.org/10.1111/j.1551-2916.2009.03035.x.
[186] S.J. Rodrigues, R.P. Chartoff, D.A. Klosterman, M. Agarwala, N. Hecht, Solid freeform fabrication of functional silicon nitride ceramics by laminated object manufacturing, Proc. Solid Free. Fabr. Symp. Austin (2000) 1–8.
[187] Y. Zhang, X. He, S. Du, J. Zhang, Al2O3 Ceramics Preparation by LOM (Laminated Object Manufacturing), Int. J. Adv. Manuf. Technol. 17 (2001) 531–534, https://doi.org/10.1007/s001700170154.
[188] L. Rueschhoff, W. Costakis, M. Michie, J. Youngblood, R. Trice, Additive manufacturing of dense ceramic parts via direct ink writing of aqueous alumina suspensions, Int. J. Appl. Ceram. Technol. 13 (2016) 821–830, https://doi.org/10.1111/ijac.12557.
[189] W.J. Costakis, L.M. Rueschhoff, A.I. Diaz-Cano, J.P. Youngblood, R.W. Trice, Additive manufacturing of boron carbide via continuous filament direct ink writing of aqueous ceramic suspensions, J. Eur. Ceram. Soc. 36 (2016) 3249–3256, https://doi.org/10.1016/j.jeurceramsoc.2016.06.002.
[190] U. Scheithauer, E. Schwarzer, H.-J. Richter, T. Moritz, Thermoplastic 3D Printing—An Additive Manufacturing Method for Producing Dense Ceramics, Int. J. Appl. Ceram. Technol. 12 (2015) 26–31, https://doi.org/10.1111/ijac.12306.
[191] E. Peng, D. Zhang, J. Ding, Ceramic robocasting: recent achievements, potential, and future developments, Adv. Mater. 30 (2018) 1802404, https://doi.org/10.1002/adma.201802404.
[192] A. Shahzad, I. Lazoglu, Direct Ink Writing (DIW) of Structural and Functional Ceramics: Recent Achievements and Future Challenges, Compos. Part B Eng. 225 (2021), 109249, https://doi.org/10.1016/j.compositesb.2021.109249.
[193] A. Ghazanfari, W. Li, M.C. Leu, J.L. Watts, G.E. Hilmas, Additive manufacturing and mechanical characterization of high density fully stabilized zirconia, Ceram. Int. 43 (2017) 6082–6088, https://doi.org/10.1016/j.ceramint.2017.01.154.
[194] T. Huang, M.S. Mason, G.E. Hilmas, M.C. Leu, Freeze-form extrusion fabrication of ceramic parts, Virtual Phys. Prototyp. 1 (2006) 93–100, https://doi.org/10.1080/17452750600649609.
[195] M.S. Mason, T. Huang, R.G. Landers, M.C. Leu, G.E. Hilmas, Aqueous-based extrusion of high solids loading ceramic pastes: process modeling and control, J. Mater. Process. Technol. 209 (2009) 2946–2957, https://doi.org/10.1016/j.jmatprotec.2008.07.004.
[196] A. Ghazanfari, W. Li, M.C. Leu, G.E. Hilmas, A novel freeform extrusion fabrication process for producing solid ceramic components with uniform layered radiation drying, Addit. Manuf. 15 (2017) 102–112, https://doi.org/10.1016/j.addma.2017.04.001.
[197] S. Esslinger, A. Grebhardt, J. Jaeger, F. Kern, A. Killinger, C. Bonten, R. Gadow, Additive Manufacturing of β-Tricalcium Phosphate Components via Fused Deposition of Ceramics (FDC), Mater. (Basel) (2021) *14*, https://doi.org/10.3390/ma14010156.
[198] J.-P. Kruth, M.C. Leu, T. Nakagawa, Progress in additive manufacturing and rapid prototyping, CIRP Ann. 47 (1998) 525–540, https://doi.org/10.1016/S0007-8506(07)63240-5.
[199] M. Faes, J. Vleugels, F. Vogeler, E. Ferraris, Extrusion-Based Additive Manufacturing of ZrO2 Using Photoinitiated Polymerization, CIRP J. Manuf. Sci. Technol. 14 (2016) 28–34, https://doi.org/10.1016/j.cirpj.2016.05.002.
[200] Crump, S.S. Apparatus and Method for Creating Three-Dimensional Objects 1992.
[201] Chee Kai Chua, Kah Fai Leong, C.S. Lim, Rapid Prototyping: Principles and Applications (with Companion CD-ROM), World Scientific Publishing Company,, 2010.
[202] ISO/ASTM, I.O. for S.; F2792), 52900:2015 (ASTM Additive Manufacturing—General Principles and Terminology.
[203] A. Hazeveld, J.J.R. Huddleston Slater, Y. Ren, Accuracy and reproducibility of dental replica models reconstructed by different rapid prototyping techniques, Am. J. Orthod. Dentofac. Orthop. 145 (2014) 108–115, https://doi.org/10.1016/j.ajodo.2013.05.011.
[204] B. Khatri, K. Lappe, M. Habedank, T. Mueller, C. Megnin, T. Hanemann, Fused Deposition Modeling of ABS-Barium Titanate Composites: A Simple Route towards Tailored Dielectric Devices, Polym. (Basel) (2018) *10*, https://doi.org/10.3390/polym10060666.
[205] O.A. Mohamed, S.H. Masood, J.L. Bhowmik, Optimization of fused deposition modeling process parameters: a review of current research and future prospects, Adv. Manuf. 3 (2015) 42–53, https://doi.org/10.1007/s40436-014-0097-7.
[206] V.L. Tsang, S.N. Bhatia, Three-dimensional tissue fabrication, Adv. Drug Deliv. Rev. 56 (2004) 1635–1647.
[207] K.V. Wong, A. Hernandez, A review of additive manufacturing, ISRN Mech. Eng. 2012 (2012), 208760, https://doi.org/10.5402/2012/208760.

[208] S. T, S. P, A. M.S, A Review on Advancements in Applications of Fused Deposition Modelling Process, Rapid Prototyp. J. 26 (2020) 669–687, https://doi.org/10.1108/RPJ-08-2018-0199.
[209] S. Danforth, Fused deposition of ceramics: a new technique for the rapid fabrication of ceramic components, Mater. Technol. 10 (1995) 144–146, https://doi.org/10.1080/10667857.1995.11752614.
[210] M.-W. Sa, B.-N.B. Nguyen, R.A. Moriarty, T. Kamalitdinov, J.P. Fisher, J.Y. Kim, Fabrication and Evaluation of 3D Printed BCP Scaffolds Reinforced with ZrO2 for Bone Tissue Applications, Biotechnol. Bioeng. 115 (2018) 989–999, https://doi.org/10.1002/bit.26514.
[211] L. Gorjan, R. Tonello, T. Sebastian, P. Colombo, F. Clemens, Fused Deposition Modeling of Mullite Structures from a Preceramic Polymer and γ-Alumina, J. Eur. Ceram. Soc. 39 (2019) 2463–2471, https://doi.org/10.1016/j.jeurceramsoc.2019.02.032.
[212] M. Allahverdi, S.C. Danforth, M. Jafari, A. Safari, Processing of advanced electroceramic components by fused deposition technique, J. Eur. Ceram. Soc. 21 (2001) 1485–1490, https://doi.org/10.1016/S0955-2219(01)00047-4.
[213] M.A. Jafari, W. Han, F. Mohammadi, A. Safari, S.C. Danforth, N. Langrana, A novel system for fused deposition of advanced multiple ceramics, Rapid Prototyp. J. 6 (2000) 161–175, https://doi.org/10.1108/13552540010337047.
[214] N. Singh, R. Singh, I.P.S. Ahuja, On Development of Functionally Graded Material Through Fused Deposition Modelling Assisted Investment Casting from Al2O3/SiC Reinforced Waste Low Density Polyethylene, Trans. Indian Inst. Met. 71 (2018) 2479–2485, https://doi.org/10.1007/s12666-018-1378-9.
[215] D. Drummer, S. Cifuentes-Cuéllar, D. Rietzel, Suitability of PLA/TCP for Fused Deposition Modeling, Rapid Prototyp. J. 18 (2012) 500–507, https://doi.org/10.1108/13552541211272045.
[216] Q. Wei, Y. Wang, X. Li, M. Yang, W. Chai, K. Wang, Y. zhang, Study the Bonding Mechanism of Binders on Hydroxyapatite Surface and Mechanical Properties for 3DP Fabrication Bone Scaffolds, J. Mech. Behav. Biomed. Mater. 57 (2016) 190–200, https://doi.org/10.1016/j.jmbbm.2015.12.007.
[217] N.A.S. Mohd Pu'ad, R.H. Abdul Haq, H. Mohd Noh, H.Z. Abdullah, M.I. Idris, T. C. Lee, Review on the fabrication of fused deposition modelling (FDM) composite filament for biomedical applications, Mater. Today Proc. 29 (2020) 228–232, https://doi.org/10.1016/j.matpr.2020.05.535.
[218] N.A. Conzelmann, L. Gorjan, F. Sarraf, L.D. Poulikakos, M.N. Partl, C.R. Müller, F. J. Clemens, Manufacturing Complex Al2O3 Ceramic Structures Using Consumer-Grade Fused Deposition Modelling Printers, Rapid Prototyp. J. 26 (2020) 1035–1048, https://doi.org/10.1108/RPJ-05-2019-0133.
[219] P. Nevado, A. Lopera, V. Bezzon, M.R. Fulla, J. Palacio, M.A. Zaghete, G. Biasotto, A. Montoya, J. Rivera, S.M. Robledo, et al., Preparation and in Vitro Evaluation of PLA/Biphasic Calcium Phosphate Filaments Used for Fused Deposition Modelling of Scaffolds, Mater. Sci. Eng. C. 114 (2020), 111013, https://doi.org/10.1016/j.msec.2020.111013.
[220] T.N.A.T. Rahim, A.M. Abdullah, H.M. Akil, D. Mohamad, Z.A. Rajion, Preparation and Characterization of a Newly Developed Polyamide Composite Utilising an Affordable 3D Printer, J. Reinf. Plast. Compos. 34 (2015) 1628–1638, https://doi.org/10.1177/0731684415594692.
[221] A.M. Abdullah, T.N.A. Tuan Rahim, D. Mohamad, H.M. Akil, Z.A. Rajion, Mechanical and Physical Properties of Highly ZrO2 /β-TCP Filled Polyamide 12 Prepared via Fused Deposition Modelling (FDM) 3D Printer for Potential Craniofacial Reconstruction Application, Mater. Lett. 189 (2017) 307–309, https://doi.org/10.1016/j.matlet.2016.11.052.
[222] E. Nyberg, A. Rindone, A. Dorafshar, W.L. Grayson, Comparison of 3D-Printed Poly-ε-Caprolactone Scaffolds Functionalized with Tricalcium Phosphate, Hydroxyapatite, Bio-Oss, or Decellularized Bone Matrix, Tissue Eng. Part A 23 (2017) 503–514, https://doi.org/10.1089/ten.tea.2016.0418.
[223] A. Arnesano, S. Kunjalukkal Padmanabhan, A. Notarangelo, F. Montagna, A. Licciulli, Fused Deposition Modeling Shaping of Glass Infiltrated Alumina for Dental Restoration, Ceram. Int. 46 (2020) 2206–2212, https://doi.org/10.1016/j.ceramint.2019.09.205.
[224] M. Revilla-León, Ö.M. Additive manufacturing technologies used for processing polymers: current status and potential application in prosthetic dentistry, J. Prosthodont 28 (2019) 146–158.
[225] F2792–12a, A.I. (2013) Standard Terminology for Additive Manufacturing Technologies (ASTM International, West Conshohocken, PA, 2012). P. Jain, AM Kuthe, Feasibility Study of Manufacturing Using Rapid Prototyping: FDM Approach. Procedia Eng 634–11.
[226] D. Ibrahim, T.L. Broilo, C. Heitz, M.G. de Oliveira, H.W. de Oliveira, S.M. W. Nobre, J.H.G. dos Santos Filho, D.N. Silva, Dimensional Error of Selective Laser Sintering, Three-Dimensional Printing and PolyJet™ Models in the Reproduction of Mandibular Anatomy, J. Cranio-Maxillofac. Surg. 37 (2009) 167–173, https://doi.org/10.1016/j.jcms.2008.10.008.
[227] A. Pugalendhi, R. Ranganathan, S. Ganesan, Impact of Process Parameters on Mechanical Behaviour in Multi-Material Jetting, Mater. Today Proc. 46 (2021) 9139–9144, https://doi.org/10.1016/j.matpr.2019.12.106.
[228] K. Kumar, G.S. Kumar, An Experimental and Theoretical Investigation of Surface Roughness of Poly-Jet Printed Parts, Virtual Phys. Prototyp. 10 (2015) 23–34, https://doi.org/10.1080/17452759.2014.999218.
[229] Kim, G.D.; Oh, Y.T. A Benchmark Study on Rapid Prototyping Processes and Machines: Quantitative Comparisons of Mechanical Properties, Accuracy, Roughness, Speed, and Material Cost. *Proc. Inst. Mech. Eng. Part B J. Eng. Manuf.* 2008, *222*, 201 – 215, doi:10.1243/09544054JEM724.
[230] P. Gay, D. Blanco, F. Pelayo, A. Noriega, P. Fernández, Analysis of factors influencing the mechanical properties of flat polyjet manufactured parts, Procedia Eng. 132 (2015) 70–77, https://doi.org/10.1016/j.proeng.2015.12.481.
[231] C. Guo, M. Zhang, B. Bhandari, Model Building and Slicing in Food 3D Printing Processes: A Review, Compr. Rev. Food Sci. Food Saf. 18 (2019) 1052–1069, https://doi.org/10.1111/1541-4337.12443.
[232] Gao, W.; Zhang, Y.; Nazzetta, D.C.; Ramani, K.; Cipra, R.J. RevoMaker: Enabling Multi-Directional and Functionally-Embedded 3D Printing Using a Rotational Cuboidal Platform. In Proceedings of the 28th Annual ACM Symposium on User Interface Software & Technology; Association for Computing Machinery: New York, NY, USA, 2015; pp. 437–446.
[233] H. Fayazfar, F. Liravi, U. Ali, E. Toyserkani, Additive Manufacturing of High Loading Concentration Zirconia Using High-Speed Drop-on-Demand Material Jetting, Int. J. Adv. Manuf. Technol. 109 (2020) 2733–2746, https://doi.org/10.1007/s00170-020-05829-2.
[234] B. Derby, Inkjet Printing Ceramics: From Drops to Solid, J. Eur. Ceram. Soc. 31 (2011) 2543–2550, https://doi.org/10.1016/j.jeurceramsoc.2011.01.016.
[235] R. Noguera, M. Lejeune, T. Chartier, 3D Fine scale ceramic components formed by ink-jet prototyping process, J. Eur. Ceram. Soc. 25 (2005) 2055–2059, https://doi.org/10.1016/j.jeurceramsoc.2005.03.223.
[236] E. Willems, M. Turon-Vinas, B. Camargo dos Santos, B. Van Hooreweder, F. Zhang, B. Van Meerbeek, J. Vleugels, Additive manufacturing of zirconia ceramics by material jetting, J. Eur. Ceram. Soc. 41 (2021) 5292–5306, https://doi.org/10.1016/j.jeurceramsoc.2021.04.018.
[237] B. Mummareddy, D. Negro, V.T. Bharambe, Y. Oh, E. Burden, M. Ahlfors, J.-W. Choi, A. Du Plessis, J. Adams, E. MacDonald, et al., Mechanical properties of material jetted zirconia complex geometries with hot isostatic pressing, Adv. Ind. Manuf. Eng. 3 (2021), 100052, https://doi.org/10.1016/j.aime.2021.100052.
[238] J. Ebert, E. Özkol, A. Zeichner, K. Uibel, Ö. Weiss, U. Koops, R. Telle, H. Fischer, Direct inkjet printing of dental prostheses made of zirconia, J. Dent. Res. 88 (2009) 673–676, https://doi.org/10.1177/0022034509339988.
[239] E. Özkol, A.M. Wätjen, R. Bermejo, M. Deluca, J. Ebert, R. Danzer, R. Telle, Mechanical Characterisation of Miniaturised Direct Inkjet Printed 3Y-TZP Specimens for Microelectronic Applications, J. Eur. Ceram. Soc. 30 (2010) 3145–3152, https://doi.org/10.1016/j.jeurceramsoc.2010.07.016.
[240] E. Özkol, W. Zhang, J. Ebert, R. Telle, Potentials of the "Direct Inkjet Printing" Method for Manufacturing 3Y-TZP Based Dental Restorations, J. Eur. Ceram. Soc. 32 (2012) 2193–2201, https://doi.org/10.1016/j.jeurceramsoc.2012.03.006.
[241] S. Tyagi, A. Yadav, S. Deshmukh, Review on Mechanical Characterization of 3D Printed Parts Created Using Material Jetting Process, Mater. Today Proc. 51 (2022) 1012–1016, https://doi.org/10.1016/j.matpr.2021.07.073.
[242] Y. Liu, T. Cui, K. Varahramyan, All-Polymer Capacitor Fabricated with Inkjet Printing Technique, Solid. State Electron. 47 (2003) 1543–1548, https://doi.org/10.1016/S0038-1101(03)00082-0.
[243] M.A. Velasco, Y. Lancheros, D.A. Garzón-Alvarado, Geometric and mechanical properties evaluation of scaffolds for bone tissue applications designing by a reaction-diffusion models and manufactured with a material jetting system, J. Comput. Des. Eng. 3 (2016) 385–397, https://doi.org/10.1016/j.jcde.2016.06.006.
[244] N.W. Solís Pinargote, A. Smirnov, N. Peretyagin, A. Seleznev, P. Peretyagin, Direct Ink Writing Technology (3D Printing) of Graphene-Based Ceramic Nanocomposites: A Review, Nanomaterials (2020) *10*, https://doi.org/10.3390/nano10071300.
[245] T. Hafkamp, G. van Baars, B. de Jager, P. Etman, A feasibility study on process monitoring and control in vat photopolymerization of ceramics, Mechatronics 56 (2018) 220–241, https://doi.org/10.1016/j.mechatronics.2018.02.006.
[246] C. Hinczewski, S. Corbel, T. Chartier, Ceramic Suspensions Suitable for Stereolithography, J. Eur. Ceram. Soc. 18 (1998) 583–590, https://doi.org/10.1016/S0955-2219(97)00186-6.
[247] A. Bove, J.-M. Tulliani, M. Galati, F. Calignano, Investigation of the Influence of Process Parameters on Dimensional Accuracy and Post-Sintering Crack Formation in Ceramic 3D Printing for Porcelain-Based Commercial Resins, Prog. Addit. Manuf. (2022), https://doi.org/10.1007/s40964-022-00363-x.
[248] Z. Wang, C. Huang, J. Wang, B. Zou, Development of a novel aqueous hydroxyapatite suspension for stereolithography applied to bone tissue engineering, Ceram. Int. 45 (2019) 3902–3909, https://doi.org/10.1016/j.ceramint.2018.11.063.
[249] H. Wu, W. Liu, R. He, Z. Wu, Q. Jiang, X. Song, Y. Chen, L. Cheng, S. Wu, Fabrication of Dense Zirconia-Toughened Alumina Ceramics through a Stereolithography-Based Additive Manufacturing, Ceram. Int. 43 (2017) 968–972, https://doi.org/10.1016/j.ceramint.2016.10.027.
[250] C.V. Adake, P. Bhargava, P. Gandhi, Effect of Surfactant on Dispersion of Alumina in Photopolymerizable Monomers and Their UV Curing Behavior for Microstereolithography, Ceram. Int. 41 (2015) 5301–5308, https://doi.org/10.1016/j.ceramint.2014.12.066.
[251] S. Zhang, N. Sha, Z. Zhao, Surface Modification of α-Al2O3 with Dicarboxylic Acids for the Preparation of UV-Curable Ceramic Suspensions, J. Eur. Ceram. Soc. 37 (2017) 1607–1616, https://doi.org/10.1016/j.jeurceramsoc.2016.12.013.
[252] H. Xing, B. Zou, Q. Lai, C. Huang, Q. Chen, X. Fu, Z. Shi, Preparation and Characterization of UV Curable Al2O3 Suspensions Applying for Stereolithography 3D Printing Ceramic Microcomponent, Powder Technol. 338 (2018) 153–161, https://doi.org/10.1016/j.powtec.2018.07.023.
[253] J. Sun, J. Binner, J. Bai, Effect of surface treatment on the dispersion of nano zirconia particles in non-aqueous suspensions for stereolithography, J. Eur. Ceram. Soc. 39 (2019) 1660–1667, https://doi.org/10.1016/j.jeurceramsoc.2018.10.024.
[254] K.-J. Jang, J.-H. Kang, J.G. Fisher, S.-W. Park, Effect of the volume fraction of zirconia suspensions on the microstructure and physical properties of products

produced by additive manufacturing, Dent. Mater. 35 (2019) e97–e106, https://doi.org/10.1016/j.dental.2019.02.001.
[255] P.S. Sokolov, D.A. Komissarenko, G.A. Dosovitskii, I.A. Shmeleva, I.V. Slyusar', A. E. Dosovitskii, Rheological Properties of Zirconium Oxide Suspensions in Acrylate Monomers For Use In 3D Printing, Glas. Ceram. 75 (2018) 55–59, https://doi.org/10.1007/s10717-018-0028-3.
[256] D.A. Komissarenko, P.S. Sokolov, A.D. Evstigneeva, I.A. Shmeleva, A. E. Dosovitsky, Rheological and Curing Behavior of Acrylate-Based Suspensions for the DLP 3D Printing of Complex Zirconia Parts, Mater. (Basel) (2018) *11*, https://doi.org/10.3390/ma11122350.
[257] E. Johansson, O. Lidström, J. Johansson, O. Lyckfeldt, E. Adolfsson, Influence of Resin Composition on the Defect Formation in Alumina Manufactured by Stereolithography, Mater. (Basel) (2017) *10*, https://doi.org/10.3390/ma10020138.
[258] N. Alharbi, R. Osman, D. Wismeijer, Effects of Build Direction on the Mechanical Properties of 3D-Printed Complete Coverage Interim Dental Restorations, J. Prosthet. Dent. 115 (2016) 760–767, https://doi.org/10.1016/j.prosdent.2015.12.002.
[259] Kim Guk Bae Lee Sangwook, Three-Dimensional Printing: Basic Principles and Applications in Medicine and Radiology (K.H.Y.D.H.K.Y.-H.K.Y.S.K.C.-S.C.S.H.K. B.J.H.H.K.S.U.K.N.), kjr 17 (2016) 182–197, https://doi.org/10.3348/kjr.2016.17.2.182.
[260] M.M. Emami, F. Barazandeh, F. Yaghmaie, Scanning-Projection Based Stereolithography: Method and Structure, Sens. Actuators A Phys. 218 (2014) 116–124, https://doi.org/10.1016/j.sna.2014.08.002.
[261] Y. Cao, T. Shi, C. Jiao, H. Liang, R. Chen, Z. Tian, A. Zou, Y. Yang, Z. Wei, C. Wang, et al., Fabrication and Properties of Zirconia/Hydroxyapatite Composite Scaffold Based on Digital Light Processing, Ceram. Int. 46 (2020) 2300–2308, https://doi.org/10.1016/j.ceramint.2019.09.219.
[262] Griffith, M.L.; Halloran, J.W. Ultraviolet Curable Ceramic Suspensions for Stereolithography of Ceramics. In Proceedings of the American Society of Mechanical Engineers, Production Engineering Division (Publication) PED; 1994; Vol. 68–2, pp. 529 – 534.
[263] M.L. Griffith, J.W. Halloran, Freeform Fabrication of Ceramics via Stereolithography, J. Am. Ceram. Soc. 79 (1996) 2601–2608, https://doi.org/10.1111/j.1151-2916.1996.tb09022.x.
[264] G. Allen Brady, J.W. Halloran, Stereolithography of Ceramic Suspensions, Rapid Prototyp. J. 3 (1997) 61–65, https://doi.org/10.1108/13552549710176680.
[265] J.W. Halloran, V. Tomeckova, S. Gentry, S. Das, P. Cilino, D. Yuan, R. Guo, A. Rudraraju, P. Shao, T. Wu, et al., Photopolymerization of Powder Suspensions for Shaping Ceramics, J. Eur. Ceram. Soc. 31 (2011) 2613–2619, https://doi.org/10.1016/j.jeurceramsoc.2010.12.003.
[266] C.-J. Bae, A. Ramachandran, J.W. Halloran, Quantifying Particle Segregation in Sequential Layers Fabricated by Additive Manufacturing, J. Eur. Ceram. Soc. 38 (2018) 4082–4088, https://doi.org/10.1016/j.jeurceramsoc.2018.02.008.
[267] K. Zhang, K. Wei, J. Chen, B. Liang, D. Fang, R. He, Stereolithography Additive Manufacturing of Multi-Ceramic Triangle Structures with Tunable Thermal Expansion, J. Eur. Ceram. Soc. 41 (2021) 2796–2806, https://doi.org/10.1016/j.jeurceramsoc.2020.11.033.
[268] X. Li, Y. Yuan, L. Liu, Y.-S. Leung, Y. Chen, Y. Guo, Y. Chai, Y. Chen, 3D Printing of Hydroxyapatite/Tricalcium Phosphate Scaffold with Hierarchical Porous Structure for Bone Regeneration, Bio-Des. Manuf. 3 (2020) 15–29, https://doi.org/10.1007/s42242-019-00056-5.
[269] I.L. de Camargo, M.M. Morais, C.A. Fortulan, M.C. Branciforti, A Review on the Rheological Behavior and Formulations of Ceramic Suspensions for Vat Photopolymerization, Ceram. Int. 47 (2021) 11906–11921, https://doi.org/10.1016/j.ceramint.2021.01.031.
[270] H. Xing, B. Zou, S. Li, X. Fu, Study on Surface Quality, Precision and Mechanical Properties of 3D Printed ZrO2 Ceramic Components by Laser Scanning Stereolithography, Ceram. Int. 43 (2017) 16340–16347, https://doi.org/10.1016/j.ceramint.2017.09.007.
[271] Q. Lian, W. Sui, X. Wu, F. Yang, S. Yang, Additive Manufacturing of ZrO2 Ceramic Dental Bridges by Stereolithography, Rapid Prototyp. J. 24 (2018) 114–119, https://doi.org/10.1108/RPJ-09-2016-0144.
[272] X. Fu, B. Zou, H. Xing, L. Li, Y. Li, X. Wang, Effect of Printing Strategies on Forming Accuracy and Mechanical Properties of ZrO2 Parts Fabricated by SLA Technology, Ceram. Int. 45 (2019) 17630–17637, https://doi.org/10.1016/j.ceramint.2019.05.328.
[273] M. Zhou, W. Liu, H. Wu, X. Song, Y. Chen, L. Cheng, F. He, S. Chen, S. Wu, Preparation of a Defect-Free Alumina Cutting Tool via Additive Manufacturing Based on Stereolithography – Optimization of the Drying and Debinding Processes, Ceram. Int. 42 (2016) 11598–11602, https://doi.org/10.1016/j.ceramint.2016.04.050.
[274] Z. Wu, W. Liu, H. Wu, R. Huang, R. He, Q. Jiang, Y. Chen, X. Ji, Z. Tian, S. Wu, Research into the Mechanical Properties, Sintering Mechanism and Microstructure Evolution of Al2O3-ZrO2 Composites Fabricated by a Stereolithography-Based 3D Printing Method, Mater. Chem. Phys. 207 (2018) 1–10, https://doi.org/10.1016/j.matchemphys.2017.12.021.
[275] A. Licciulli, C. Esposito Corcione, A. Greco, V. Amicarelli, A. Maffezzoli, Laser Stereolithography of ZrO2 Toughened Al2O3, J. Eur. Ceram. Soc. 25 (2005) 1581–1589, https://doi.org/10.1016/j.jeurceramsoc.2003.12.003.
[276] C. Bae, A. Ramachandran, Chung, P.S. K, Ceramic Stereolithography: Additive Manufacturing for 3D Complex Ceramic Structures, J. Korean Ceram. Soc. 54 (2017) 470–477.
[277] Chen, Z.; Li, D.; Zhou, W. Process Parameters Appraisal of Fabricating Ceramic Parts Based on Stereolithography Using the Taguchi Method. *Proc. Inst. Mech. Eng. Part B J. Eng. Manuf.* 2012, *226*, 1249–1258, doi:10.1177/0954405412442607.
[278] N.T. Nguyen, N. Delhote, M. Ettorre, D. Baillargeat, L. Le Coq, R. Sauleau, Design and Characterization of 60-GHz Integrated Lens Antennas Fabricated through Ceramic Stereolithography, IEEE Trans. Antennas Propag. 58 (2010) 2757–2762, https://doi.org/10.1109/TAP.2010.2050447.
[279] S.J. Leigh, C.P. Purssell, J. Bowen, D.A. Hutchins, J.A. Covington, D.R. Billson, A Miniature Flow Sensor Fabricated by Micro-Stereolithography Employing a Magnetite/Acrylic Nanocomposite Resin, Sens. Actuators A Phys. 168 (2011) 66–71, https://doi.org/10.1016/j.sna.2011.03.058.
[280] S. Kirihara, T. Niki, Three-Dimensional Stereolithography of Alumina Photonic Crystals for Terahertz Wave Localization, Int. J. Appl. Ceram. Technol. 12 (2015) 32–37, https://doi.org/10.1111/ijac.12320.
[281] F. Scalera, C. Esposito Corcione, F. Montagna, A. Sannino, A. Maffezzoli, Development and Characterization of UV Curable Epoxy/Hydroxyapatite Suspensions for Stereolithography Applied to Bone Tissue Engineering, Ceram. Int. 40 (2014) 15455–15462, https://doi.org/10.1016/j.ceramint.2014.06.117.
[282] G. Mitteramskogler, R. Gmeiner, R. Felzmann, S. Gruber, C. Hofstetter, J. Stampfl, J. Ebert, W. Wachter, J. Laubersheimer, Light Curing Strategies for Lithography-Based Additive Manufacturing of Customized Ceramics, Addit. Manuf. 1–4 (2014) 110–118, https://doi.org/10.1016/j.addma.2014.08.003.
[283] Pfaffinger, M.; Mitteramskogler, G.; Gmeiner, R.; Stampfl, J. Thermal Debinding of Ceramic-Filled Photopolymers. In Proceedings of the 20th Symposium on Composites; Trans Tech Publications Ltd, 2015; Vol. 825, pp. 75–81.
[284] A. Bertsch, S. Zissi, J.Y. Jézéquel, S. Corbel, J.C. André, Microstereophotolithography Using a Liquid Crystal Display as Dynamic Mask-Generator, Microsyst. Technol. 3 (1997) 42–47, https://doi.org/10.1007/s005420050053.
[285] Kaneko, Y.; Takahashi, K. UV Exposure System for Photolithography and Rapid Prototyping Using DMD Projector. In Proceedings of the SID Conference Record of the International Display Research Conference; 2001; pp. 1339 – 1342.
[286] G. Hadipoespito, Y. Yang, H. Choi, G. Ning, X. Li, Digital Micromirror Device Based Microstereolithography for Micro Structures of Transparent Photopolymer and Nanocomposites, Proc. Solid Free. Fabr. Symp. (2003) 13–24.
[287] C. Sun, N. Fang, D.M. Wu, X. Zhang, Projection Micro-Stereolithography Using Digital Micro-Mirror Dynamic Mask, Sens. Actuators A Phys. 121 (2005) 113–120, https://doi.org/10.1016/j.sna.2004.12.011.
[288] L, H. Digital Micromirror Device. 2009.
[289] R. Bogue, 3D Printing: The Dawn of a New Era in Manufacturing? Assem. Autom. 33 (2013) 307–311, https://doi.org/10.1108/AA-06-2013-055.
[290] M.D. Monzón, R. Paz, E. Pei, F. Ortega, L.A. Suárez, Z. Ortega, M.E. Alemán, T. Plucinski, N. Clow, 4D Printing: Processability and Measurement of Recovery Force in Shape Memory Polymers, Int. J. Adv. Manuf. Technol. 89 (2017) 1827–1836, https://doi.org/10.1007/s00170-016-9233-9.
[291] O. Santoliquido, P. Colombo, A. Ortona, Additive manufacturing of ceramic components by digital light processing: a comparison between the "bottom-up" and the "top-down" approaches, J. Eur. Ceram. Soc. 39 (2019) 2140–2148, https://doi.org/10.1016/j.jeurceramsoc.2019.01.044.
[292] M.P. Lee, G.J.T. Cooper, T. Hinkley, G.M. Gibson, M.J. Padgett, L. Cronin, Development of a 3D Printer Using Scanning Projection Stereolithography, Sci. Rep. 5 (2015) 9875, https://doi.org/10.1038/srep09875.
[293] R. He, W. Liu, Z. Wu, D. An, M. Huang, H. Wu, Q. Jiang, X. Ji, S. Wu, Z. Xie, Fabrication of Complex-Shaped Zirconia Ceramic Parts via a DLP-Stereolithography-Based 3D Printing Method, Ceram. Int. 44 (2018) 3412–3416, https://doi.org/10.1016/j.ceramint.2017.11.135.
[294] R. Felzmann, S. Gruber, G. Mitteramskogler, P. Tesavibul, A.R. Boccaccini, R. Liska, J. Stampfl, Lithography-based additive manufacturing of cellular ceramic structures, Adv. Eng. Mater. 14 (2012) 1052–1058, https://doi.org/10.1002/adem.201200010.
[295] P. Tesavibul, R. Felzmann, S. Gruber, R. Liska, I. Thompson, A.R. Boccaccini, J. Stampfl, Processing of 45S5 Bioglass® by Lithography-Based Additive Manufacturing, Mater. Lett. 74 (2012) 81–84, https://doi.org/10.1016/j.matlet.2012.01.019.
[296] J. Schmidt, P. Colombo, Digital Light Processing of Ceramic Components from Polysiloxanes, J. Eur. Ceram. Soc. 38 (2018) 57–66, https://doi.org/10.1016/j.jeurceramsoc.2017.07.033.
[297] U. Scheithauer, E. Schwarzer, G. Ganzer, A. Kornig, W. Becker, E. Reichelt, M. Jahn, A. Har-tel, H.J. Richter, T. Moritz, et al., Micro-Reactors Made by Lithography-Based Ceramic Manufacturing (LCM). In *Additive Manufacturing and Strategic Technologies in Advanced Ceramics*; John Wiley & Sons, Ltd (2016) 31–41. ISBN 9781119236016.
[298] A.D. Lantada, A. de Blas Romero, M. Schwentenwein, C. Jellinek, J. Homa, Lithography-Based Ceramic Manufacture (LCM) of Auxetic Structures: Present Capabilities and Challenges, Smart Mater. Struct. 25 (2016) 54015, https://doi.org/10.1088/0964-1726/25/5/054015.
[299] J. Rauchenecker, J. Rabitsch, M. Schwentenwein, T. Konegger, Additive manufacturing of aluminum nitride ceramics with high thermal conductivity via digital light processing, Open Ceram. 9 (2022), 100215, https://doi.org/10.1016/j.oceram.2021.100215.
[300] J. Guo, Y. Zeng, P. Li, J. Chen, Fine Lattice Structural Titanium Dioxide Ceramic Produced by DLP 3D Printing, Ceram. Int. 45 (2019) 23007–23012, https://doi.org/10.1016/j.ceramint.2019.07.346.
[301] C. Marsico, M. Øilo, J. Kutsch, M. Kauf, D. Arola, Vat Polymerization-Printed Partially Stabilized Zirconia: Mechanical Properties, Reliability and Structural

Defects, Addit. Manuf. 36 (2020), 101450, https://doi.org/10.1016/j.addma.2020.101450.
[302] M. Revilla-León, N. Al-Haj Husain, L. Ceballos, M. Özcan, Flexural Strength and Weibull Characteristics of Stereolithography Additive Manufactured versus Milled Zirconia, J. Prosthet. Dent. 125 (2021) 685–690, https://doi.org/10.1016/j.prosdent.2020.01.019.
[303] Y. Lu, Z. Mei, J. Zhang, S. Gao, X. Yang, B. Dong, L. Yue, H. Yu, Flexural Strength and Weibull Analysis of Y-TZP Fabricated by Stereolithographic Additive Manufacturing and Subtractive Manufacturing, J. Eur. Ceram. Soc. 40 (2020) 826–834, https://doi.org/10.1016/j.jeurceramsoc.2019.10.058.
[304] S.-Y. Lee, C.-P. Jiang, Development of a Three-Dimensional Slurry Printing System Using Dynamic Mask Projection for Fabricating Zirconia Dental Implants, Mater. Manuf. Process. 30 (2015) 1498–1504, https://doi.org/10.1080/10426914.2014.984208.
[305] J.M. Suominen, E.J. Frankberg, P.K. Vallittu, E. Levänen, J. Vihinen, T. Vastamäki, R. Kari, L.V.J. Lassila, Three-Dimensional Printing of Zirconia: Characterization of Early Stage Material Properties, Biomater. Investig. Dent. 6 (2019) 23–31, https://doi.org/10.1080/26415275.2019.1640608.
[306] M. Borlaf, A. Serra-Capdevila, C. Colominas, T. Graule, Development of UV-Curable ZrO2 Slurries for Additive Manufacturing (LCM-DLP) Technology, J. Eur. Ceram. Soc. 39 (2019) 3797–3803, https://doi.org/10.1016/j.jeurceramsoc.2019.05.023.
[307] Y. Wang, Z. Wang, S. Liu, Z. Qu, Z. Han, F. Liu, L. Li, Additive manufacturing of silica ceramics from aqueous acrylamide based suspension, Ceram. Int. 45 (2019) 21328–21332, https://doi.org/10.1016/j.ceramint.2019.07.118.
[308] E. Schwarzer, S. Holtzhausen, U. Scheithauer, C. Ortmann, T. Oberbach, T. Moritz, A. Michaelis, Process development for additive manufacturing of functionally graded alumina toughened zirconia components intended for medical implant application, J. Eur. Ceram. Soc. 39 (2019) 522–530, https://doi.org/10.1016/j.jeurceramsoc.2018.09.003.
[309] Y. Zeng, Y. Yan, H. Yan, C. Liu, P. Li, P. Dong, Y. Zhao, J. Chen, 3D Printing of Hydroxyapatite Scaffolds Withgood Mechanical and Biocompatible Properties by Digital Light Processing, J. Mater. Sci. 53 (2018) 6291–6301, https://doi.org/10.1007/s10853-018-1992-2.
[310] T. Zheng, W. Wang, J. Sun, J. Liu, J. Bai, Development and Evaluation of Al2O3–ZrO2 Composite Processed by Digital Light 3D Printing, Ceram. Int. 46 (2020) 8682–8688, https://doi.org/10.1016/j.ceramint.2019.12.102.
[311] B. Inserra, B. Coppola, L. Montanaro, J.-M. Tulliani, P. Palmero, Preparation and Characterization of Ce-ZrO2/Al2O3 Composites by DLP-Based Stereolithography, J. Eur. Ceram. Soc. (2022), https://doi.org/10.1016/j.jeurceramsoc.2022.08.037.
[312] Zhang, S.; Miyanaji, H.; Yang, L.; Zandinejad, A.A.; Dilip, J.J.S.; Stucker, B. An Experimental Study of Ceramic Dental Porcelain Materials Using a 3D Print (3DP) Process. 2014.
[313] M.M. Methani, M. Revilla-León, A. Zandinejad, The potential of additive manufacturing technologies and their processing parameters for the fabrication of all-ceramic crowns: a review, J. Esthet. Restor. Dent. 32 (2020) 182–192, https://doi.org/10.1111/jerd.12535.
[314] H. Seitz, W. Rieder, S. Irsen, B. Leukers, C. Tille, Three-dimensional printing of porous ceramic scaffolds for bone tissue engineering, J. Biomed. Mater. Res. Part B Appl. Biomater. 74B (2005) 782–788, https://doi.org/10.1002/jbm.b.30291.
[315] O.A. Mohamed, S.H. Masood, J.L. Bhowmik, Experimental Investigation of Time-Dependent Mechanical Properties of PC-ABS Prototypes Processed by FDM Additive Manufacturing Process, Mater. Lett. 193 (2017) 58–62, https://doi.org/10.1016/j.matlet.2017.01.104.
[316] M. Schmidt, M. Merklein, D. Bourell, D. Dimitrov, T. Hausotte, K. Wegener, L. Overmeyer, F. Vollertsen, G.N. Levy, Laser Based Additive Manufacturing in Industry and Academia, CIRP Ann. 66 (2017) 561–583, https://doi.org/10.1016/j.cirp.2017.05.011.
[317] D. Olivier, J.A. Travieso-Rodriguez, S. Borros, G. Reyes, R. Jerez-Mesa, Influence of Building Orientation on the Flexural Strength of Laminated Object Manufacturing Specimens, J. Mech. Sci. Technol. 31 (2017) 133–139, https://doi.org/10.1007/s12206-016-1212-4.
[318] ISO/ASTM, I.O. for S. ASTM 52900: 2015 (ASTM F2792) Additive Manufacturing—General Principles—Terminology. ISO Geneva, Switz.
[319] M.H. Farshidianfar, A. Khajepour, A.P. Gerlich, Effect of real-time cooling rate on microstructure in laser additive manufacturing, J. Mater. Process. Technol. 231 (2016) 468–478, https://doi.org/10.1016/j.jmatprotec.2016.01.017.
[320] Govil, K.; Kumar, V.; Pandey, D.P.; Praneeth, R.; Sharma, A. Additive Manufacturing and 3D Printing: A Perspective. In Proceedings of the Advances in Engineering Design; Prasad, A., Gupta, S.S., Tyagi, R.K., Eds.; Springer Singapore: Singapore, 2019; pp. 321–334.
[321] J.S. Woods, K. Veltman, M.A.J. Huijbregts, F. Verones, E.G. Hertwich, Towards a meaningful assessment of marine ecological impacts in life cycle assessment (LCA), Environ. Int. 89–90 (2016) 48–61, https://doi.org/10.1016/j.envint.2015.12.033.
[322] H.S. Sidhu, S. Kumar, Design and fabrication of prosthetic leg, A J. Compos. Theory 12 (2019) 973–981.
[323] Yakout, M.; Elbestawi, M.A.; Veldhuis, S.C. A Review of Metal Additive Manufacturing Technologies. In Proceedings of the Manufacturing Engineering and Process VII; Trans Tech Publications Ltd, 2018; Vol. 278, pp. 1–14.
[324] A.D. Lantada, P.L. Morgado, J. Stampfl, Additive Manufacturing Technologies for Enhancing the Development Process of Biodevices, in: A.D. Lantada (Ed.), Handbook on Advanced Design and Manufacturing Technologies for Biomedical Devices, Springer, US: Boston, MA, 2013, pp. 181–205. ISBN 978-1-4614-6789-2.
[325] Subodh Kumar, A.K.S. Choudhary, Anand Kishore Singh, A.K. Gupta, A comparison of additive manufacturing technologies, Int. J. Innov. Res. Sci. Technol. 3 (2016) 147–152.
[326] L. Chen, Y. He, Y. Yang, S. Niu, H. Ren, The research status and development trend of additive manufacturing technology, Int. J. Adv. Manuf. Technol. 89 (2017) 3651–3660, https://doi.org/10.1007/s00170-016-9335-4.
[327] B. Zareiyan, B. Khoshnevis, Interlayer adhesion and strength of structures in contour crafting - effects of aggregate size, extrusion rate, and layer thickness, Autom. Constr. 81 (2017) 112–121, https://doi.org/10.1016/j.autcon.2017.06.013.
[328] G.J. Gibbons, R. Williams, P. Purnell, E. Farahi, 3D printing of cement composites, Adv. Appl. Ceram. 109 (2010) 287–290, https://doi.org/10.1179/174367509X12472364600878.
[329] S.C. Paul, Y.W.D. Tay, B. Panda, M.J. Tan, Fresh and hardened properties of 3D printable cementitious materials for building and construction, Arch. Civ. Mech. Eng. 18 (2018) 311–319, https://doi.org/10.1016/j.acme.2017.02.008.
[330] B. Vrancken, L. Thijs, J.-P. Kruth, J. Van Humbeeck, Heat Treatment of Ti6Al4V Produced by Selective Laser Melting: Microstructure and Mechanical Properties, J. Alloy. Compd. 541 (2012) 177–185, https://doi.org/10.1016/j.jallcom.2012.07.022.
[331] W. Oropallo, L.A. Piegl, Ten challenges in 3D printing, Eng. Comput. 32 (2016) 135–148, https://doi.org/10.1007/s00366-015-0407-0.